

**NETWORK LEVEL MANIPULATION OF NEURONAL POPULATIONS VIA
MICROTECHNOLOGY: EPILEPSY ON A CHIP**

by

Lacey Anne Cirinelli

B.S. Bioengineering, The Pennsylvania State University, 2005

Submitted to the Graduate Faculty of
Swanson School of Engineering in partial fulfillment
of the requirements for the degree of
Doctor of Philosophy

University of Pittsburgh

2014

UNIVERSITY OF PITTSBURGH
SWANSON SCHOOL OF ENGINEERING

This dissertation was presented

by

Lacey Anne Cirinelli

It was defended on

November 24, 2014

and approved by

X. Tracy Cui, Ph.D., Associate Professor, Department of Bioengineering

Lance A. Davidson, Ph.D., Associate Professor, Department of Bioengineering

Kacey G. Marra, Ph.D., Associate Professor, Departments of Plastic Surgery &
Bioengineering

Rebecca P. Seal, Ph.D., Assistant Professor, Department of Neurobiology

Dissertation Director:

Lance A. Davidson, Ph.D., Associate Professor, Department of Bioengineering

Copyright © by Lacey Cirinelli

2014

NETWORK LEVEL MANIPULATION OF NEURONAL POPULATIONS VIA MICROTECHNOLOGY: EPILEPSY ON A CHIP

Lacey Anne Cirinelli, Ph.D.

University of Pittsburgh, 2014

Recent studies indicate that oscillations between functional states (ex: ictal, post-ictal) in epilepsy are due to fluctuations in neuronal network firing patterns. However, current epilepsy models are often limited to non-mechanistically identifying the most likely anti-epileptic drug candidates. Therefore, expanding research to the network level is a promising way to examine the mechanisms underlying mental pathologies and possibly assess better ways to treat them. Microtechnology, which allows for control of the local microenvironment, is a reliable way to study whole networks, but is rarely applied to neurological disease. The objective of this project is to combine microtechnology with standard neuroscience techniques in an effort to create a platform for high throughput testing of anti-epileptic drugs. To achieve this, we create “epileptic” neuronal networks *in vitro*, characterize network morphology and phenotypic connectivity, and evaluate network activity modulation due to genetic manipulations related to epilepsy. This project focuses on the gene SCN1a, which codes for the voltage gated sodium channel Na_v1.1. Mutations in SCN1a are linked to Generalized Epilepsy with Febrile Seizures Plus. The central hypothesis is that mutations in SCN1a affect activity properties of individual neurons, thus impacting recurrent activity in small networks, and that examining these networks may provide insight into pathways involved in seizure propagation.

TABLE OF CONTENTS

PREFACE.....	XII
1.0 INTRODUCTION.....	1
1.1 EPILEPSY & SCN1A.....	2
1.1.1 Epilepsy Overview	2
1.1.2 Causes & Mechanisms of Epilepsy.....	3
1.1.3 Epilepsy Therapies: Pharmaceuticals.....	6
1.1.4 Epilepsy Therapies: Surgical.....	7
1.1.5 Current Epilepsy Research.....	8
1.1.6 Current Epilepsy Models	10
1.2 MOLECULAR BIOLOGY & GENETICS.....	13
1.2.1 Cell Culture	13
1.2.2 Plasmid Generation	14
1.2.3 Controlling Gene Expression to Understand the Molecular Mechanisms of Epilepsy	15
1.3 MICROTECHNOLOGY	17
1.3.1 Microcontact Printing	17
1.3.2 Controlling Network Geometry	19
1.4 CALCIUM IMAGING	22

1.4.1	Calcium Imaging & Neuronal Activity.....	22
1.5	SUMMARY	23
2.0	CREATION OF WILD TYPE AND MUTANT SCN1A NEURONAL CULTURES.....	25
2.1	INTRODUCTION	25
2.1.1	Generalized Epilepsy with Febrile Seizures Plus, Type II & SCN1a	25
2.1.2	SCN1a/Nav1.1 Studies	28
2.2	MATERIALS & METHODS	31
2.2.1	LB Agar Plates	31
2.2.2	Culturing Plasmids	31
2.2.3	Plasmid Preparations	32
2.2.4	Assaying DNA Concentration.....	34
2.2.5	Endotoxin Removal & Ethanol Precipitation	34
2.2.6	Restriction Digest.....	35
2.2.7	Gel Electrophoresis.....	35
2.2.8	DNA Sequencing	36
2.2.9	Neuronal Harvest, Plating, and Culture.....	36
2.2.10	Nucleofection.....	37
2.2.11	Transfection Efficiency and Co-Transfection Efficiency Calculations ...	38
2.3	RESULTS	39
2.4	DISCUSSION.....	45
2.5	CONCLUSIONS	46

3.0	PHENOTYPIC CHARACTERIZATION OF SMALL NEURONAL NETWORKS CONTAINING WILD TYPE OR MUTANT SCNA1 GENES	47
3.1	INTRODUCTION	47
3.1.1	Nav1.1 Expression	48
3.2	MATERIALS & METHODS	50
3.2.1	Immunocytochemistry.....	50
3.2.2	Epifluorescence Imaging.....	52
3.2.3	Image Analysis & Statistics	53
3.3	RESULTS	54
3.4	DISCUSSION.....	80
3.5	CONCLUSIONS	82
4.0	FUNCTIONAL ANALYSIS OF DEFINED NETWORKS	83
4.1	INTRODUCTION	83
4.1.1	Calcium Imaging, Epilepsy, and Constrained Neuronal Networks.....	83
4.1.2	GEFS⁺ and AEDs.....	85
4.2	MATERIALS & METHODS	87
4.2.1	Master Fabrication	87
4.2.2	Stamp Fabrication	88
4.2.3	Coverslip Preparation	88
4.2.4	Stamping Protocol	89
4.2.5	Neuronal Harvest, Nucleofection, and Culture.....	90
4.2.6	Time-Lapse Calcium Imaging	90
4.2.7	Statistical Analysis.....	91

4.2.8	<i>In Vitro</i> Toxicology Testing.....	92
4.3	RESULTS	93
4.4	DISCUSSION.....	114
4.5	CONCLUSIONS	116
5.0	PROJECT SUMMARY.....	117
5.1	EPILEPSY ON A CHIP	120
APPENDIX.....		121
LIST OF ACRONYMS		121
BIBLIOGRAPHY		123

LIST OF TABLES

Table 1: Comparison of Current Epilepsy Models [52]	12
Table 2: Plasmid List	33
Table 3: ICC Primary Antibodies List.....	51
Table 4: ICC Secondary Antibodies List	52
Table 5: Time-to-Fmax P-values, Effect Size, & Trends for Valproic Acid Trials	104
Table 6: Time-to-Fmax P-values, Effect Size, & Trends for Induced VPA Trials	105
Table 7: Time-to-Fmax P-values, Effect Size, & Trends for Carbamazepine Trials	110
Table 8: Time-to-Fmax P-values, Effect Size, & Trends for Induced CBZ Trials	111

LIST OF FIGURES

Figure 1: Causes of Epilepsy	4
Figure 2: Mechanisms of Epilepsy.....	5
Figure 3: Step-by-step photolithography process	18
Figure 4: Step-by-step process for casting a PDMS stamp	19
Figure 5. Examples of Constrained Neural Networks	21
Figure 6: GEFS⁺ Spectrum	26
Figure 7: Nav1.1 Protein Diagram.....	27
Figure 8: Sodium Current, Membrane Potential, & Sodium Channel Conformation	30
Figure 9. Plasmid map of SCN1a.....	33
Figure 10: Gel Electrophoresis of Digested and Undigested Plasmids	40
Figure 11: Co-Transfection Efficiency	42
Figure 12: Transfection Efficiency in Neurons	44
Figure 13: Representative Images of Nav1.1 Expression	57
Figure 14: Nav1.1 Expression Over Time for Individual Genotypes.....	58
Figure 15: Nav1.1 Expression Across Genotypes at a Given Age	59
Figure 16: Representative Images of Parvalbumin Expression	61
Figure 17: Parvalbumin Expression over Time for Individual Genotypes	62
Figure 18: Parvalbumin Expression Across Genotypes at a Given Age.....	63

Figure 19: Representative Images of Vglut1 Expression	65
Figure 20: Vglut1 Expression Over Time for Individual Genotypes	66
Figure 21: Vglut1 Expression Across Genotypes at a Given Age.....	67
Figure 22: Representative Images of Nav1.1-MAP2 Co-localization.....	69
Figure 23: Representative Images of Nav1.1-Tau1 Co-localization.....	70
Figure 24: Nav1.1 Co-localization with MAP2 and Tau1	71
Figure 25: Representative Images of Nav1.1-Parvalbumin Co-expression.....	73
Figure 26: Nav1.1-Parvalbumin Co-localization Over Time for Individual Genotypes	74
Figure 27: Nav1.1-Parvalbumin Co-localization Across Genotypes at a Given Age	75
Figure 28: Representative Images of Nav1.1-VGlu1 Co-expression.....	77
Figure 29: Nav1.1-Vglut1 Co-localization in Individual Genotypes Across Time.....	78
Figure 30: Nav1.1-Vglut1 Co-localization Across Genotypes at a Given Age	79
Figure 31: Microcontact Printing Ring Patterns	94
Figure 32: Average Number of Cells per Ring Network.....	95
Figure 33: Valproic Acid & Carbamazepine Induced Cell Death	97
Figure 34: Representative Traces of Baseline Calcium Activity	99
Figure 35: Connection Between Time-to-F_{max} and Cell Activity	101
Figure 36: Representative Calcium Traces Following VPA	106
Figure 37: Representative Calcium Traces Following BMI & VPA	107
Figure 38: Representative Calcium Traces Following CBZ	112
Figure 39: Representative Calcium Traces Following BMI & CBZ.....	113

PREFACE

I owe my deepest gratitude to a number of individuals, without whom this work would not have been possible. To my advisors: Dr. Henry Zeringue for allowing me to run with an idea, and to Dr. Lance Davidson for his mentoring, guidance, encouragement, and willingness to take on this project. To my lab mates: Shawn Burton, M.S., who taught me almost everything I know about cell culture and molecular biology techniques; to Dr. Ashwin Vishwanathan for his advice on microcontact printing and calcium imaging analysis; and to Dr. Rich Stoner for general encouragement. And, to my thesis committee for their suggestions and patience.

I would like to acknowledge Dr. Harvey Borovetz, Dr. Sanjeev Shroff, & The University of Pittsburgh's Bioengineering Department for supporting me financially along with The University of Pittsburgh's Provost Office and The Center for the Neural Basis of Cognition. A very special thank you to Dr. Peter Strick for being a true advocate for students.

Additionally, I would like to recognize Dr. Al George, Jr. for kind donation of the SCN1a plasmids and Dr. Michael Gold for the use of and advice regarding his calcium imaging rig.

Last but not least, a very special thank you to my family. To my parents for their unconditional love and support; to my brother, Ethan, for continually pushing me; to my husband, Todd, for his never-ending support (and for putting up with my thesis-related stress); and to Jack and Gus for putting a smile on my face when I needed it most.

1.0 INTRODUCTION

Studies indicate that the short-term vacillation between normal and abnormal brain function in neurological diseases like dementia and epilepsy may result from changes in neuronal network activity [1]. With over 600 nervous system disorders affecting 50 million Americans annually, research should be expanded to the network level to search for clues on how neurological diseases work [2].

On average, the human brain contains 100 billion neurons with hundreds of cell types and an estimated 100 trillion interconnections [3]. These interconnections are influenced by chemical and mechanical signals and appear to play a critical role in brain function [3]. Unfortunately, the central nervous system's complexity and compactness, along with some brain regions' unknown connectivity and inaccessibility, makes it difficult to study networks *in vivo*. Additionally, traditional neuroscience methods often focus on single cell activity. Even though single cell data provides valuable information, it does not shed light on how changes in that single cell's activity impact the network as a whole [4]. While small *in vitro* networks can be created to overcome these limitations, they form random connections which introduce unwanted variability from dish to dish. A possible way around this is to plate cells on patterned surfaces with defined size and geometry, thus controlling connectivity while reducing network complexity and inaccessibility [5-7]. The technique of microcontact printing is a common way to create patterned substrates for culturing neurons *in vitro* [5, 8]. By combining the traditionally

engineering-based technique of microcontact printing with classical neuroscience methods, we 1) evaluate artificially-generated *in vitro* networks of cultured neurons and 2) evaluate these artificial networks as our *in vitro* model of Generalized Epilepsy with Febrile Seizures Plus, Type II - a disease rarely studied in neurons *in vitro*.

1.1 EPILEPSY & SCN1A

1.1.1 Epilepsy Overview

Worldwide, more than 50 million people are afflicted with epilepsy- a collection of over 40 disorders marked by a predisposition to recurrent, unpredictable seizures [9] [10]. The strict definition of epilepsy is a neurological disorder where abnormal electrical activity in the brain causes loss-of-consciousness and seizures [11]. However, the symptoms of epilepsy vary widely based on which type of epilepsy a patient has. Some patients experience absence, or petite mal seizures, where they appear inattentive, become unresponsive, and stare off into space for the duration of the seizure [12]. Others experience alternating periods of muscle clenching and relaxation known as tonic-clonic, or grand mal, seizures [12].

Regardless of type, epilepsy is thought to affect 2 to 3 million people in the United States, although a recent study from Hesdorffer *et al.* indicates that as many as 12 million Americans run the risk of developing epilepsy in their lifetime due to age or genetic predisposition [13] [14]. In addition to being at least as prevalent as breast cancer, epilepsy can also be as deadly: up to 50,000 Americans die of epilepsy-related deaths each year [15]. Epilepsy-related deaths occur due to a variety of causes including suicide, since epilepsy patients are 4 to 6 times as likely to

develop depression compared to the general public, seizure-related accidents, development of status epilepticus (prolonged seizures lasting longer than five minutes), and SUDEP, or sudden unexplained death in epilepsy, where otherwise healthy patients die unexpectedly with no apparent cause [16] [17] [18] [19].

Finally, epilepsy can be contracted at any point in life, is not specific to race or gender, and can have either a genetic component or a physical origin (ex: traumatic brain injury) [20]. Regardless of basis, epilepsies are classified as being either partial or generalized. Partial seizures originate from, and are localized to, a specific area of the brain, while generalized seizures propagate throughout both cerebral hemispheres simultaneously.

1.1.2 Causes & Mechanisms of Epilepsy

In addition to epilepsy being a collection of chronic seizure disorders as opposed to a single disease, there is also no underlying cause for epilepsy. A variety of factors may cause a normal brain network to be disrupted leading to chronic seizure activity (Figure 1). For instance, physical injuries like traumatic brain injury (linked to Post-Traumatic Epilepsy) [21] or ischemic stroke (linked to Epilepsy with Cerebrovascular Diseases) can cause a patient to develop chronic seizures [22]. Genetic mutations can also disrupt network function. For example, mutations in SCN1a are linked to Generalized Epilepsy with Febrile Seizures Plus, Type II [23] while mutations in PRICKLE1 are linked to Progressive Myoclonic Epilepsy with ataxia [24]. Additionally, abnormal brain development or connectivity with or without a genetic basis can lead to chronic seizures as in the case of Juvenile Myoclonic Epilepsy (abnormal thalamo-cortico structure) [25] and Temporal Lobe Epilepsy (decreased Default Mode Network connections) [26].

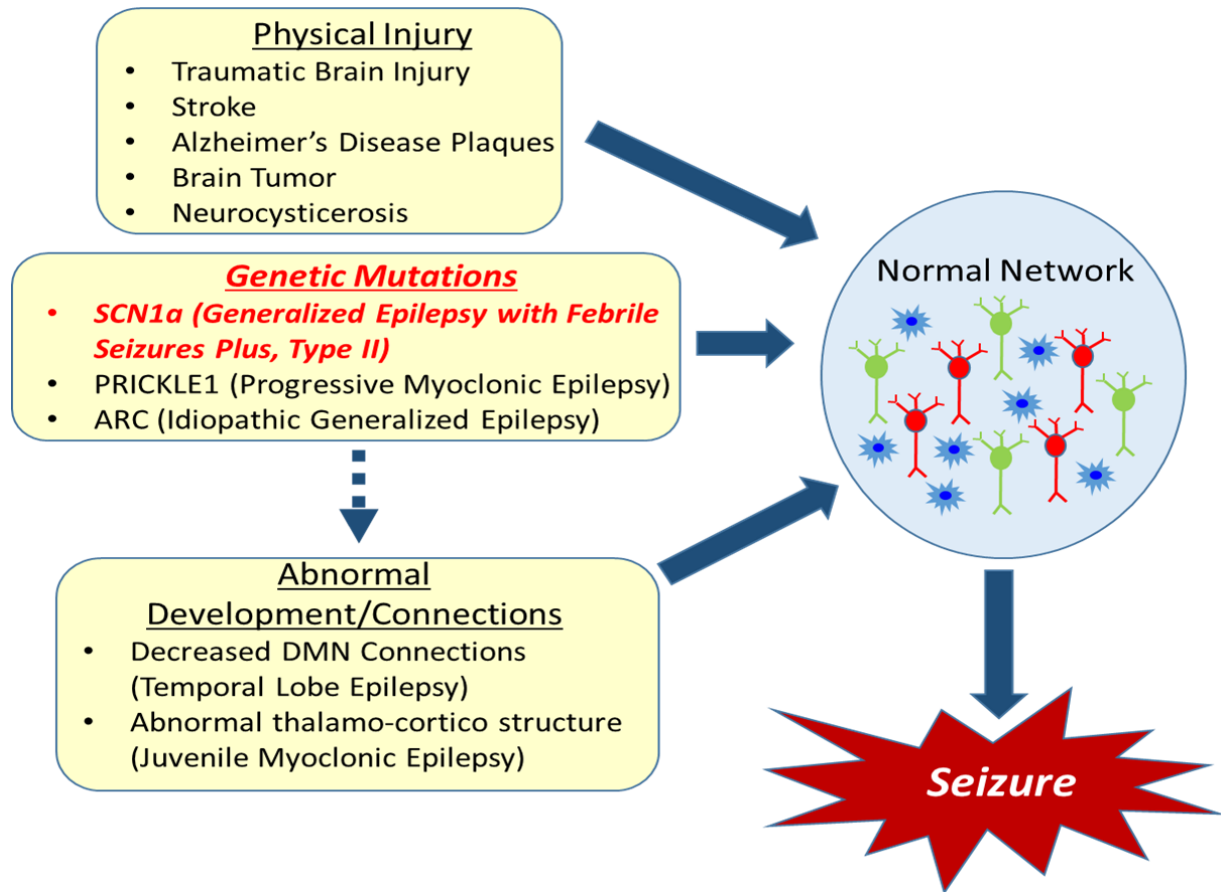


Figure 1: Causes of Epilepsy

Above: Multiple causes underlying epileptogenesis. Those in red are examined in this project.

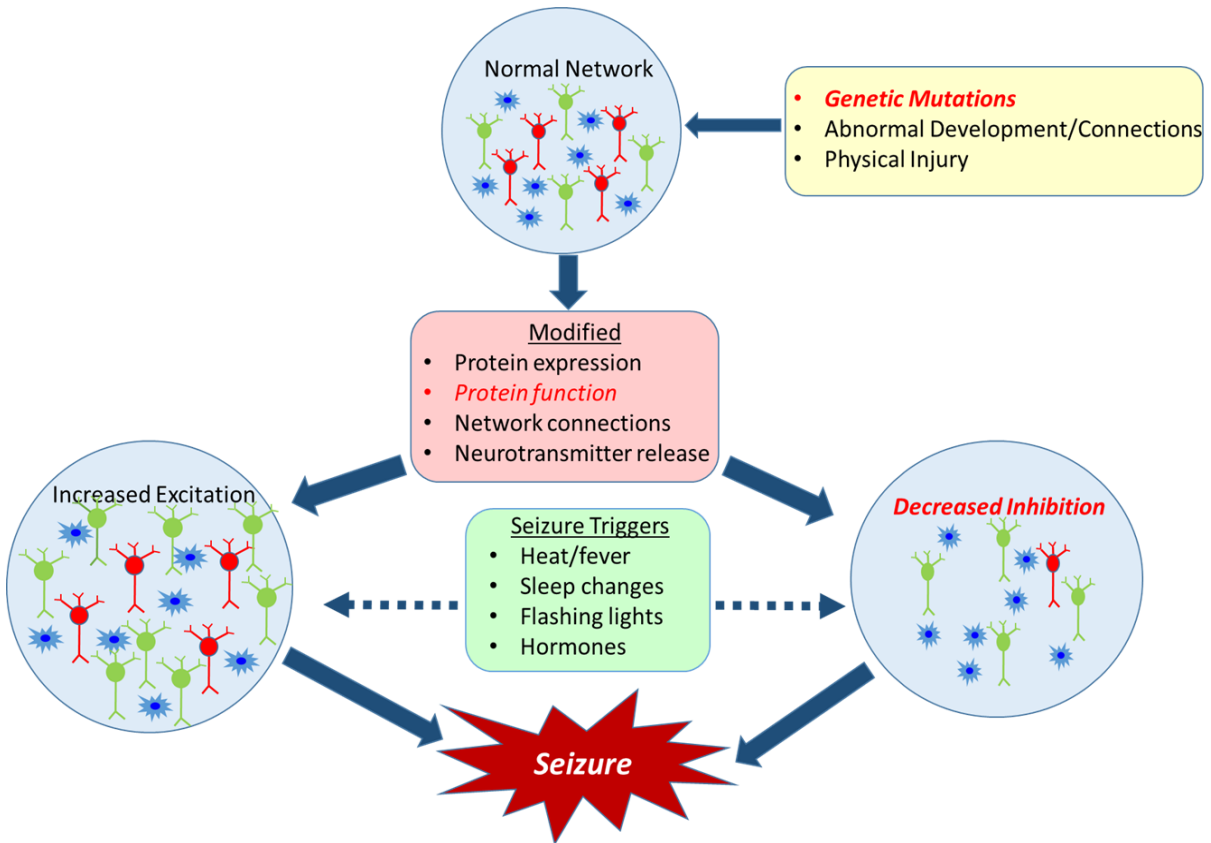


Figure 2: Mechanisms of Epilepsy

Above: Examples of mechanisms underlying epileptogenesis. Those in red are examined in this project.

In addition to multiple causes underlying epilepsy, there are also a number of mechanisms influencing how a network is disrupted (Figure 2). For example, protein function or expression can be modified as can synapse development, network connectivity, and neurotransmitter release. All mechanisms lead to either an overall increase in network excitation or an overall decrease in network inhibition, which ultimately makes patients more likely to seize spontaneously or following a seizure trigger like fever or flashing lights.

1.1.3 Epilepsy Therapies: Pharmaceuticals

Despite epilepsy's prevalence, it remains one of the least understood chronic disorders in the world [27]. While there is no cure, many cases can be controlled with medication or surgery. Typically, the first course of treatment involves anti-epileptic drugs (AEDs). Effective AEDs usually work by increasing network inhibition (by increasing GABA levels, for example) or by decreasing network excitation (by blocking glutamate release, for example) [28]. About 60% of patients achieve seizure-free status on their first or second AED [29]. However, the odds of pharmacologically-based seizure cessation drop dramatically with each subsequent AED tried, with a less than 4% chance of seizure cessation likely after the second AED [30] [31]. The underlying reason why some patients are able to control seizures with AEDs while others with the same syndrome are not is not fully known, but variation in individual genetics is thought to play a role [32]. Because patients typically need to be slowly introduced to and weaned off of AEDs, the time between diagnosis and successful treatment can vary greatly from patient to patient, and significantly increases with each failed AED trial [30].

In addition to selecting the proper AED, determining an appropriate dosage can be complicated. Because patients have varying degrees of drug tolerance, with some experiencing

drug toxicity at low levels and others being able to stand higher doses, “standard” dosages do not exist [33]. Therefore, clinicians often slowly adjust dosages over time to balance drug efficacy with side effects like dizziness, fatigue, headache, and weight gain or loss. Patients who are able to control seizures for 2-10 years on AEDs are sometimes permitted to stop AED use. However, patients often relapse, typically within two years [29].

1.1.4 Epilepsy Therapies: Surgical

AEDs eliminate seizures in 60-70% of epilepsy patients and reduce seizures in another 20-30%. [10] [34]. Patients with unsuccessful or incomplete AED treatment often face more drastic surgical options including tissue resections, vagus nerve stimulation, gamma knife surgery, and deep brain stimulation are available [34, 35]. Tissue resection and gamma knife surgeries selectively remove areas of the brain linked to seizure activity [36, 37]. Stimulation procedures, on the other hand, act as pacemakers to regulate brain activity [38, 39]. However, not all surgical treatments are available for all patients. In fact, deep brain stimulation is currently the only surgical option available to treat all types of epilepsy [40]. However, safety and efficacy results for deep brain stimulation are still inconclusive and the procedure is yet to be approved for U.S. patients by the FDA [41, 42]. On the other hand, traditional surgical interventions are well established but are often only options for patients with partial epilepsies because generalized epilepsies lack well-defined seizure origin sites. Additionally, patients whose seizures originate in eloquent areas of the brain (those that control speech, vision, or motor skills), are not considered good surgical candidates. Therefore, out of the patients who do not achieve seizure-free status following AED therapy, less than 10% of adults actually undergo surgery [43].

Unfortunately, even after surgery, many patients require AEDs, albeit at lower doses. The combination of surgery and AEDs successfully eliminates seizures in approximately 70% of patients whose seizures cannot be controlled by AEDs alone [31]. Another 10% of surgical patients experience significant seizure reduction with a surgery/AED combination [31]. However, surgical long-term success varies. Although success rates differ based on the type of surgery performed, approximately 38% of adults who undergo traditional epilepsy surgeries relapse within 5 years, and 53% relapse within 10 years [44]. Similar results are seen in children [45].

As currently available options fail to give many patients the seizure-free status they so desperately crave, continuing effort should be given to developing new drugs and therapies.

1.1.5 Current Epilepsy Research

Despite being the most common neurological disease in the world, epilepsy's public and private funding is greatly reduced compared to other neurological disorders [46]. For example, in 2009, Alzheimer's research received an average of \$129/patient and multiple sclerosis received an average of \$280/patient [15]. Epilepsy, which afflicts almost 12 million more patients worldwide than Alzheimer's and M.S. combined, received only \$35/patient in funding [15]. Part of the underfunding may be because advances in anti-epileptic drugs (AEDs) have made many epilepsies manageable, leading to the mistaken belief that all epilepsies can be controlled. Additionally, the fact that epilepsy can be deadly is not widely known, and is often not even discussed between doctors and their patients [47, 48]. Furthermore, most epileptics are not in a constant state of seizure, and many suffer from absence, or staring seizures, as opposed to the more obvious grand mals. This makes epilepsy less visible to the public at large compared to

diseases like cancer, Parkinson's, or muscular dystrophy where patients have apparent signs of illness that may garner more public empathy. Whatever the reason, epilepsy's comparative underfunding means that research into new therapies needs to be cost-conscious.

In spite of dwindling research funds, the epilepsy community has continued to reassess research goals. In 2000, the White House-initiated conference, "Curing Epilepsy: Focus on the Future," outlined 17 benchmarks for epilepsy research. Benchmarks fell into three categories: 1.) creating better therapies with fewer side-effects, 2.) developing methods to prevent epilepsy in at-risk individuals, and 3.) understanding the mechanisms behind epileptogenesis [49]. In 2005 and 2007, the benchmarks were expanded to emphasize a need for the creation and validation of new models that could be used to test novel therapies, to identify AEDs that may be most effective in treating a given patient, and to determine which patients are likely to experience adverse side-effects or develop intractable seizures [50] [51]. As a result, the National Institute of Neurological Disorders and Stroke is pushing for reevaluation of current epilepsy models and investigation into the feasibility of "personalized therapies," which test an individual patient's genotype against available treatments to determine which method(s) and dose(s) will be most effective with the least side effects.

In summary, according to NINDS, new epilepsy models should achieve the following goals:

- Be capable of quickly testing multiple therapies (high through-put testing);
- Have the potential to be used in personalized medicine;
- Allow for the examination of disease mechanism;
- Model chronic epilepsy as opposed to acute seizures;
- Be inexpensive

1.1.6 Current Epilepsy Models

Historically, AED safety and efficacy have been tested using animal models because they allow for system wide drug-effects to be monitored. Mice have long been considered the gold standard and a number of transgenic rodent models exist for the most common types of epilepsy. More recently, simpler animals like zebrafish and *Drosophila* have been introduced as epilepsy models because their genome can be quickly and cheaply modified and they allow for high-throughput AED testing [52-54].

However, not all transgenic animal models of epilepsy demonstrate spontaneous seizures, so external stimuli often need to be applied [55]. External stimuli are also used to create acute seizure models in healthy animals if a genetic model is not available. Two of the most commonly used external stimuli are electroshock and chemoconvulsants [55] [52]. Electroconvulsive thresholding (ECT) or maximal electroshock (MES) models involve passing a known amount of electrical current through the animal's head to induce seizures. Similarly, chemoconvulsant models revolve around giving animals convulsant drugs like Metrazol, bicuculline, or nicotine [55]. Both ECT/MES and chemoconvulsant models are popular because they can be used to inexpensively screen large numbers of drugs, but chemoconvulsants are preferred as they tend to give electrical and behavioral results more-similar to those seen in humans [55] [52]

Regardless of whether a model animal is genetically modified or not, no whole animal model allows researchers to examine the mechanisms behind AED cessation of chronic seizures *in vivo* [56]. Additionally, some disagreement exists as to whether an acute seizure in an otherwise healthy animal constitutes a valid model of chronic disease, especially when the cellular and molecular basis of epileptogenesis cannot be examined [57]. To examine the origin

of epilepsy and to complement whole animal studies, *in vitro* models of epilepsy have been developed.

The three common *in vitro* epilepsy models used are slice, primary cell culture, and dissociated single cells. Like all other epilepsy models, these three preparations have individual benefits and drawbacks (Table 1). Slice work provides the most information regarding *in vivo* network connectivity. Furthermore, tissue can be isolated from genetically modified animals which simultaneously provides samples with underlying pathology and all of the normal tissue composition present in a whole animal. However, precise exposure to extracellular solutions like AEDs may be limited in slice work because of the bath solutions necessary to keep the slice viable [58]. Additionally, acute slices can only be used for a few hours or days [58]. Dissociated single cells and primary cell cultures are convenient for examining ion channel expression and kinetics, which is quite helpful as many epilepsies are linked to ion channel defects. Dissociated single cells, however, often lose their dendritic arbor when they are transplanted from *in vivo* to *in vitro* culture [52]. Primary cell cultures, like slices, are sensitive to their culture conditions and include multiple cell types which may be difficult to identify during experimentation. Additionally, most primary cell cultures used as genetic models of epilepsy are not neurons at all but are actually comprised of non-neuronal cells expressing one or more neuronal protein. Thus, there is a significant lack of an *in vitro* epilepsy model comprised of genetically modified primary neuronal cultures.

Table 1: Comparison of Current Epilepsy Models [52]

Comparison of Current Epilepsy Models				
	Name	Description	Pros	Cons
<i>In vivo</i>	Human/Family Studies	Clinical trials for epilepsy therapies or genetic studies tracing phenotypes, and where available, genotypes of families with a history of seizure-disorders.	In humans, chronic, may transition to personalized medicine	Expensive, hard to find controls, difficult to get statistically significant sample sizes, can only model 1 form of epilepsy at a time, family studies can be very labor intensive
	Genetically Induced Animal Models	Animals modified to express a gene associated with epilepsy. Common sources: mice, zebrafish, drosophila	May be mechanistic, can see therapy's effect on the whole animal	Expensive, can only model 1 form of epilepsy at a time, may not be mechanistic, may still require external stimuli
	Pharmacologically Induced Animal Models	Seizures triggered by exposing an animal to a chemoconvulsant like BMI or Metrazol. Common sources: mice, rat, zebrafish	Inexpensive, similar electrical activity as humans, potential to model various AEDs quickly, can easily be modified to model various types of epilepsy	Acute seizures
	Electrically Induced Animal Models	Seizures triggered by exposing an animal to electrical current. Common Sources: mice	Inexpensive, potential to model various AEDs quickly, can easily be modified to model various types of epilepsy	Acute seizures
<i>In vitro</i>	Slices	Healthy or genetically-modified tissue slices exposed to pharmacological agents like BMI, PTZ, or 4-AP to trigger seizure activity. Common sources: mice, rat	Inexpensive, potential to model various AEDs quickly, can easily be modified to model various types of epilepsy	May be acute seizures, simple, short-term, genetic samples may be expensive
	Cell Culture	Genetically, pharmacologically, or electrically induced seizures in dissociated cultures of cells. Common sources: HEK293, mice, rat, CHO	Inexpensive, potential to model various AEDs quickly, long or short term, can easily be modified to model various types of epilepsy, may transition to personal medicine, can examine network mechanisms	Simple, genetic models often involve expression of neuronal proteins in non-neuronal cells
	Dissociated Single Cells	Single cells removed from a subject with underlying pathology. Common sources: humans, mice	Can be inexpensive (rodent), chronic, may transition to personal medicine	Can be expensive (human), simple, short-term, no network information, can only model 1 form of epilepsy at a time, invasive
Computational Models	Macroscopic	Large scale models primarily composed of principle excitatory cells and inhibitory interneurons	Inexpensive, potential to model various AEDs quickly, can be modified to model various types of epilepsy	Simple, do not take cellular or molecular characteristics into account
	Biophysical	Examine biophysical or molecular properties related to seizure activity in single cell or small network models.	Inexpensive, potential to model various AEDs quickly, can be modified to model various types of epilepsy,	Limited by computational power available

1.2 MOLECULAR BIOLOGY & GENETICS

1.2.1 Cell Culture

Maintaining *in vitro* neuronal cultures is a practice that began over a century ago with Roux's 1885 embryonic chicken medullary and Harrison's 1907 frog neural tube explants [59-61]. While the basic protocol remains the same, many variations have been developed to improve individual culture success. In 1959, Renato Dulbecco modified Eagle's basal media to create the DMEM still commonly used to culture neurons today [62]. DMEM is often supplemented with serum, a portion of blood plasma which is high in proteins and growth factors, that helps promote glial proliferation. Glia are thought to be necessary for healthy neuronal development because cultures that lack glia appear to develop fewer or less efficient synapses [63]. However, glia introduce variability and glial overgrowth is detrimental when patterning cultures because it can allow cells to spread out beyond the pattern limits. To check glial overgrowth, the anti-metabolic agent cytosine arabinoside (AraC) is often added to media between days *in vitro* (DIV) 2 and 10 [64, 65]. Although effective at killing rapidly proliferating cells like glia, AraC can negatively impact neurons as well, especially in low-density cultures [66, 67] [68]. In 2004, Brewer *et al.* developed Neurobasal, a modified form of DMEM/F12 specifically designed for culturing embryonic hippocampal neurons which made the use of primary neuronal cultures more practical for research purposes [69]. Neurobasal has reduced levels of some amino acids and lacks serum, thus promoting neuronal development while limiting glial proliferation. Unlike serum supplemented media, B27 supplemented Neurobasal yields cultures composed of less than 0.5% glia that are viable for over four weeks [69].

A combination of serum positive DMEM and B27/Glutamax supplemented Neurobasal is used in this project as it is optimal for culturing nucleofected embryonic rat hippocampal neurons [70].

1.2.2 Plasmid Generation

With sequencing of the human genome, came genetic advances in molecular biology. In particular, plasmids- double-stranded, often circular, DNA molecules found in bacteria- became a common way to create genetic models of disease. In genetic engineering, plasmids act as a vector for transferring external DNA into host cells. Vectors are created in a multi-step process beginning when a gene of interest is inserted into a plasmid containing an antibody resistant gene, a multiple cloning site, and a replication origin.

Although plasmids can replicate on their own within a host, they lack the ability to transfer their DNA to a new host without some form of transfer. Therefore, once a desired plasmid vector is created, it is inserted into competent bacteria that are adept at taking up heterogeneous DNA through transformation. Bacterial transformation was initially discovered in 1928 by Frederick Griffith using *Streptococcus pneumoniae* [71]. It became a widely used molecular cloning technique in the 1970s when Mandel and Higa determined that *Escherichia coli* could be transformed after induction of artificial competence [72]. Inducing artificial competence is often achieved using methods like calcium chloride transformation where non-competent cells are incubated in a cold solution of divalent cations, like calcium chloride, then heat shocked. Although the exact mechanism is unknown, two prevailing theories are that divalent cations shield negatively charged DNA allowing it to conjugate onto the cells'

negatively charged surface, or that the sudden change from cold to hot conditions weakens the cells' surface, creating pores for foreign materials to pass through.

A more recent method of transformation, electroporation, induces competence by briefly exposing cells to an electric field which creates holes in the cell membrane allowing foreign material like plasmid DNA to enter. Immediately after the electric field is removed, the holes in the cell membrane are repaired preventing cell death. In the early 2000s, Amaxa developed nucleofection - an electroporation method that could be used to transfect previously difficult to transfect primary cells like neurons.

1.2.3 Controlling Gene Expression to Understand the Molecular Mechanisms of Epilepsy

Although much epilepsy research has been done using chemically or electrically induced seizures, nearly 100 genetic animal models of epilepsy have been created in recent years [73]. While induced epilepsy models are helpful in screening new AEDs, genetic models have helped identify other genes, ion channels, and post-synaptic receptors impacted by mutations in human epilepsy-related genes [73]. These animals provide a platform for studying the pathology underlying chronic seizure disorders, but the complexity of the whole animal can limit mechanistic study. Additionally, transgenic animal models can be expensive and time-consuming to create [74]. Therefore, *in vitro* models are used as an alternative for evaluating the mechanisms underlying epilepsy [74].

Many *in vitro* models use plasmids to introduce exogenous genes to study the molecular basis of epilepsy (note: this project uses plasmids encoding the gene SCN1a and the voltage-gated sodium channel it codes for, Na_v1.1). In one early study, Sugawara *et al* transfected a human embryonic kidney cell line with a plasmid encoding the alpha subunit of Na_v1.1 to study

Severe Myoclonic Epilepsy of Infancy (SMEI) [75]. Sugawara's group observed transfected cells had extremely low inward sodium currents during whole-cell patch clamp, indicating a sodium channel loss-of-function.

Similarly, Mantegazza *et al* co-transfected the human embryonic kidney cell line tsA-20a with a fluorescently-tagged human Nav1.1 associated β 1 subunit and a plasmid expressing an M145T mutation in human Nav1.1 [76]. Cell functionality was examined using whole-cell patch clamping. Again, a reduction in current densities indicated a loss-of-function. Additionally, cells expressing the mutant Nav1.1 channels had slower sodium currents and required less electrical stimuli to trigger action potentials.

Finally, Sugiura *et al* examined loss-of-function mutations including A1685V (used in this project) and A1685D in HEK293 cells [77]. In this case, both A1685V and A1685D cells displayed decreased sodium current density compared to cells expressing wild type SCN1a regardless of β subunit expression. However, the presence of the β subunit did result in some sodium current, indicating that the β subunit may be able to partially counteract some loss-of-function effects for some mutations. However, the authors stress that the results need to be re-examined in neurons.

Non-neuronal cells expressing neuronal proteins have provided useful information regarding a protein of interest, but it is imperative that protein function be examined in neuronal cultures so their interplay with other ion channels can be explored. Non-neuronal models simply do not allow researchers to determine if and how other ion channels may compensate for epilepsy-related mutations that ultimately influence the disease's mechanism. Additionally, non-neuronal cells do not exhibit the same connectivity seen in neurons.

1.3 MICROTECHNOLOGY

1.3.1 Microcontact Printing

Microtechnology is defined as any technology performed near the one micron scale. Improvements in microtechnology have made studying the relationship between network geometry and function possible because surface chemistry can be controlled and uniform submicron substrates can be repeatedly created [78] [79]. In addition to controlling surface topology, microfabrication can be used to control cell-cell and cell-medium interactions, which is useful because the local microenvironment affects cell behavior [68, 79, 80]. In general, microtechnology provides researchers with a powerful tool to create precise models for examining cells' interactions with themselves and their environment [81].

While there are many microtechniques available, this project uses microcontact printing - a method similar to using a rubber ink stamp. Stamps create patterns by either selectively modifying the surface (with polylysine for example) to make certain regions more desirable for cell adhesion, or by using a pattern's geometry to manipulate cell growth as neurons tend to stay on larger areas where they can spread as opposed to restricted areas where they may not be able to extend processes [82] [83].

To begin microcontact printing, a master mold must be made using photolithography, a process where a photosensitive resin called a photoresist is applied to a substrate then exposed to UV light filtered through a photomask containing the desired pattern (Figure 3). After the substrate is developed to remove excess photoresist, a process similar to developing photographic film, only the reverse of the desired pattern remains. Once a suitable master mold has been fabricated, polydimethylsiloxane (PDMS), a silicon-based polymer is poured over top

(Figure 4). As the PDMS cures, in the master, an elastomeric stamp containing the desired pattern is produced. After curing and any necessary post-processing is complete, the stamp is ready to be “inked” with the molecule of choice.

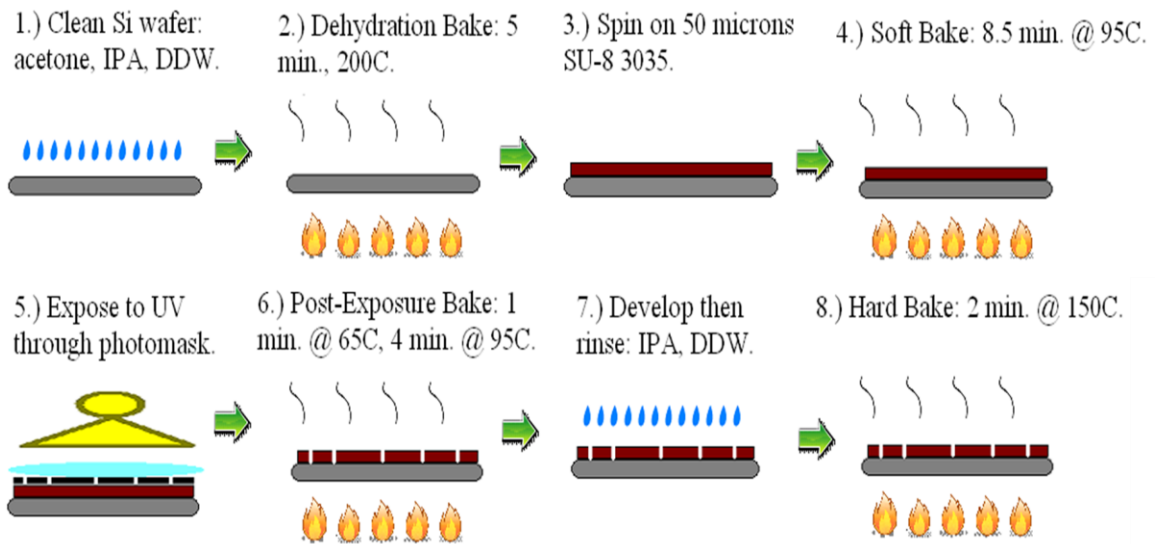


Figure 3: Step-by-step photolithography process

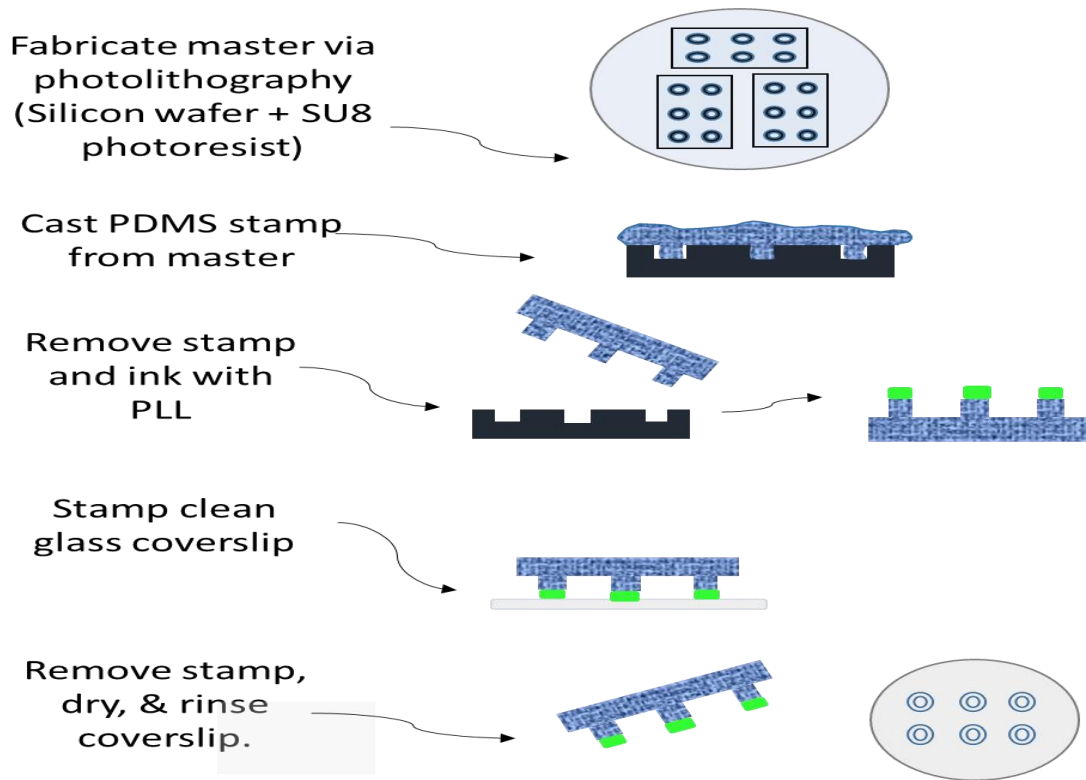


Figure 4: Step-by-step process for casting a PDMS stamp

1.3.2 Controlling Network Geometry

As microtechnology became more popular in neuroscience, more emphasis was placed on determining if and how patterned substrates impact culture composition and development. Numerous researchers have explored the link between network geometry and functionality (Figure 5) [84]. [78, 85-88]. Various studies have determined that patterned cultures exhibit a

strong capacity for self-organization, forming a similar ratio of excitatory and inhibitory neurons regardless of pattern size, extending undifferentiated neurons within 24 hours of plating similar to unpatterned cultures, forming spontaneous connections with neighboring cells, and displaying connections and electrical properties similar to those found *in vivo* [83, 89-91]. Therefore, patterned primary cell cultures appear to reduce the randomness and variability typically seen in dissociated *in vitro* cultures while providing networks with characteristics similar to their *in vivo* counterparts and relatively simple network structures that are accessible to a variety of experimental set-ups.

The pattern used in this project is based on the ring-shaped patterns created by Vishwanathan *et al* (Figure 5, top right) [92]. Vishwanathan created small, ring-shaped networks composed of 40 to 60 neurons using microcontact printing. Networks were incubated with calcium sensitive fluorophores, exposed to baths of either HEPES-buffered saline (HBS), bicuculline methiodide (BMI), or tetrodotoxin (TTX), and stimulated with single or paired electrical pulses. Time-lapse calcium imaging allowed the activity of the entire ring network to be quantified by changes in fluorescence intensity. While there was no unprovoked activity, reverberatory activity, defined as network activity persisting >2 s after the cessation of the input stimulus, was observed in several cultures of DIV 10-14 E18-E19 hippocampal rat neurons. This activity, which persisted even after cessation of the external stimulus, could be viewed as an example of memory because the network essentially “remembered” the stimulus after it was removed.

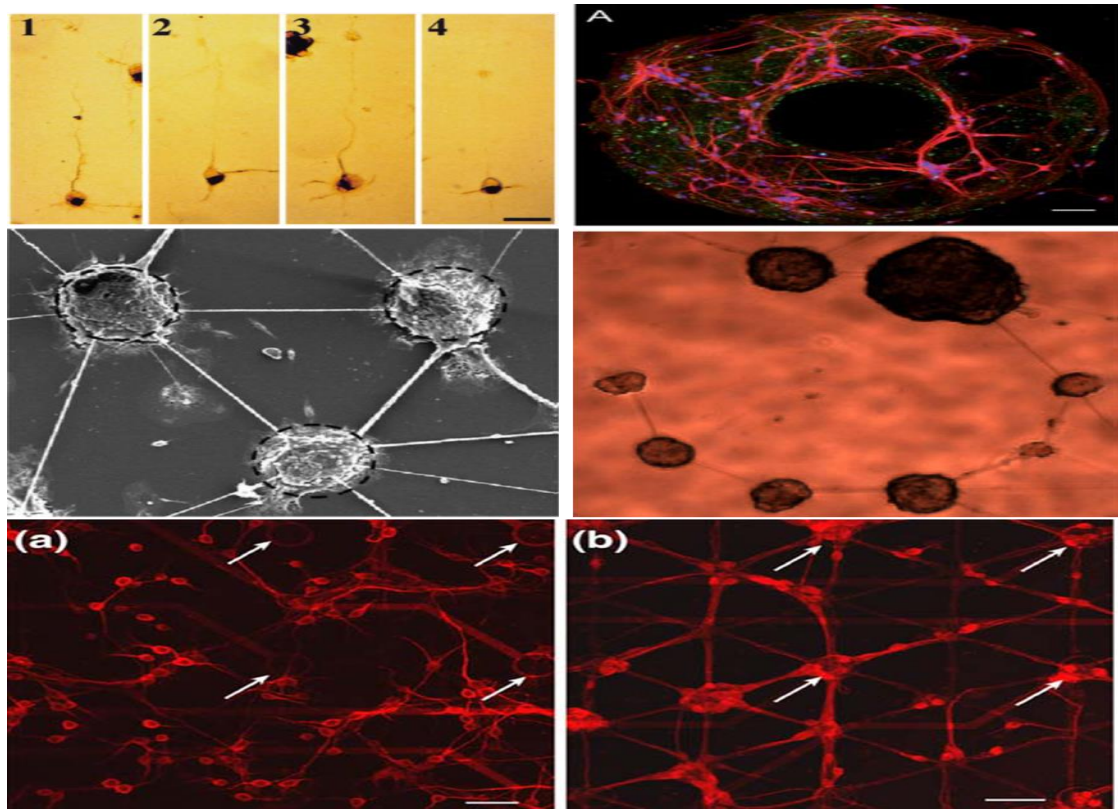


Figure 5. Examples of Constrained Neural Networks

Top Left: Immunostained patterned DIV 3 hippocampal neurons stained for MAP2 (orange); scale bar: 50 μm [91] Top Right: MAP2-stained (red) networks of rat hippocampal neurons on FITC-tagged polylysine rings (green); blue: Hoechst stained nuclei; scale bar: 50 μm . [92]. Middle: SEM of clusters of neurons on 100 μm polylysine islands (left); micrograph of clusters of neurons on 100 μm polylysine islands forming a circular network (right) [90]. Bottom: DIV 7 unpatterned (left) and patterned (right) neural networks grown on planar microelectrode arrays; arrows indicate electrodes. Red: MAP2 stained processes; scale bar: 50 μm [93].

1.4 CALCIUM IMAGING

1.4.1 Calcium Imaging & Neuronal Activity

Network activity can be observed directly from time-lapse calcium imaging which infers cellular activity from intracellular calcium levels. To prepare cultures for calcium imaging, cells are exposed to fluorescently labeled calcium sensitive dyes and monitored under a microscope. Changes in the dye's fluorescence intensity are then recorded and analyzed over time. Time dependent changes in calcium are used to extrapolate information regarding a cell's activity based on the fact that intracellular calcium levels rise in the soma and axon following an action potential.

The first calcium imaging dyes were derived from the luminescent jellyfish protein, aequorin. Many of today's dyes, however, are based on work done by Roger Tsien's group at U.C. Berkeley in the 1980s. In 1985, Tsien synthesized the ratiometric calcium imaging dye Fura-2 [94]. Its derivative, Fura-2AM, is used in this project.

Fura-2AM is a high affinity, ratiometric dye that includes an acetoxymethyl (AM) ester. Fura-2 readily binds to free calcium, but does not easily pass through the cell membrane. The addition of an AM group makes the dye more lipophilic, allowing it to more readily enter cells. Once inside a cell, esterases hydrolyze the AM ester, allowing the dye to freely bind to calcium [95]. When Fura-2 family dyes bind calcium, their absorption wavelength shifts from 380 nm to 340 nm. The ratio of 340/380 emissions can then be used to extrapolate intracellular calcium levels or to infer cell activity. Although the fluorophore's decay time makes it impossible to visualize individual action potentials, calcium imaging is exceedingly useful in studying signal propagation throughout a network. Additionally, unlike other calcium sensitive dyes, Fura-2

family dyes emit at 510 nm regardless of the surrounding calcium levels. This feature prevents variables like cell thickness or dye concentration from confounding results. Furthermore, using a ratiometric method as opposed to a single-wavelength dye limits the effects of photobleaching and dye leakage.

1.5 SUMMARY

In summary, epilepsy is a common neurological disease that is rarely studied in neurons *in vitro*. Available cell culture techniques and molecular biology methods allow for dissociated neuronal cultures to be transfected with exogenous DNA. The availability of epilepsy-related plasmids makes the creation of an *in vitro* neuronal epilepsy model quite feasible. Furthermore, pairing *in vitro* cell culture with microtechnology, specifically microcontact printing, may help reduce the variability often seen in dissociated cell cultures. Additionally, *in vitro* cultures would allow for examination of whole network activity, which plays an important role in seizure propagation. Calcium imaging is often used to examine network activity in *in vitro* cultures and could easily be used to study epileptogenesis.

Therefore, we propose to create and evaluate a potential *in vitro* epilepsy model that is inexpensive, can be used for high-throughput testing of multiple AEDs, can study either chronic or acute seizures, and could have future potential in personalized medicine. Such research would fill a significant gap in the epilepsy field. Additionally, we propose to evaluate the use of constrained geometry in reducing *in vitro* variability in an effort to clearly examine how genetic modifications impact network functionality.

Specifically, we will focus on the gene SCN1a which is associated with Generalized Epilepsy with Febrile Seizures Plus, Type II (GEFS⁺). SCN1a and the voltage-gated sodium channel it codes for, Na_v1.1, has been extensively studied *in vivo* and in non-neuronal *in vitro* cultures. To complete this project, we will address the following specific aims:

1.) **Create wild type and mutant SCN1a neuronal cultures.** This Aim is focused on demonstrating small neuronal networks containing wild type and mutant Na_v1.1 ion channels can be created *in vitro*. Specifically, we propose to generate SCN1a plasmids and use them to culture genetically modified neuronal networks via nucleofection.

2. **Characterize the phenotype of small neuronal networks containing wild type or mutant SCN1a genes.** The working hypothesis for this aim is that mutations in SCN1a affect the electrophysiological properties of individual neurons, but may also affect network composition. The goal of this aim is to characterize network composition including Na_v1.1 expression. Specifically, we propose to assess if transfection with SCN1a plasmids alters overall Na_v1.1 expression levels as well as Na_v1.1 expression levels and patterns in excitatory, inhibitory, and glial cells.

3. **Perform functional analysis of defined networks.** The working hypothesis for this aim is that changes in activity due to SCN1a mutations impact network functionality. Specifically, the modification of SCN1a subunits should modify the activity properties of constrained networks. We propose to assess the impact of genetic modification on network functionality through time-lapse calcium imaging of constrained networks.

This research is innovative because standard biological approaches for studying genetics are rarely combined with microcontact printing to examine neurological disease and because a neuron-based *in vitro* model of epilepsy would fill an obvious need in current epilepsy research.

2.0 CREATION OF WILD TYPE AND MUTANT SCN1A NEURONAL CULTURES

2.1 INTRODUCTION

This chapter is focused on methods needed to create small *in vitro* neuronal networks expressing wild type and mutant Na_v1.1 ion channels. The foundation for this chapter is that the common neurological disease, epilepsy, has a well-documented genetic component. However, epilepsy-related genetic mutations are not often studied *in vitro* in neurons, but instead are examined in non-neuronal cells expressing one or more neuronal proteins. Non-neuronal studies are helpful in identifying how a protein of interest may work, but they fail to consider other missing neuronal proteins and connections. Therefore, a clear next step to *in vitro* epilepsy research is to transition from non-neuronal networks to neuronal networks.

2.1.1 Generalized Epilepsy with Febrile Seizures Plus, Type II & SCN1a

While there are over 40 types of epilepsy, this project focuses on Generalized Epilepsy with Febrile Seizures Plus, Type II (GEFS⁺). GEFS⁺ is a spectrum disorder ranging from mild, sporadic seizures with normal mental development to catastrophic Severe Myoclonic Epilepsy of Infancy (SMEI), which often presents with ataxia and mental handicap, forcing patients to require lifelong care (Figure 6) [96] [97].

GEFS⁺ can be caused by a variety of genetic mutations, but all of them involve the gene SCN1a [98]. SCN1a is a gene located at 2q22-24 that encodes the protein Na_v1.1- a voltage-gated sodium channel α subunit found throughout the central nervous system (Figure 7) [99]. GEFS⁺-related SCN1a mutations appear to be either missense or loss-of-function mutations that result in a decrease in network inhibition [100]. We focus on mutations in SCN1a because it is arguably the most well studied epilepsy-related gene known.

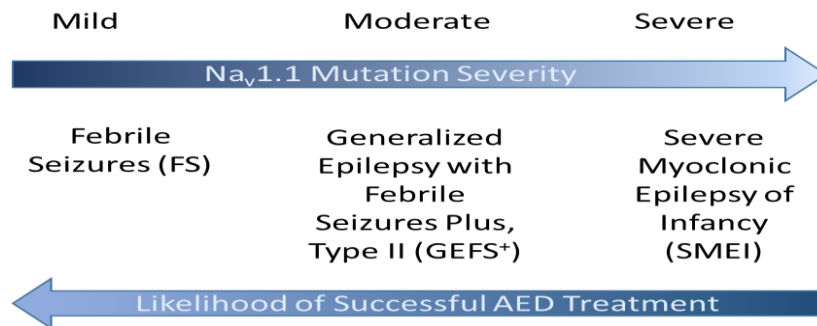


Figure 6: GEFS⁺ Spectrum

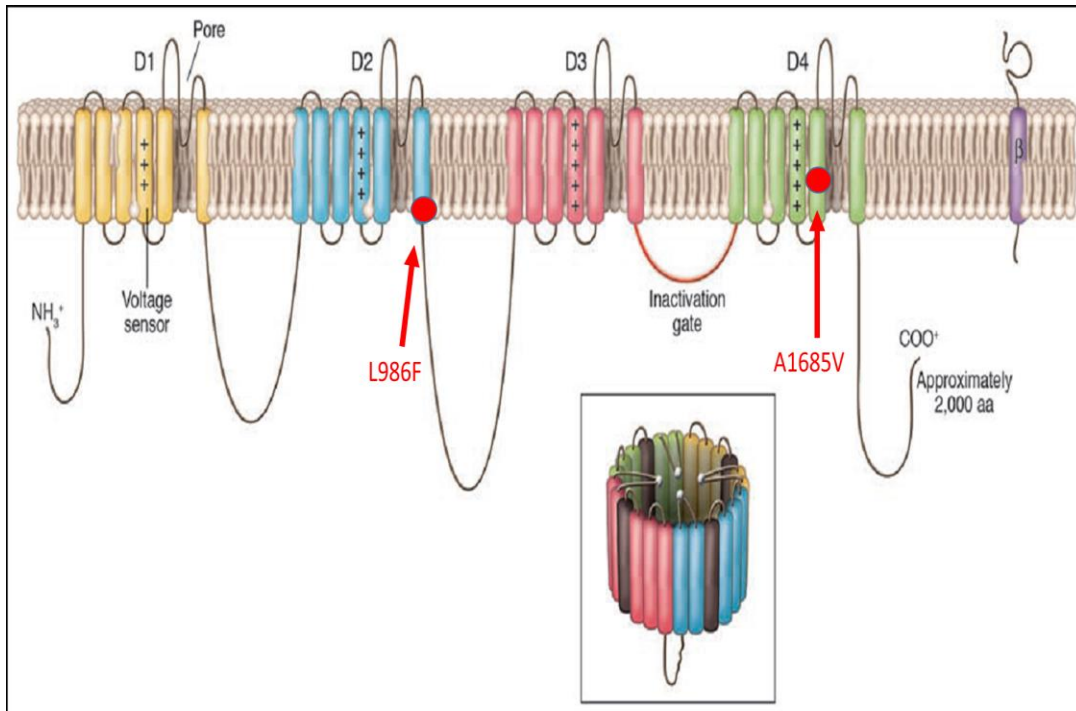


Figure 7: Nav1.1 Protein Diagram

Above: Nav1.1- a monomer composed of four homogenous domains (DI-DIV), each containing six transmembrane segments. The DI domain contains several positively charged amino acids which act as a voltage sensor. The four domains associate to form a voltage-gated, sodium permeable pore (inset) [101]. Locations of mutations used in this project shown in red.

Along with isoforms Nav1.2 and Nav1.6, Nav1.1 is responsible for initiating and propagating action potentials throughout the central nervous system of mammals [102]. All voltage gated sodium channels alternate between open, closed, and inactive conformations. Channels are closed at resting potential and open to allow an influx of sodium ions in response to local depolarization. This causes an increase in intracellular ion concentration and membrane potential. As membrane potential increases, the channel quickly inactivates as the inactivation gate binds together.

Since transmembrane α -subunits normally create sodium currents in response to depolarization, defects in the genes that encode them can result in altered sodium current. We examine two loss of function mutations: A1685V and L986F, which appear to reduce or eliminate sodium channel currents in inhibitory cells, resulting in a lack of network inhibition which ultimately makes networks more likely to exhibit seizure activity. Most SCN1a loss-of-function mutations lead to Severe Myoclonic Epilepsy of Infancy (SMEI) in humans, as seen with the L986F missense mutation [103]. The A1685V mutation, however, has been linked to both SMEI and the less extreme GEFS⁺ (sometimes interchangeably referred to as PEFS⁺ in literature) [23, 103, 104].

2.1.2 SCN1a/Nav1.1 Studies

The consequences of an SCN1a loss-of-function (LOF) has been studied in genetically modified mice [105] [106] [107]. LOF mice present with little if any sodium currents or action potentials in hippocampal GABAergic inhibitory neurons, and reduced sodium currents and low firing rates in cerebellar GABAergic Purkinje cells (Figure 8). This indicates that inhibitory neurons are highly reliant on Nav1.1 for proper function. Interestingly, excitatory pyramidal cells' sodium

currents are not affected indicating that excitatory cells either do not express Nav1.1 or that they express other voltage gated sodium channels that can compensate for Nav1.1's loss. Additionally, Yu noted a small up-regulation of Nav1.3 in a subset of hippocampal interneurons. As Nav1.3 expression generally wanes as Nav1.1 expression increases, increased Nav1.3 expression indicated that Nav1.1 was not being expressed and that inhibitory neurons were compensating by expressing Nav1.3. Ogiwara *et al* later confirmed high levels of Nav1.1 in inhibitory neurons via immunocytochemistry.

Nav1.1 mutations have also been studied *in vitro*, but rarely in neuronal cultures [102]. Various Nav1.1 modifications have been examined using HEK 293 cells, xenopus oocytes, and TSA201 cells, all transfected to express Nav1.1 [76, 103, 108, 109]. However, these models examine Nav1.1 in an isolated setting without the presence of other sodium channels or other proteins expressed in the brain, and are therefore, limited as mechanistic models for new drugs.

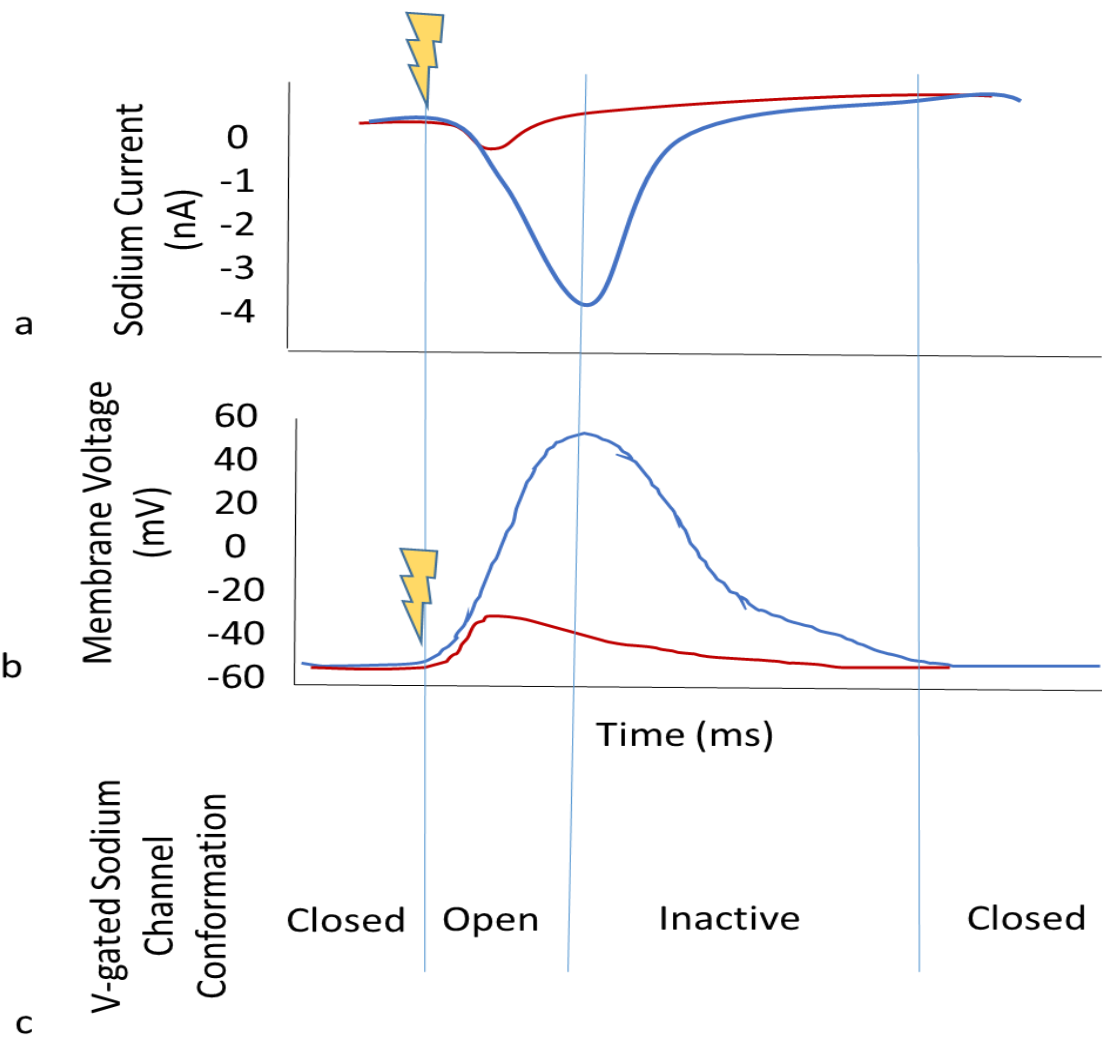


Figure 8: Sodium Current, Membrane Potential, & Sodium Channel Conformation

Above: a) Sodium current vs. time for normal (blue) and loss-of-function (red) channels. b) Membrane potential vs. time for normal (blue) and loss-of-function (red) channels. c) Voltage gated sodium channel conformation. vs. time. Stimulation shown by lightning bolts. [110] [111].

2.2 MATERIALS & METHODS

2.2.1 LB Agar Plates

In order to introduce the desired DNA into mammalian cells, we used bacteria to propagate the plasmid. In brief, agar plates for bacterial growth were made. Kanamycin was added to plates used to grow SCN1a WT, A1685V, or L986F cultures while ampicillin was added to plates used to grow pLL3.74-dsRed. 4% (w/v) LB agar was added to DDW and mixed for 10 minutes before being autoclaved. The sterile solution was then placed in a 55°C water bath for 15 min until the flask was cool enough to touch. After adding any desired antibiotics (1 µL 50 mg/mL ampicillin per mL agar solution or 2 µL of 25 mg/mL kanamycin per mL agar solution), the plates were poured and cooled for 20 minutes before being stored upside down at 4°C.

2.2.2 Culturing Plasmids

Once agar plates were available, bacterial cultures were developed. To do so, LB agar plates containing the desired antibiotic were warmed, upside down, for two hours prior to streaking. A loopful of slightly thawed transfected bacteria was removed using a sterilized inoculating loop and gently streaked over an agar plate. The plate was allowed to sit for 15 minutes until excess liquid was absorbed. Plates were then stored, inverted, at 30°C for SCN1a plasmids or 37°C for pLL3.74-dsRed. After 24-48 hours, the plates were removed from the incubator, wrapped with parafilm, and stored at 4°C or used to create broth cultures for mini- and midi-preparations.

To prepare mini-prep broths, 3 mL of LB containing the same concentration of antibiotics as the LB agar plates, were transferred to a vial. One small, isolated colony from an agar plate

was picked and dropped into the culture vial. The vial was then loosely sealed and shook at 175 rpm (at 30°C for SCN1a plasmids or 37°C for pLL3.74-dsRed) overnight until cloudy.

LB cultures with appropriate antibiotics were then used directly for mini-preps or to develop Terrific broth (TB) cultures for midi-preps.

Original SCN1a plasmid stocks were a kind gift from Dr. Al George, Jr. Original pLL3.74-dsRed stocks were a kind give of the Dr. Luk Van Parijs lab.

2.2.3 Plasmid Preparations

A number of plasmids were central to this project including two mutant SCN1a plasmids (A158V and L986F), a wild type SCN1a plasmid, and several fluorescent markers (Table 2, Figure 9).

A midi-prep was used to isolate moderate yields of plasmid DNA. Because the cells were EndA⁺, a guanidine hydrochloride wash was included. LB cultures were expanded in Terrific broth (TB) to improve plasmid yield. Briefly, 1 µL of antibiotic per mL and 750 µL of cells from an LB starter colony was added to Terrific broth. After shaking at 240 rpm, 30°C, overnight, cells were harvested by centrifuging for 10 minutes at 21°C, 4200 rpm then resuspended and processed following the Wizard midiprep protocol (Promega, Madison, WI). The final DNA concentration was assayed using the NanoDrop 1000 (Thermo Scientific, Waltham, MA) and aliquots were stored at -20°C.

Table 2: Plasmid List

Plasmid	Size (bp)
SCN1a WT	10451
SCN1a A1685V	10451
SCN1a L986F	10451
pLL3.74-dsRed	7650
Pmax-GFP	3486
m-Cherry	4381

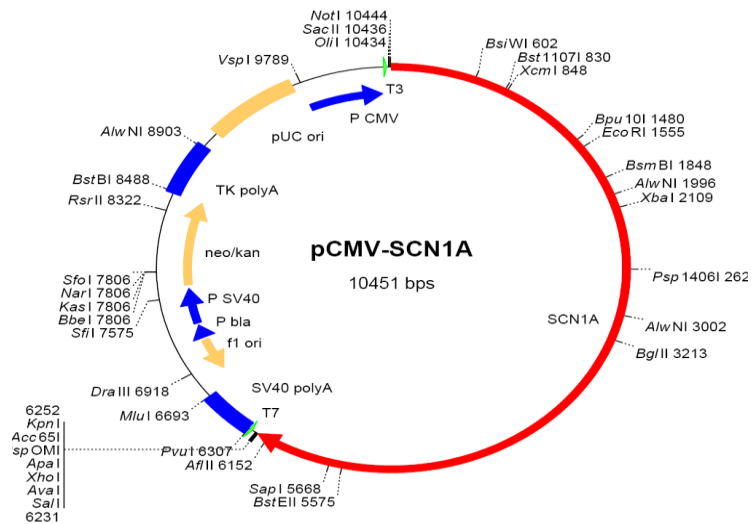


Figure 9. Plasmid map of SCN1a

2.2.4 Assaying DNA Concentration

Once DNA was prepared, the concentration was assayed using 1 μ L of sample and the NanoDrop 1000 (sterile DDW was used for a blank for all samples). DNA concentrations were also assayed after endotoxin-free ethanol precipitation. Samples with an A_{260}/A_{280} value below 1.8 were discarded as they were not pure enough for nucleofection.

2.2.5 Endotoxin Removal & Ethanol Precipitation

Prior to nucleofection, DNA was cleaned to remove endotoxins which are common in plasmid DNA preparations. The following protocol (repeated once per sample) and UltraClean Endotoxin Removal Kit were used (MO Biolabs, Carlsbad, CA). 1/10 volume of Endotoxin Removal Reagent was added to the DNA sample, vortexed until the solution was homogenous, incubated on ice for 5 minutes, and heated at 65°C for 10 minutes. The solution was then centrifuged for 5 minutes at 4°C and the clear aqueous phase was transferred to a new tube using endotoxin-free pipette tips. The final DNA solution was then centrifuged for 5 minutes at 4°C.

Following endotoxin removal, DNA samples were concentrated using an endotoxin-free ethanol precipitation, as ethanol removes hydration shells around DNA molecules, allowing more concentrated DNA solutions to form. 1/10 volume of endotoxin-free 5M sodium chloride was added to the DNA and mixed followed by two volumes of endotoxin-free EtOH. The DNA was then incubated on ice for 30 minutes and centrifuged for 15 minutes at 4°C. After discarding the supernatant, the DNA pellet was washed with 1 mL of 70% endotoxin-free EtOH, inverted to mix, and centrifuged again for 5 minutes at 4°C. The supernatant was discarded and the pellet was allowed to dry in a laminar flow hood for 15-30 minutes before being resuspended in

endotoxin-free water. The new DNA concentration was assayed using a NanoDrop 1000 and DNA aliquots were stored at -20°C until needed.

2.2.6 Restriction Digest

Prior to gel electrophoresis, plasmids were linearized using restriction digest. SCN1aWT, A1685V, and L986F samples were digested using HindIII with NEB2 and BSA (New England BioLabs, Ipswich, MA). PLL3.74-dsRed samples were digested using SalI with NEB2 buffer and BSA (New England Biolabs, Ipswich, MA). All components were vortexed before 1-2 µg of DNA, 100x BSA, and NEB buffer were added to a microtube. DDW was added to a final volume of 20 µL followed by 0.2 µL enzyme. The solution was flicked to mix, then spun to collect, and incubated overnight at 37°C.

2.2.7 Gel Electrophoresis

DNA size was analyzed using a 1.2% polyacrylamide gel and an electrical field. 1x TAE and agarose were added to a flask and heated until clear. The solution was then cooled to 57°C before 1.5 µL EtBr was added to the gel. The agarose solution was quickly poured into a tray with combs and allowed to solidify for 20 minutes. After removing the combs, and orientating the wells, 1x TAE buffer was added until the gel was submerged and all wells were covered. 10 µL of sample containing 2 µL of 5x loading buffer was added per well then 1.5 µL of EtBr was added to the loading buffer opposite the loading wells. A 1 kb GeneRuler DNA ladder (Thermo Scientific, Pittsburgh, PA) was run in each gel to assess DNA size. The gel was run for 45

minutes at 115 V before being visualized under UV light using GelDoc software (Bio Rad, Hercules, CA).

2.2.8 DNA Sequencing

Plasmid DNA was sequenced at the University of Pittsburgh Genomics and Proteomics Core Laboratories using Sanger sequencing and T3 primer. Following sequencing, a BLAST search was performed on the resultant sequence to verify the plasmid encoding SCN1a.

2.2.9 Neuronal Harvest, Plating, and Culture

All experiments were performed using E18-E19 rat hippocampal neurons isolated from freshly harvested tissue. However, some supplemental cultures were obtained from Brain Bits (Brain Bits, LLC, Springfield, IL) or from harvested hippocampal tissue stored in Hibernate-E media supplemented with 2% B27 and 0.5 mM glutamax (Life Technologies, Grand Island, NY) for 1-2 days.

E18-E19 rat pups were sacrificed in accordance with University of Pittsburgh IACUC guidelines. The hippocampal tissue was dissected and dissociated in HEPES-buffered, $\text{Ca}^{2+}/\text{Mg}^{2+}$ -free Hank's BSS before being plated onto coverslips. To do so, a timed pregnant female was euthanized via carbon dioxide asphyxiation and cervical dislocation. All embryos were collected and decapitated. After removing the scalp and skull, the brain was isolated using forceps. The cortex was then isolated from the midbrain and olfactory bulbs, the dura was removed, and the cortical lobes were separated. The cortex was then trimmed leaving behind the hippocampus and a small portion of the surrounding cortex. The tissue was rinsed with HBSS and digested using

trypsin-EDTA. After incubating for 15 minutes and being rinsed with HBSS, the tissue was dissociated using a combination of DNase and firepolished Pasteur pipettes (one smoothed pipette, one reduced to half the original diameter, and one reduced to one third the original diameter). The cells were then spun down (10 min, 4°C, 1800 rpm), counted using Trypan blue and a cell cytometer, and diluted to the desired density. In this case, a final density of 1×10^5 cells/mL was desired. However, cells were plated at 1.67×10^5 cells/mL to account for nucleofection related cell death, which is documented at around 40% [70]. Plating media was composed of 96% Neurobasal, 2% B27 (50x), 1% pen-strep, 0.25% 200 mM glutamate, and 0.125% 10 mM glutamate in 10 mM HCl.

2.2.10 Nucleofection

Nucleofection was used to introduce plasmid DNA into neuronal cultures. For this project, the Rat Neuron Nucleofector Kit (Lonza, Walkersville, MD) was used immediately after cells were dissociated. Briefly, cells were counted and $1-6 \times 10^6$ cells were aliquoted for transfection (typically 4×10^6 cells were used). Aliquots were spun at 10g for 5 minutes at room temperature. The supernatant was then discarded and cell pellets were resuspended in 100 μ L of nucleofection solution. 1-3 μ g of DNA was added to the cell solution and briefly flicked to mix. A fluorescent marker (pLL3.74-dsRed, GAP43-RFP, Pmax-GFP, or m-cherry) was added to each SCN1a sample as a transfection marker. The cell solution was then transferred to a certified nucleofection cuvette and exposed to program O-03 on the Amaxa Nucleofection Device (Lonza, Walkersville, MD). 500 μ L of warmed RPMI media (Life Technologies, Grand Island, NY) was added to the cuvette and cells were immediately transferred to a 1.5 mL microtube and placed in a 37°C, 5% CO₂ incubator for 5 minutes to allow cells to recover. The desired quantity of cells

was then added to a microtube containing nucleofection media (DMEM + 10% fetal bovine serum + 10 µg/mL pen-strep) before being transferred to a dish containing stamped coverslips and plating media. After 2-4 hours in an incubator, 25% of the media was exchanged with a reduced serum media (DMEM + 5% fetal bovine serum + 10 µg/ml pen-strep). After 24 hours, 75% of the media was exchanged with plating media (outlined in 2.2.9) to remove nucleospheres and preserve patterning. To limit glial proliferation, one quarter of media was exchanged with AraC positive feeding media at DIV 4 and, as needed, after DIV 11 (96% Neurobasal, 2% B27 (50x), 1% pen-strep, and 0.25% 200 mM glutamine, 5 µM final concentration AraC).

2.2.11 Transfection Efficiency and Co-Transfection Efficiency Calculations

In order to assess the uniformity of transfection for two plasmids at once, cells were transfected simultaneously with equal DNA masses of m-Cherry and Pmax-GFP. On DIV 7, cells were fixed in 4% PFA for 10 minutes, rinsed in PBS three times (5 minutes each), and mounted with Vectasheild with DAPI (Vector Labs, Burlingame, CA). Transfection efficiency for each individual plasmid was then assessed along with co-transfection efficiency using a Leica DMI 4000B fluorescent microscope (Leica Microsystems, Buffalo Grove, IL).

Additionally, the transfection efficiency of pLL3.74-dsRed was assessed for all cultures on DIV 4, 8, and 12. Results were reported as the mean \pm standard error of the mean. Statistical differences between days was assessed per genotype using a 1-way ANOVA and post-hoc Scheffe test [112].

2.3 RESULTS

This chapter focused on the generation of SCN1a plasmids, the transfection of rat hippocampal neurons, and the culturing of small networks of control and transfected cells. The results of these experiments are outlined below.

To assess the success of plasmid generation, gel electrophoresis and DNA sequencing was used. Restriction digest of pLL3.74-dsRed plasmid resulted in 3 bands between 2000 and 2500 bp (Fig. 10). Anticipated results were 3 bands at 2137, 2514, and 2955 bp for pLL3.74-dsRed, indicating successful generation of pLL3.74-dsRed. Restriction digest of SCN1a plasmids resulted in 1 band between 5000-6000 bp, 1 band around 3500 bp, and 1 band near 2000 bp (Figure 10). Anticipated results were 3 bands at 1089, 3533, and 5810 bp for SCN1a, indicating successful generation of SCN1a WT, A1685V, and L986F plasmids. Additionally, following sequencing, a BLAST search resulted in a 98-99% identity and 0% gap with BC172767.1 for SCN1aWT, A1685V, and L986F plasmids. BC172767.1 is a synthetic construct of *homo sapien* SCN1a. Gel electrophoresis and BLAST search results combined indicate that the plasmids were indeed SCN1a variants.

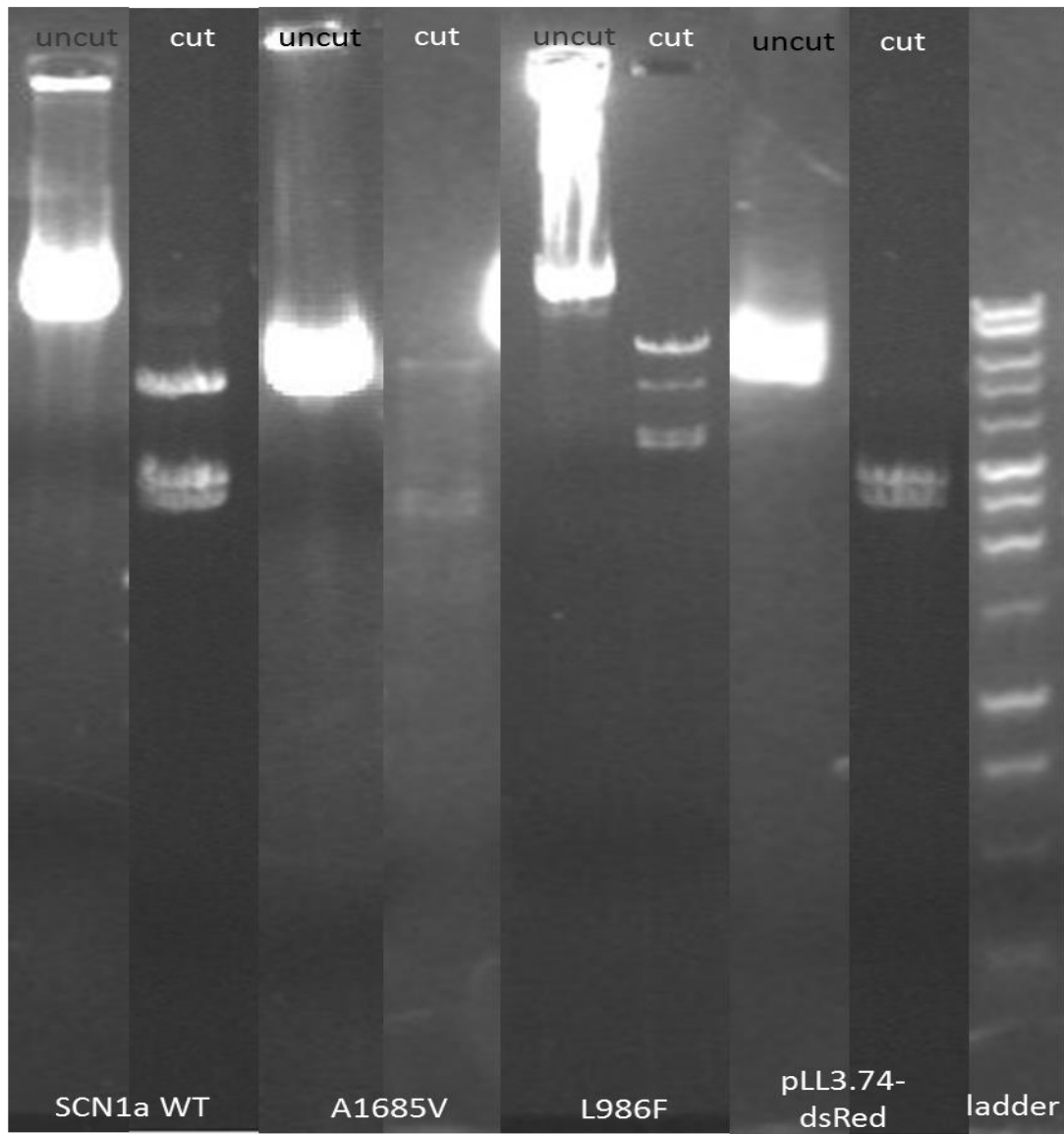


Figure 10: Gel Electrophoresis of Digested and Undigested Plasmids

Above: agarose gel displaying undigested (uncut) and digested (cut) plasmids.

To confirm that multiple plasmids could be co-transfected with close to 100% co-expression, Pmax-GFP and m-cherry were co-transfected into neurons (Figure 11). Co-transfection efficiency was determined to be $89\% \pm 3$, coinciding with co-transfection efficiencies seen by other researchers [113]. Additionally, $94\% \pm 3$ of GFP⁺ cells expressed m-cherry and $94\% \pm 5$ of m-cherry⁺ cells expressed GFP. This confirms the long-accepted theory that the presence of one co-transfected plasmid is also indicative of the other's presence.

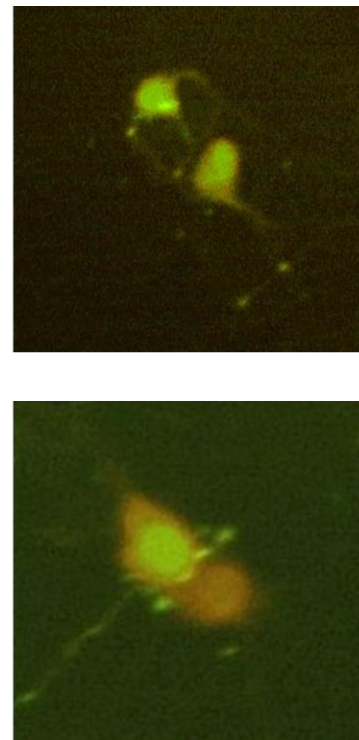
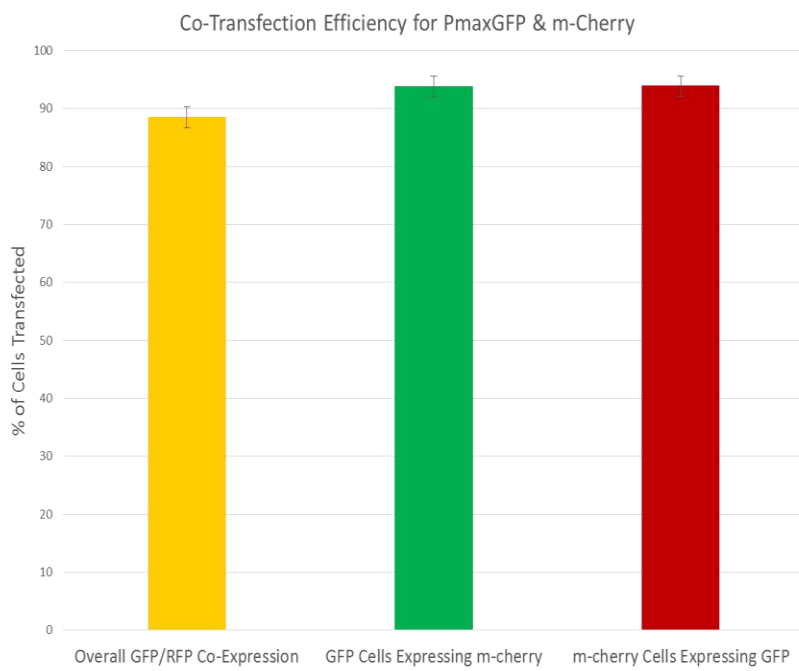


Figure 11: Co-Transfection Efficiency

Above: Left: DIV 7 co-transfection efficiency for neurons transfected with Pmax-GFP and m-cherry. Yellow: total GFP/m-cherry co-expression, Green: % of Pmax-GFP⁺ neurons also expressing m-cherry, Red: m-cherry⁺ cells also expressing Pmax-GFP. Error bars indicate standard error of the mean. Right: examples of Pmax-GFP/m-cherry co-expression (green: Pmax-GFP, red: m-cherry).

Cultures were maintained for approximately two weeks and transfection efficiency was examined at DIV 4 (Figure 12a), 8 (Figure 12b), and 12 (Figure 12c). Significance was evaluated using a 1-way ANOVA and post-hoc Scheffe test. Transfection efficiency was compared across days for individual genotypes and across genotypes on a given day (Figure 12). In general, we observed slightly lower transfection efficiencies for SCN1a-pLL-3.74-dsRed vs. Pmax-mCherry, possibly due to the larger plasmid size. Average transfection efficiencies were $76\% \pm 2$ overall on DIV 4, $75\% \pm 2$ on DIV 8, and $62\% \pm 2$ overall on DIV 12. These transfection values are in line with those expected by Amaxa [70], although other researchers have reported a wide range of transfection efficiencies from <10% to more than 90% [114-117]. This variability is likely due to differences in culturing and transfection techniques. There was no significant difference in transfection efficiencies across genotypes and transfection efficiencies were fairly stable over time. pLL3.74-dsRed and L986F cells displayed transfection efficiencies that did not significantly change over time. However, SCN1a WT cells displayed a significant drop in transfection efficiency from DIV 4 to 12 (p value: 0.035). Similarly, A1685V cultures displayed a significant loss of transfection efficiency from DIV 4 to 12 and DIV 8 to 12 (p values: 0.00 and 0.004 respectively). This may be due general cell death and/or because the transfection began to become unstable by DIV 12 as the nucleofection kit used for these studies only provides stable gene expression for 12-14 days [70].

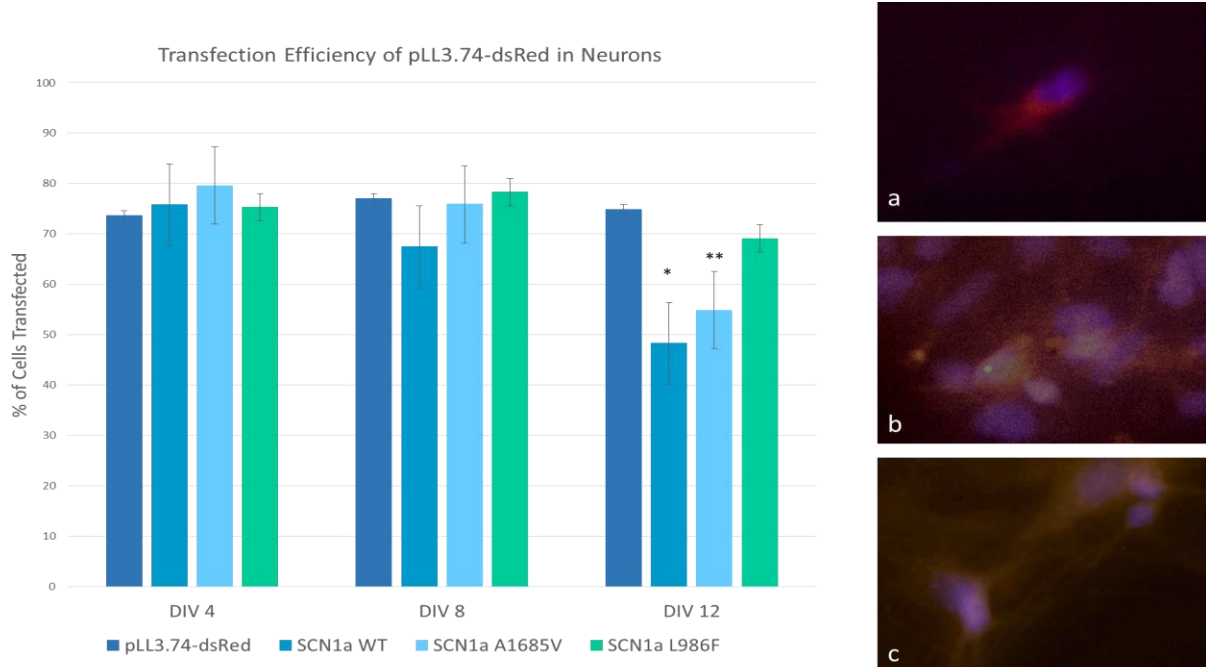


Figure 12: Transfection Efficiency in Neurons

Above: Left: Transfection efficiency for pLL3.74-dsRed in neuronal cultures across time $12 \pm$ standard error. Statistically significant differences across days, within the same genotype is represented by * and ** ($p < 0.05$ or $p < 0.01$ respectively), as determined by 1-way ANOVA and post-hoc Scheffe test. Right: representative images of pLL3.74-dsRed expression on DIV4 (a), DIV8 (b), and DIV12 (c) (blue: nuclei, red: pLL3.74-Red). DIV 4, 8, and 12 n: pLL3.74-dsRed (n=12, 11, 11), SCN1a WT (n=10, 10, 12), SCN1a A1685V (n=12, 12, 12), SCN1a L986F (n=11, 10, 12).

2.4 DISCUSSION

In general, we demonstrated the successful creation of SCN1a plasmids as well as the ability to transfect and culture neurons for at least two weeks. Additionally, we were able to achieve transfection efficiencies near 75% for all genotypes through DIV 8- greatly exceeding the 5-30% transfection efficiency generally obtained when transfecting neurons using other techniques like calcium phosphate precipitation or lipofection [118]. Furthermore, our nucleofection method displayed co-localization of nearly 95% for co-transfected plasmids, confirming that the presence of one co-transfected plasmid is indicative of the other in this preparation.

Overall, plasmid generation was fairly straightforward. The A1685V (mild) mutant proved much easier to generate than the more severe L986F mutant which took several attempts. Additionally, observational data also indicated differences between genotypes as some issues arose regarding transfected cell viability early on. Early transfected cultures were maintained using only serum-free Neurobasal in an effort to minimize glial expression. Un-transfected (negative control) cells tolerated this protocol well, being easily maintained for up to three weeks. Cells transfected only with fluorescent markers like Pmax-GFP or dsRed-PLL3.74 and those expressing SCN1a WT or A1685V showed reduced viability (10-12 day culture length) in a serum-free environment, most likely a residual effect of the harsh transfection conditions. L986F transfected cultures, however, presented with the lowest cell viability initially with cultures rarely surviving past one week. The decreased viability with reduced serum may indicate that nucleofected cells, especially those expressing severe mutations, may rely more heavily on glial support. When the other extreme of all serum media was used, checking glial proliferation became difficult and transfected cultures were often overtaken by glia. This may be because the transfection method resulted in increased cell death early on thus increasing the

initial glial population, because the transfected cells were more sensitive to AraC and thus more likely to die after exposure at DIV 4-7 or, because the mutations, which may impact network functionality or composition, made the cultures more delicate and less viable. However, once a combination of serum⁺ media for the first 48 hours followed by serum-free media for the remainder of culture life was implemented, L986F cultures were easily maintained for 2-3 weeks. This culture method was well-tolerated for remaining genotypes as well.

Lastly, nucleofection provided a repeatable way to co-express plasmids across genotypes, although the method's stability beginning at DIV 12 does currently limit the length of experiments. While this preparation may be best for examining the early stages of disease, modifications like the use of viral vectors could allow for an extension of experiment length.

2.5 CONCLUSIONS

In summary, this chapter served as an important building block for the rest of the project as it allowed us to develop genetically modified neuronal networks that could be evaluated for use in epilepsy research. One downside, however, is that because the cultures are already expressing native SCN1a/Na_v1.1 (and will continue to do so to some extent depending on transfection efficiency), assessing levels of native to mutant SCN1a/Na_v1.1 is problematic. Therefore, we relied on phenotypical and functional activity to assess the transfections impact.

3.0 PHENOTYPIC CHARACTERIZATION OF SMALL NEURONAL NETWORKS CONTAINING WILD TYPE OR MUTANT SCN1A GENES

3.1 INTRODUCTION

Changes in genetic makeup often modify protein expression or function. In loss-of-function situations, affected proteins may be expressed but have altered function or the affected protein may be expressed at lower levels, both leading to changes in network composition. Neural plasticity allows the brain to adapt to network changes over time, so it is possible that a dynamic system like the brain could attempt to compensate for smaller scale changes in network activity, as a result of modified protein function. To that end, this chapter focuses on examining whether $\text{Na}_v1.1$ expression levels are modified in SCN1a mutant cultures and whether $\text{Na}_v1.1$ expression patterns vary, suggesting a compensatory mechanism may be reshaping the network. The working hypothesis for this study is that mutations in SCN1a affect the functional properties of individual neurons and, therefore, may affect the composition of the network comprised of those neurons. Additionally, forced expression of SCN1a may alter expression patterns of $\text{Na}_v1.1$, so neuronal phenotypes should be evaluated. To test this hypothesis, we evaluate patterns of connectivity through $\text{Na}_v1.1$ co-localization with parvalbumin (largely expressed in inhibitory interneurons), vesicular glutamate transporter 1 (an excitatory cell marker), and the microtubule associated proteins MAP2 and Tau1 (dendritic and axonal markers, respectively).

3.1.1 Na_v1.1 Expression

Wild type Na_v1.1 is a 260 kDa transmembrane protein expressed mainly in neuronal cell bodies and proximal processes in human brains [119]. In the human hippocampus, Na_v1.1 appears to be present in the dentate hilus, stratum granulosum, and subicular complex of the hippocampus and is “readily detected” in CA2 and CA3 pyramidal neurons [119]. In rodents, Na_v1.1 has long been thought to be expressed in the soma and dendrites of excitatory and inhibitory neurons [120]. Prior work in our lab using the SCN1a plasmids from this project indicated that Na_v1.1 was largely expressed in the soma of visual cortex neurons [121]. More recent studies have provided conflicting results regarding Na_v1.1 expression. Gong *et al* determined that Na_v1.1 expression was prominent in the rat hippocampus, with most expression occurring in somas but some expression occurring in pyramidal cell dendrites [122]. However, Duflocq *et al* indicated that Na_v1.1 is predominantly expressed in the AIS and Nodes of Ranvier in various regions of the mouse hippocampus [123]. They observed that most Na_v1.1⁺ cells appeared to be interneurons except in CA3 where it is expressed by a few pyramidal cells. Similarly, Ogiwara *et al* examined Na_v1.1 expression in mouse cortex and hippocampus and indicated that Na_v1.1 is predominantly expressed in the axon initial segment of parvalbumin positive (PV⁺) interneurons in the cortex as well as the soma and axons of PV⁺ interneurons in the hippocampus, with extremely low levels of expression in excitatory cells [124] [107]. Other studies indicate that approximately 4% of rat pyramidal cell layer neurons in CA3 also express Na_v1.1 in proximal portions of the AIS [125]. Additionally, cultured rat glia have demonstrated Na_v1.1 expression along with two other voltage-gated sodium channel isoforms, Na_v1.5 and Na_v1.6 [126]. Na_v1.1 over-expression in glia is thought to possibly play a role in spreading seizure activity throughout the cortex [127].

Parvalbumin (PV) is a calcium-binding protein involved in calcium signaling. In the hippocampus, PV is primarily expressed by GABAergic interneurons, specifically those targeting pyramidal cells [128]. Most PV⁺ interneurons are fast-spiking and responsible for providing network inhibition. Changes in parvalbumin expression have been linked to neurological disorders. Loss-of-function mutation in a PV⁺ cell's voltage-gated sodium channel would likely reduce network inhibition, and therefore increase overall excitability, and possibly cause seizure-like activity. Previous studies have shown that a 20% reduction in network inhibition can lead to overwhelming synchronized cortical activity, and even a small reduction in inhibition can generate bursting behavior [129].

Vesicular glutamate transporter 1 (Vglut1) is the main vesicular glutamate transporter in the human hippocampus [130]. Pyramidal neurons and granule cells in CA1, 2, and 3 show strong Vglut1 expression and although glia do not appear to express Vglut1 *in vivo*, co-localization has been observed *in vitro* [131, 132]. In rats, Vglut1 is largely expressed in the hippocampus, thalamus, cortex, and cerebellum [133].

In summary, this chapter focuses on evaluating how modifying the genotype of some cells in a network affect protein expression in the network as a whole. In part, we are interested in any compensatory methods that may be at work to counteract a reduction in overall inhibition, but we are also examining if forced expression of Na_v1.1 leads to modified protein localization within the cell. To date, studies indicate that Na_v1.1 is localized to the soma and dendrites of excitatory cells, the axon initial segment of parvalbumin expressing inhibitory cells, and the soma of glia. Additionally, Na_v1.1 is thought to have higher expression levels in inhibitory vs. excitatory cells.

3.2 MATERIALS & METHODS

3.2.1 Immunocytochemistry

Cellular phenotype was evaluated using immunocytochemistry and a variety of primary and secondary antibodies (Table 3 & Table 4). Fresh paraformaldehyde solution was prepared by combining 76% (v/v) warm DDW, 4% (w/v) paraformaldehyde, and enough 10N NaOH to clear the solution. Next, 10% (v/v) 10x PBS, 0.5% (v/v) 1 M MgCl₂, 2% (v/v) 0.5 M EDTA, and 4% (w/v) sucrose were added and the solution was mixed on an orbital until clear. NaOH and glacial HCl were added until a pH of 7.4 was achieved. Cells were fixed for 10 minutes at room temperature in pre-warmed PFA then washed in PBS three times, 5 minutes each. Next, cells were permeabilized in a 0.3% Triton-X100 solution for 10 minutes and washed three more times in PBS, 5 minutes each. Cells were then blocked in a 5% BSA and 5% GSA solution for one hour. After blocking, coverslips were transferred to parafilm containing 1^o antibodies diluted in 1% BSA and incubated for one hour at room temperature (see below). Following another PBS wash (3 times, 5 minutes each), coverslips were transferred to parafilm containing 2^o antibodies diluted in 1% BSA (see below). Samples were incubated in the dark for one hour at room temperature before being washed with PBS (3 times, 5 minutes each) and DDW (5 times) to remove excess salt. After excess water was removed, samples were placed on microscope slides containing Vectasheild with DAPI and allowed to air dry in the dark for 20 minutes before being sealed with nail polish, imaged, and stored in the dark at 4°C.

To ensure non-specific binding did not occur, the following controls were performed prior to experimentation:

- 1.) **Negative Primary Antibody:** Samples were fixed and stained as outlined, but the primary antibody was replaced with 5% GSA/5% BSA.
- 2.) **Double-staining Negative Secondary Antibody:** All double staining samples were exposed to one primary antibody and the other secondary that would be present.

Table 3: ICC Primary Antibodies List

1° Antibodies				
Host	Antibody	Dilution	Source	Catalog #
Rabbit	Anti-Nav1.1	1:125	Santa Cruz (Santa Cruz, CA)	SC 28754
Mouse	Anti-Parvalbumin	1:300	Millipore (Billerica, MA)	MAB 1572
Mouse	Anti-MAP2	1:300	Sigma (St. Louis, MO)	M 4403
Mouse	Anti-Tau1	1:300	Millipore (Billerica, MA)	MAB 3420
Guinea Pig	Anti-Vglut1	1:200	Millipore (Billerica, MA)	AB 5905

Table 4: ICC Secondary Antibodies List

2° Antibody				
Host	Antibody	Dilution	Source	Catalog #
Goat	Alexa 488 Anti-Rabbit	1:200	Invitrogen (Carlesbad, CA)	A 11008
Goat	Alexa 647 Anti-Mouse	1:200	Invitrogen (Carlesbad, CA)	A 21235
Goat	Alexa 647 Anti-Guinea Pig	1:200	Invitrogen (Carlesbad, CA)	A 21450

3.2.2 Epifluorescence Imaging

Immunocytochemistry samples were imaged using a Leica DMI 4000B upright microscope with Leica EL6000 and CTR4000 light sources, Leica DFC 350FX camera, and LAS software. Images were taken under 40x objective using the following filter cubes: A 11513872 (blue), L5 11513880 (green), N2.1 11513882 (red), and Y5 11513888 (far red). Prior to imaging experimental samples, imaging settings were determined using control samples. Once optimal settings were determined, they were recorded and maintained for all remaining samples from that trial. Additionally, in order to reduce bleed-through, sequential images were taken beginning with far red, then red, green, and blue.

3.2.3 Image Analysis & Statistics

Images collected with LAS software were imported and analyzed using ImageJ v.1.47 (NIH, Bethesda, MD). To assess co-localization, the JACoP ImageJ plug-in was used to calculate the Mander's co-localization co-efficient [112]. For overall Nav1.1, parvalbumin, and Vglut1 expression, co-localization was defined as the percentage of nuclei (blue) expressing each specific protein (far red). For Nav1.1 co-localization with MAP2, Tau1, PV, or Vglut1, co-localization was defined as the percentage of Nav1.1⁺ regions (green) expressing each specific protein (far red). In both cases, the entire field of view was used because it was comparable in cell count to ring-network studies being performed sequentially and we wanted to examine similar sized networks. Previous studies examining morphology and function of patterned vs. unpatterned networks indicate no significant differences [78]. Therefore, the expression patterns seen in unconstrained networks of similar size and cell density should translate to patterned networks. Statistical analysis was performed using a 1-way ANOVA and post-hoc Scheffe test in SPSS v. 22 (IBM, Armonk, NY).

3.3 RESULTS

This chapter focused on examining phenotypic changes introduced by genetic manipulation. *In vitro* cultures were successfully transfected with SCN1a plasmids and culture composition was examined by evaluating overall Nav1.1 (Figure 13, Figure 14, Figure 15), parvalbumin (Figure 16, Figure 17, Figure 18), and Vglut1 (Figure 19, Figure 20, Figure 21) expression. Additionally, Nav1.1 localization was evaluated for several criteria related to its potential function in the network. The first was cellular localization (where is Nav1.1 being expressed in the cell) followed by cell-type localization (which cells are expressing Nav1.1). To assess cellular localization, Nav1.1 co-localization with the somato-dendritic marker MAP2 (Figure 22 & Figure 24) and the axonal marker Tau1 (Figure 23 & Figure 24) was examined. To assess cell-type localization, Nav1.1 co-localization with PV (an inhibitory cell marker) and Vglut1 (an excitatory cell marker) was evaluated (Figure 25, Figure 26, Figure 27 & Figure 28, Figure 29, Figure 30 respectively).

All studies involved immunocytochemistry with multiple primary and secondary antibodies. Because auto-fluorescence and non-specific staining are common issues in double-labeling situations, we took precautions to address these potential pitfalls prior to experimentation. Negative primary tests were performed where both secondary antibodies were present but the primary antibodies were replaced with blocking solution. These samples did not auto-fluoresce and did not show non-specific binding for any secondary antibody combination tried. Primary antibodies were also paired with the opposite secondary antibody to ensure there was no non-specific binding between the two. Again, no non-specific binding was observed. Additionally, every experimental trial was accompanied with single primary antibody controls. For these samples, only one of the two primary antibodies being examined was present along

with both secondary antibodies allowing us to evaluate any non-specific or background fluorescence for solutions used in that staining trial. These samples were also used to determine imaging settings for that set of experimental trials.

Nav1.1 expression was evaluated for individual genotypes over time (Figure 14) as well as across genotypes on a given day (Figure 15). Significance was evaluated using a 1-way ANOVA and post-hoc Scheffe test. In all instances, Nav1.1 was expressed by both neurons and glia, largely in the soma but with some localization to the axon initial segment in neurons (Figure 13). Nav1.1 expression varied somewhat over time for individual genotypes. pLL3.74-dsRed cells showed a significant increase in endogenous Nav1.1 expression from DIV 4-12 ($45\% \pm 4$ to $65\% \pm 5$, $p = 0.026$; Figure 14b). Negative control cells displayed a similar trend (Figure 14 a) as did A1685V cells (Figure 14c). However, A1685V had significantly higher Nav1.1 expression from DIV 4 to 8 ($35\% \pm 4$ to $59\% \pm 3$, $p = 0.001$) and 8 to 12 ($35\% \pm 4$ to $59\% \pm 4$, $p = 0.002$) while the changes in negative control cells were more subtle. SCN1a WT cells, on the other hand, displayed a significant decrease in Nav1.1 expression from DIV 8 to 12 ($58\% \pm 3$ to $39\% \pm 4$, $p = 0.012$; Figure 14c), possibly indicating some compensation for forced Nav1.1 overexpression. L986F cells displayed a similar trend over time (Figure 14e). This drop in Nav1.1 expression could be due to gradual cell death as the culture nears DIV 14 or a result of the transfection losing stability.

Nav1.1 expression was also fairly consistent across genotypes on DIV 4, 8, and 12 (Figure 15). On DIV 4, negative control cells displayed a significant increase in Nav1.1 expression compared to A1685V ($54\% \pm 5$ to $36\% \pm 4$, $p = 0.044$; Figure 15a). However, by DIV 8, an average of 57% of all cells expressed Nav1.1 regardless of genotype (Figure 15b). This could indicate that a subset of A1685V are compensating for the LOF mutation by up-

regulating $\text{Na}_v1.1$ expression, but that the process takes time. By DIV 12, however, $\text{Na}_v1.1$ expression appeared sporadic (Figure 15c). Both SCN1a WT and L986F cells' $\text{Na}_v1.1$ levels were significantly lower than pLL3.74-dsRed ($39\% \pm 4.06$ and $39\% \pm 4$ vs. $65\% \pm 5$; p values of 0.002, 0.003, respectively) and negative control cells ($39\% \pm 4$ and $39\% \pm 4$ vs. $67\% \pm 4$; p = 0.011, and p = 0.014 respectively). This may be due to cell death as the cultures neared the two week mark, changes in cell proliferation, transfection transience as nucleofection is only stable for 12-14 days, or a combination of the three.

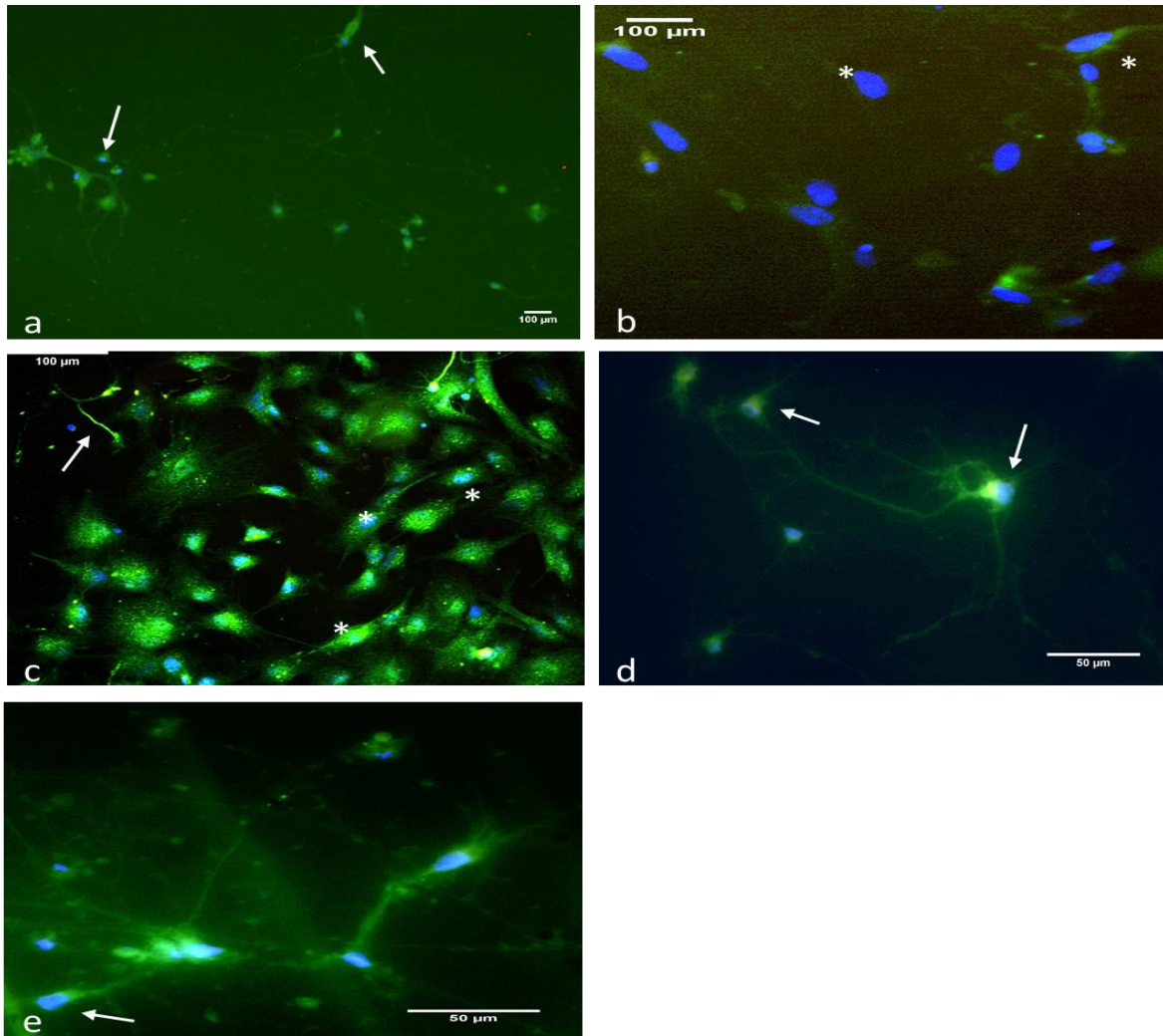


Figure 13: Representative Images of Nav1.1 Expression

Above: Representative images of Nav1.1 expression. A) Negative control cells (DIV 12), b) pLL3.74-dsRed cells (DIV 12), c) SCN1a WT cells (DIV 8), d) SCN1a A1685V (DIV 8), e) SCN1a L986F cells (DIV 8). Arrows indicate neuronal expression. * indicates glial expression. DAPI: nuclei (blue), Alexa 488: Nav_v1.1 (green).

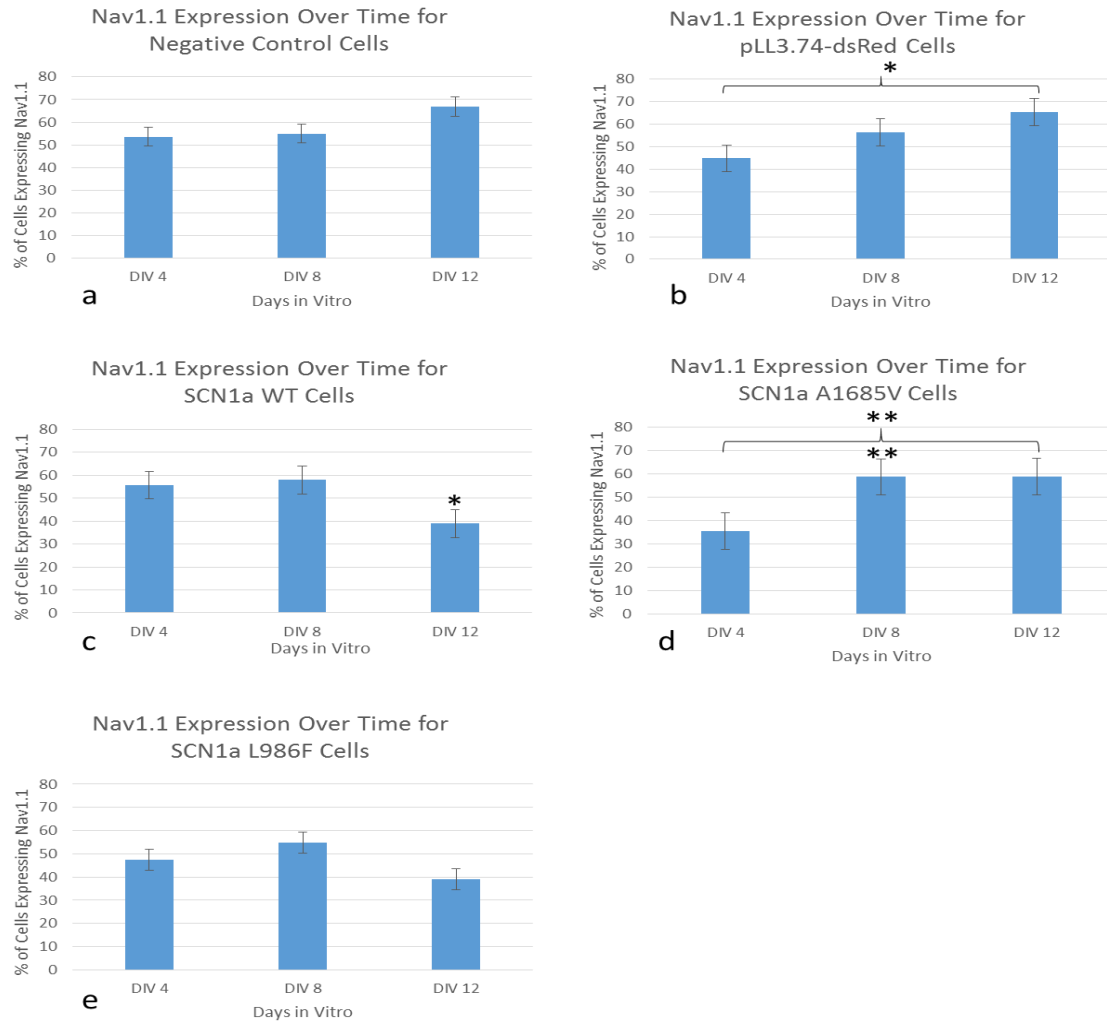


Figure 14: Nav1.1 Expression Over Time for Individual Genotypes

Above: Average Nav_v1.1 expression for individual genotypes on DIV 4, 8, and 12 ± standard error. **: p<0.01; *: 0.01 < p < 0.05 as determined by 1-way ANOVA and post-hoc Scheffe test.

a) Negative control cells (n=8, 12, 11), b) pLL3.74-dsRed cells (n=9, 9, 8), c) SCN1a WT (n=6, 9, 8), d) SCN1a A1685V (n=10, 9, 9), e) SCN1a L986F (n=9, 10, 7)

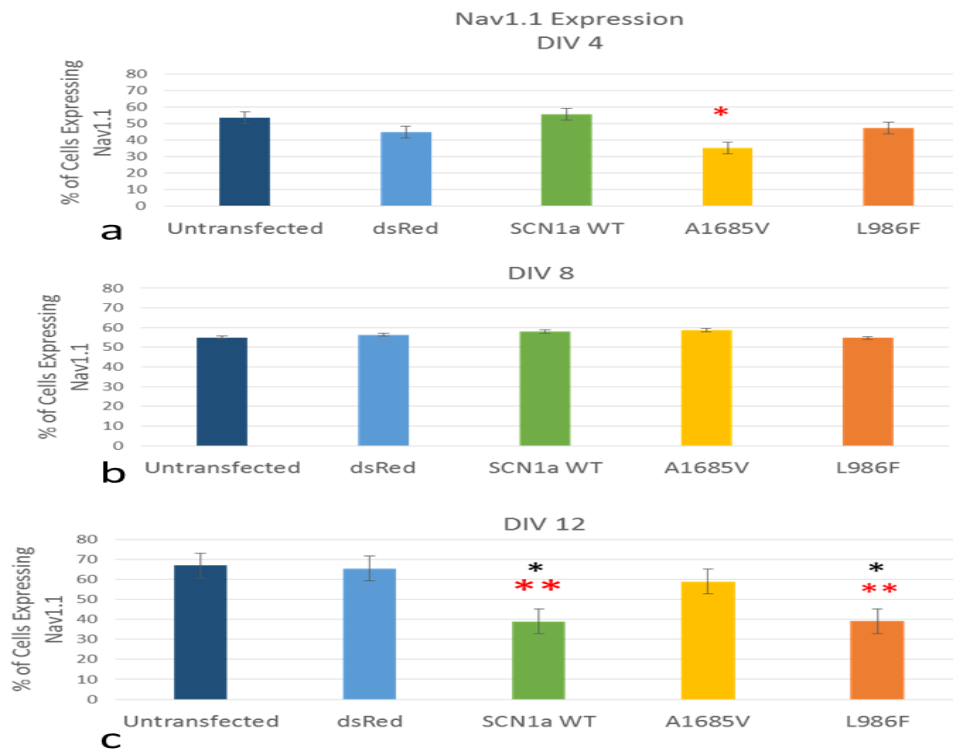


Figure 15: Nav1.1 Expression Across Genotypes at a Given Age

Above: Nav_v1.1 expression across genotypes on DIV 4, 8, and 12 ± standard error. * and ** represent significant differences from transfected controls (pLL3.74-dsRed). **: p<0.01; *: 0.01 < p < 0.05 (red: differences from negative control cells; black: differences from pLL3.74-dsRed cells) as determined by 1-way ANOVA and post-hoc Scheffe test. DIV 4, 8, and 12 n: Negative control cells (n=8, 12, 11), pLL3.74-dsRed cells (n=9, 9, 8), SCN1a WT (n=6, 9, 8), SCN1a A1685V (n=10, 9, 9), SCN1a L986F (n=9, 10, 7).

Parvalbumin (PV) expression was also examined for individual genotypes across time (Figure 17) and across genotypes on a given day (Figure 18). Significance was evaluated using a 1-way ANOVA and post-hoc Scheffe test. Parvalbumin was largely localized to the soma on neurons and did not appear to be expressed by glia (Figure 16). pLL3.74-dsRed (Figure 17b), SCN1a WT cells (Figure 17c), and A1685V cells had fairly stable PV expression over time, although WT cells did display a significant decrease in expression from DIV 8 to 12 ($35\% \pm 3$ to $20\% \pm 4$, p value: 0.021). Negative control cells had elevated PV expression on DIV 4 but by DIV 8, their PV expression had come down to dsRed and WT levels (Figure 17a). L986F mutants, on the other hand, displayed the lowest DIV 4 PV levels ($16\% \pm 5$), significantly higher expression levels on DIV 8 (58%, p value: 0.001), and a noticeable decrease on DIV 12 (26%; Figure 17e). L986F's increased PV expression on DIV 8 may indicate the network's attempt to adapt to a reduced inhibition resulting from the SCN1a mutation. The sudden decrease on DIV 12 could potentially be a result of a loss of genotype due to nucleofection's transient nature as nucleofection is only stable for 12-14 days.

PV expression across genotypes on a given day was also variable (Figure 18). On DIV 4, negative control and A1685V cells displayed the highest PV expression (Figure 18a). WT cells had comparatively lower expression levels, but both dsRed and L986F cells had significantly lower PV expression than negative controls. ($22\% \pm 3$ and $16\% \pm 3$ vs. $44\% \pm 8$, respectively; p-values of 0.049 and 0.008 respectively). By DIV 8, a trend indicated that an average of 38% of negative control, dsRed, and SCN1a WT cells were expressing PV (Figure 18). However, mutant cells were expressing comparatively higher levels of PV, possibly indicative of a subtle compensatory mechanism. By DIV 12, however, the mutant's increased PV expression was gone (Figure 18), possibly as a result of loss-of-genotype and a return to baseline PV expression.

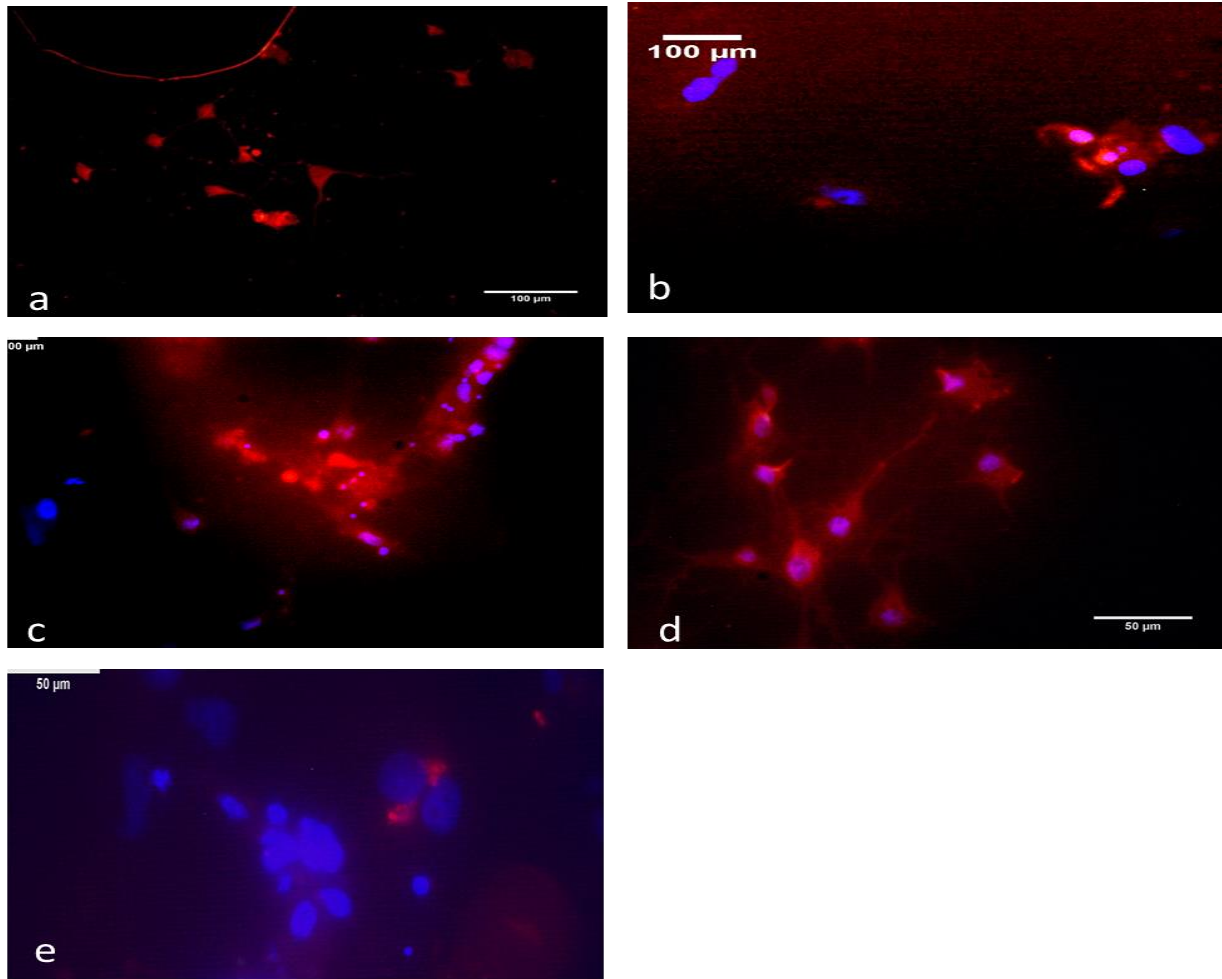


Figure 16: Representative Images of Parvalbumin Expression

Above: Representative images of parvalbumin expression. A) Negative control cells (DIV 12), b) pLL3.74-dsRed cells (DIV 12), c) SCN1a WT cells (DIV 12), d) SCN1a A1685V cells (DIV 8), e) SCN1a L986F cells (DIV 12). DAPI: nuclei (blue), Alexa 647: parvalbumin (red).

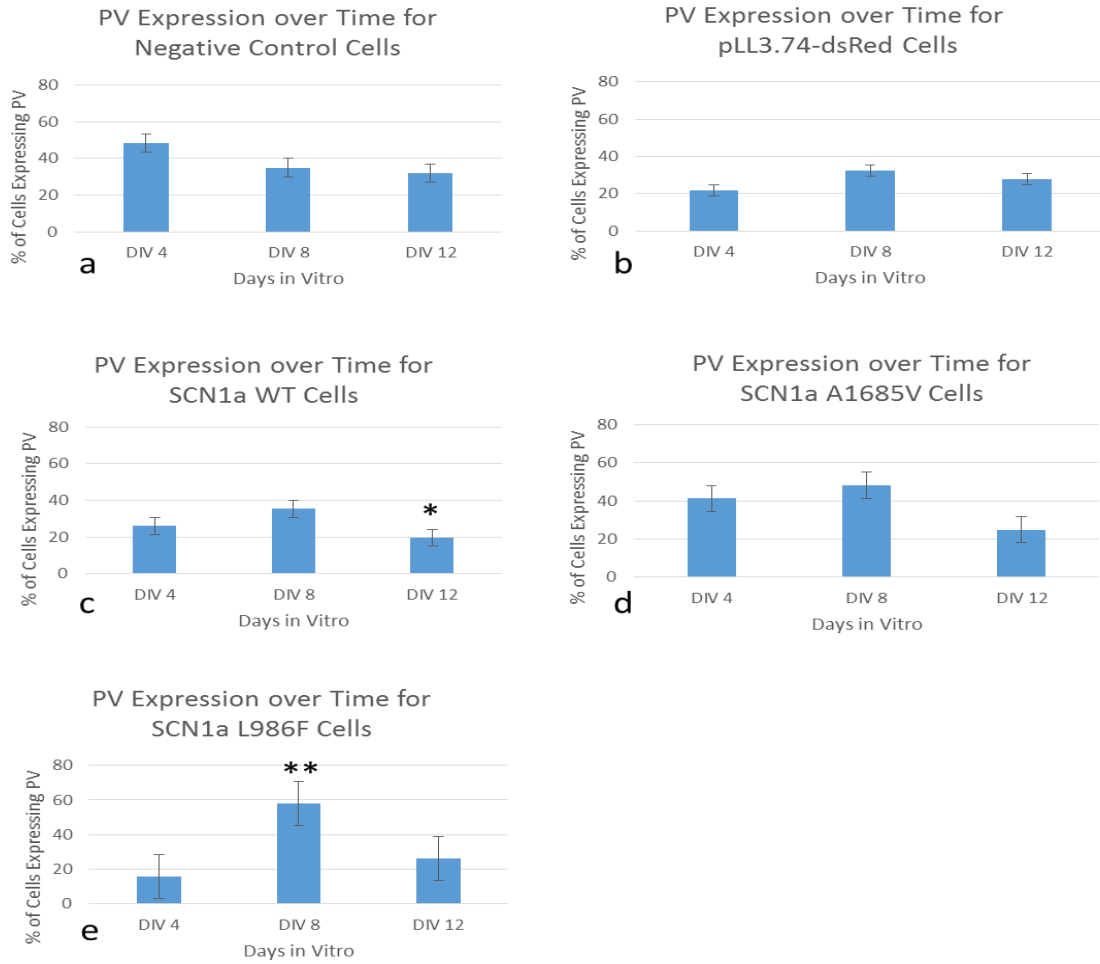


Figure 17: Parvalbumin Expression over Time for Individual Genotypes

Above: Average PV expression for individual genotypes on DIV 4, 8, and 12 \pm standard error. *: $0.01 < p < 0.05$ as determined by 1-way ANOVA and post-hoc Scheffe test. a) Negative control cells (n=6, 7, 6), b) pLL3.74-dsRed cells (n=6, 6, 6), c) SCN1a WT (n=6, 7, 6), d) SCN1a A1685V (n=6, 7, 7), e) SCN1a L986F (n=6, 6, 5).

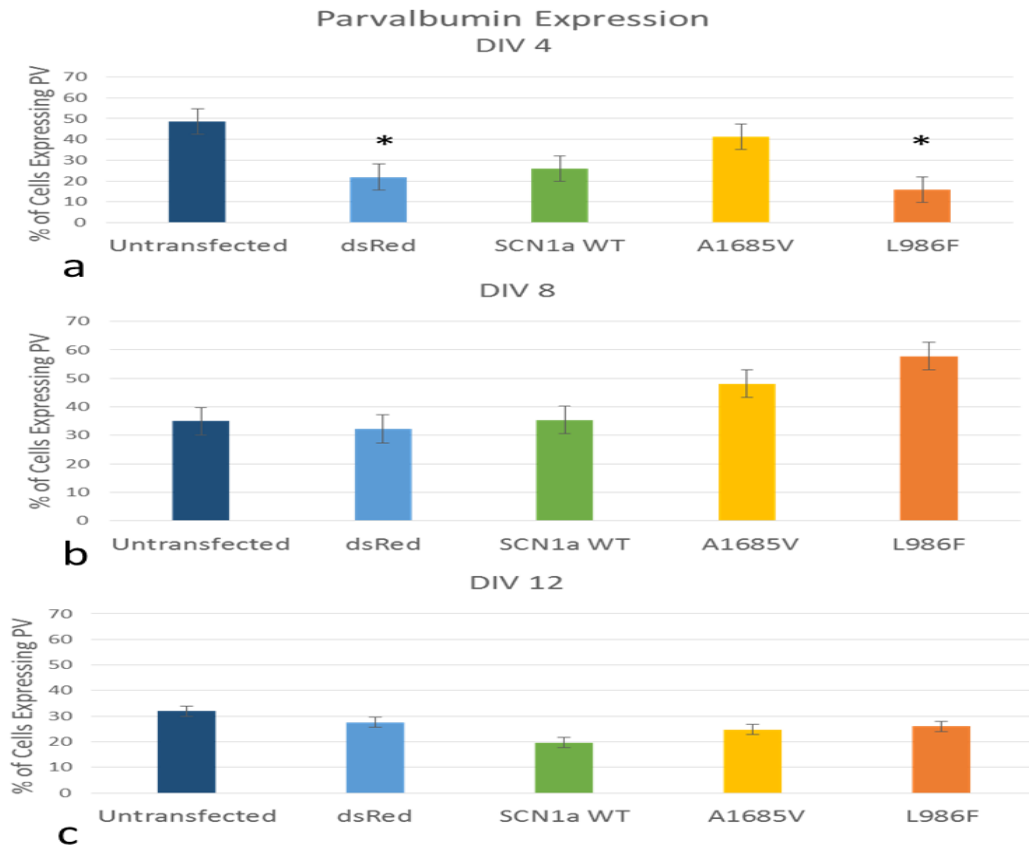


Figure 18: Parvalbumin Expression Across Genotypes at a Given Age

Above: Average PV expression across genotypes on individual days \pm standard error. * represents a significant difference from negative control cells ($p < 0.05$) as determined by 1-way ANOVA and post-hoc Scheffe test. DIV 4, 8, and 12 n: Negative control cells (n=6, 7, 6), pLL3.74-dsRed cells (n=6, 6, 6), SCN1a WT (n=6, 7, 6), SCN1a A1685V (n=6, 7, 7), SCN1a L986F (n=6, 6, 5).

Vesicular transporter 1 (Vglut1) expression was also fairly stable over time (Figure 20) and uniform across genotypes (Figure 21), making a down-regulation of Vglut1⁺ excitatory cells unlikely. Vglut1 was present in the soma of neurons and glia and appeared more punctate in the axons over time (Figure 19). SCN1a WT cells had uniform Vglut1 expression across all days (Figure 20c). A small increase in Vglut1 expression from DIV 4 to 8 followed by a small decrease in expression from DIV 8 to 12 was observed in negative control cells (Figure 20a), A1685V cells (Figure 20d), and L986F cells (Figure 20e). pLL3.74-dsRed cells displayed a similar trend, but the decrease from DIV 8 to 12 was significant in this case according to a 1-way ANOVA and post-hoc Scheffe test ($76\% \pm 5$ to $45\% \pm 6$, p value of 0.021). The slight increase in Vglut1 expression from DIV 4-8 may be due to gradual synapse maturity, as synapses begin to mature around DIV 7. The slight decrease from DIV 8 to 12 is likely due to decreased viability as the culture aged. Examining Vglut1 expression across genotypes on individual days reiterated fairly even Vglut1 expression on DIV 4 (Figure 21a), 8 (Figure 21b), and 12 (Figure 21c).

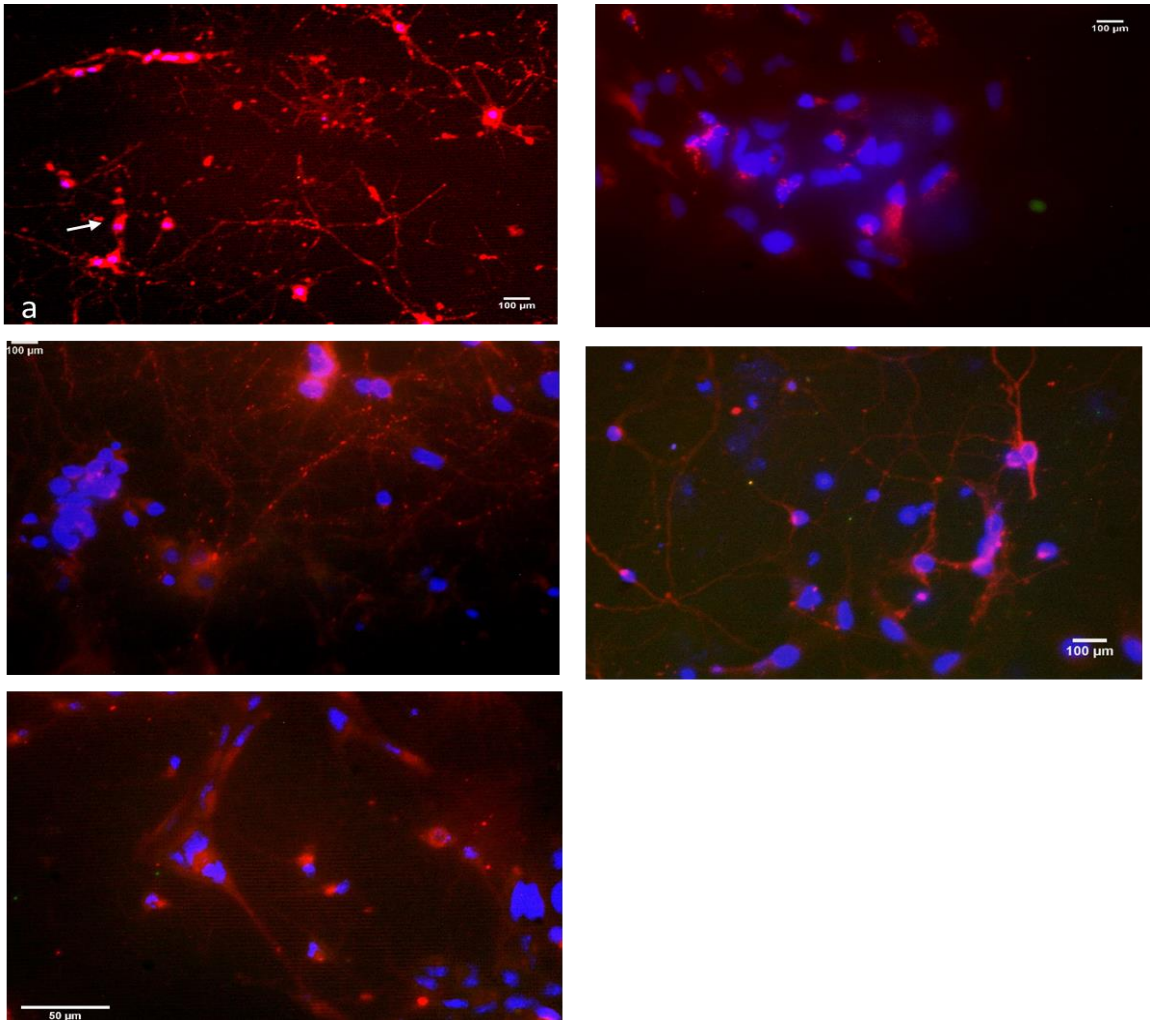


Figure 19: Representative Images of Vglut1 Expression

Above: Representative images of Vglut1 expression in a) negative control cells (DIV 12), b) pLL3.74-dsRed cells (DIV 8), c) SCN1a WT cells (DIV 8), d) SCN1a A1685V cells (DIV 8), and e) SCN1a L986F cells (DIV 4). DAPI: nuclei (blue), Alexa 647: Vglut1 (red). Arrows indicate neuronal expression.

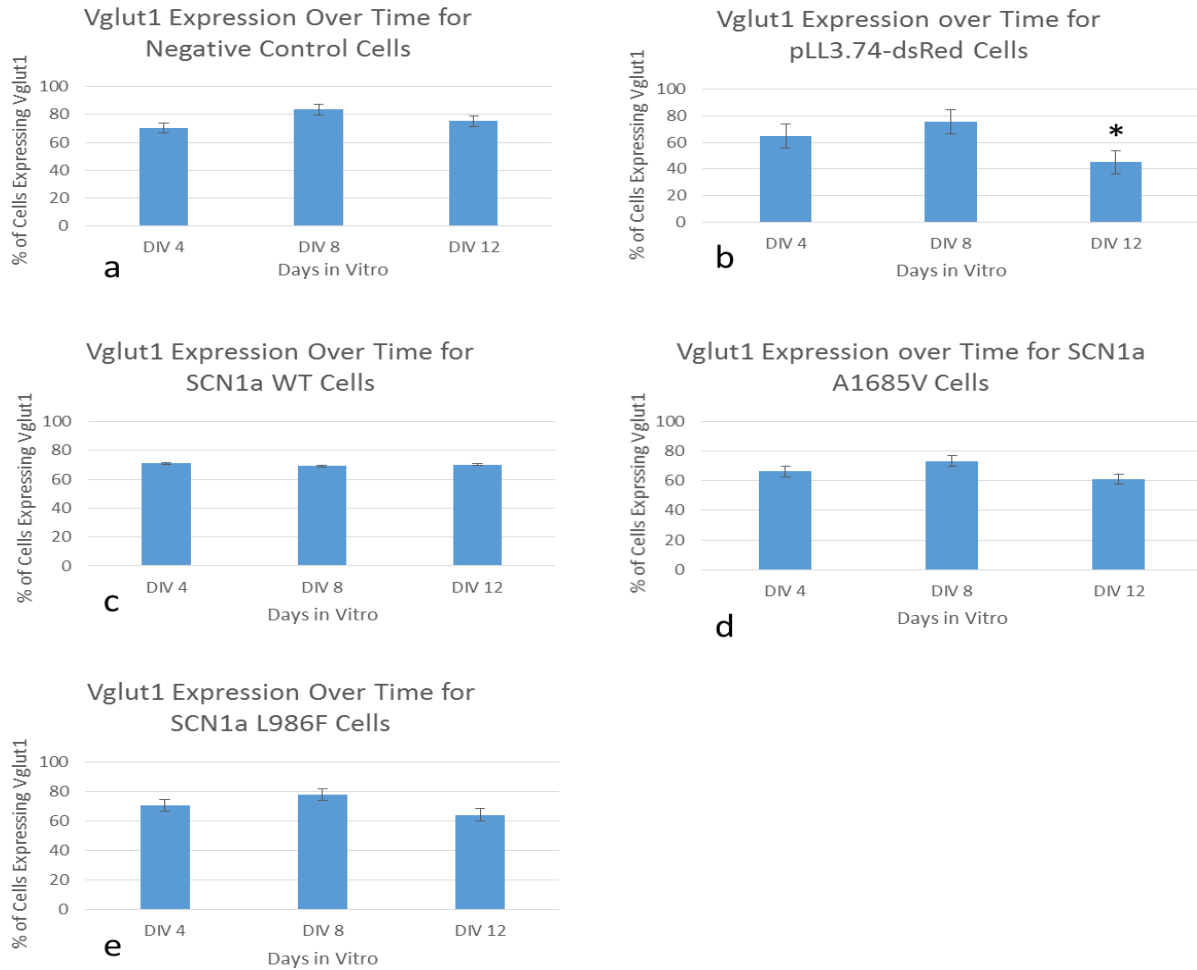


Figure 20: Vglut1 Expression Over Time for Individual Genotypes

Above: Average Vglut1 expression for individual genotypes on DIV 4, 8, and 12 \pm standard error. *: $0.01 < p < 0.05$ as determined by 1-way ANOVA and post-hoc Scheffe test. a) Negative control cells (n=6, 6, 8), b) pLL3.74-dsRed cells (n=7, 7, 6), c) SCN1a WT (n=6, 6, 7), d) SCN1a A1685V (n=6, 6, 6), e) SCN1a L986F (n=6, 7, 6).

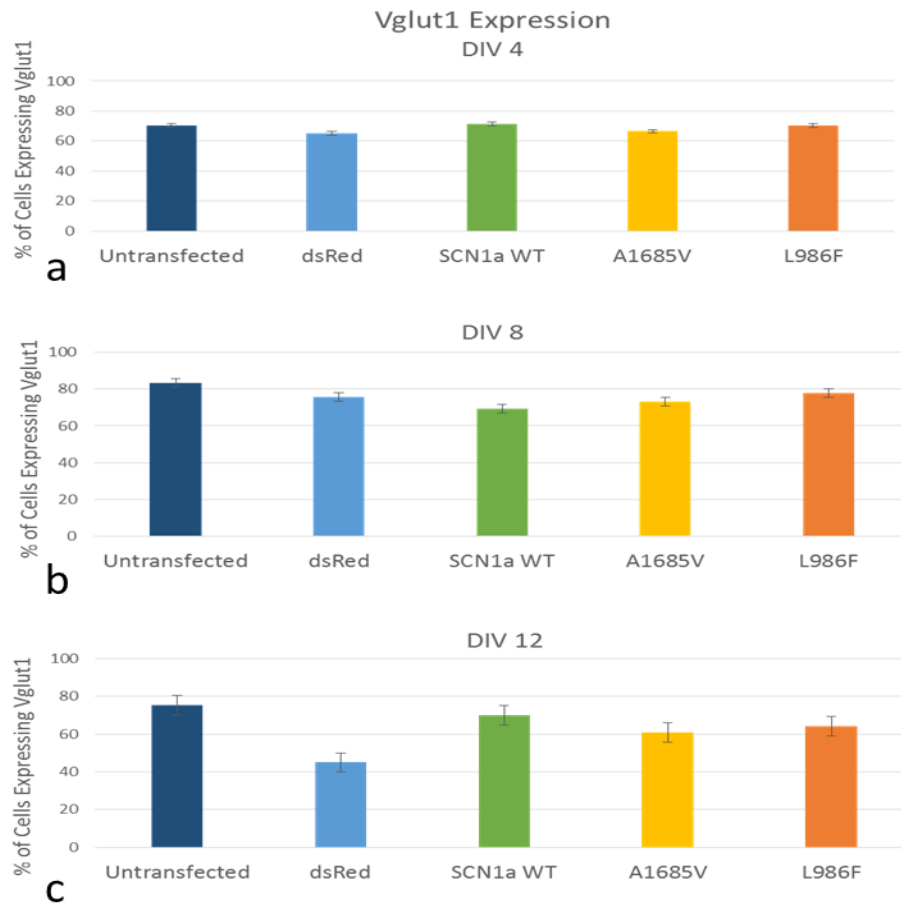


Figure 21: Vglut1 Expression Across Genotypes at a Given Age

Above: Average Vglut1 expression across genotypes on individual days \pm standard error. DIV 4, 8, and 12 n: Negative control cells (n=6, 6, 8), pLL3.74-dsRed cells (n=7, 7, 6), SCN1a WT (n=6, 6, 7), SCN1a A1685V (n=6, 6, 6), SCN1a L986F (n=6, 7, 6)

Cellular localization of Nav1.1 displayed a small shift in Nav1.1 expression in axons and dendrites (Figure 24). Nav1.1 was often expressed in the soma and axon while MAP2 was expressed in the soma and dendrites (Figure 22). Although Nav1.1 and Tau1 are expressed in the axon, Nav1.1 was generally isolated to the axon initial segment, as expected (Figure 23). Nav1.1-MAP2 co-localization in most genotypes averaged around 57%. However, Nav1.1 dendritic expression in A1685V cells was noticeably lower at 45%. Similarly, Nav1.1-Tau1 co-localization averaged 53% for negative control, pLL3.74-dsRed, and L986F cells but was comparatively lower in A1685V cells ($40\% \pm 5$). The combined reduction in axonal and dendritic expression contrasts A1685V's overall Nav1.1 expression from DIV 8 which is similar to all other genotypes (Figure 15b). This may indicate that A1685V cells have a similar number of cells expressing Nav1.1 but that the amount of Nav1.1 being expressed in processes is reduced. Additionally, Nav1.1 expression in axons was comparatively higher in SCN1aWT cells compared to negative control, pLL3.74-dsRed, and L986F cells ($74\% \pm 6$). This may indicate that transfection with SCN1a WT causes an overexpression of Nav1.1 that is predominately affecting inhibitory neurons. The combined increase in Nav1.1-Tau1 co-localization in SCN1aWT cells and decrease in A1685V cells leads to a significant difference between the two (p value: 0.026).

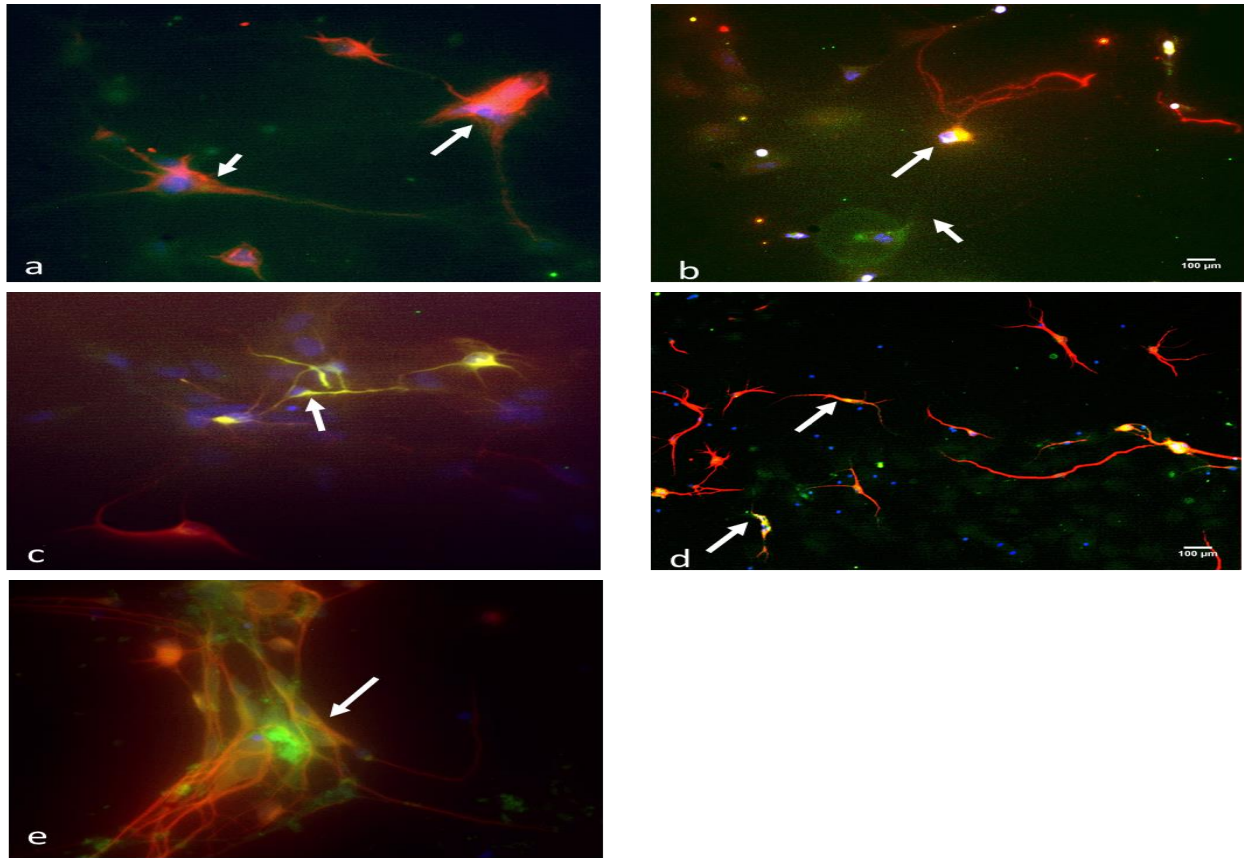


Figure 22: Representative Images of Nav1.1-MAP2 Co-localization

Above: Representative images of Nav_v1.1 and MAP2 expression for negative control (a), pLL3.74-dsRed (b), SCN1a WT (c), SCN1a A1685V (d), and SCN1a L986F (e) cells. Blue: nuclei (DAPI), green: Nav_v1.1 (Alexa 488), red: MAP2 (Alexa 647). **Arrows indicate Nav_v1.1-MAP2 co-localization in the soma and dendrites (b). Arrows indicate Nav_v1.1-MAP2 co-localization in the soma with MAP2 localization to the dendrites and Nav_v1.1 localization to the axon in a, c, d, and e. Scale is the same for a, b, c, and e.

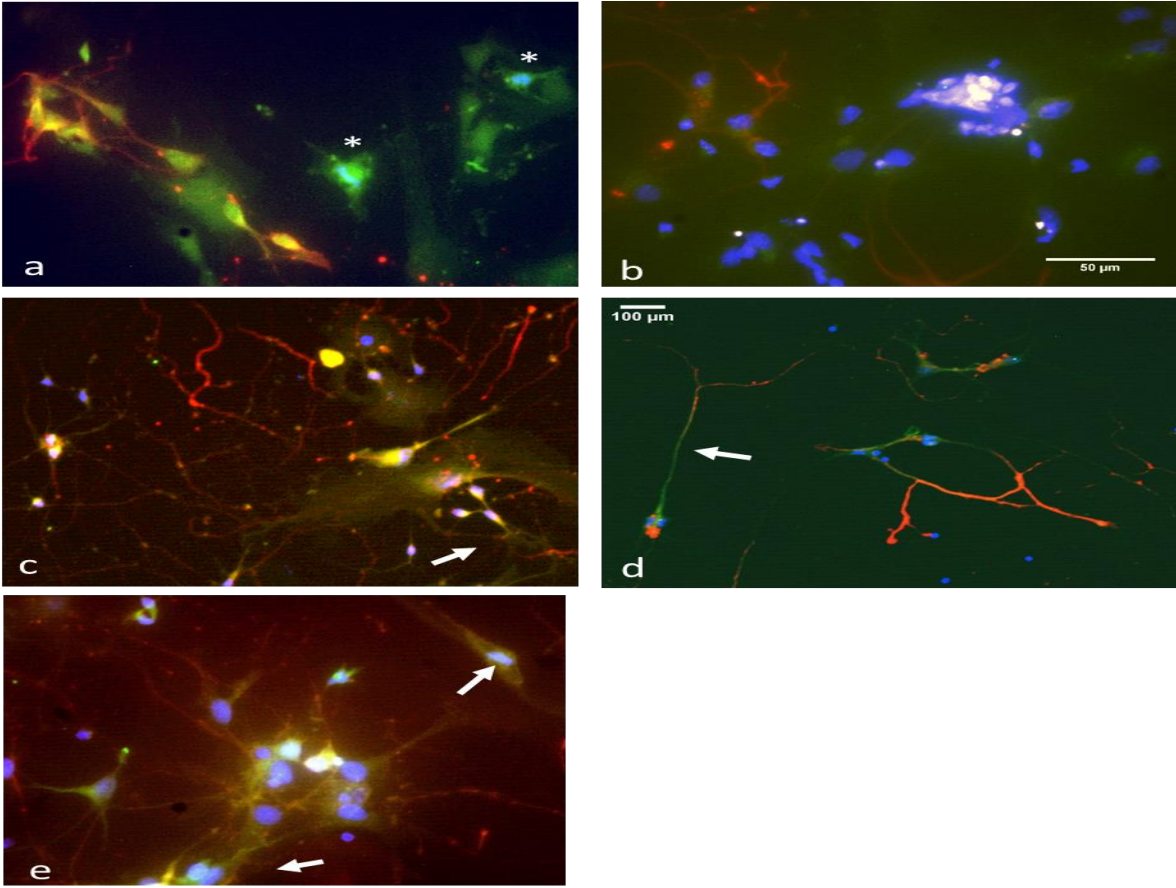


Figure 23: Representative Images of Nav1.1-Tau1 Co-localization

Above: Representative images of Nav_v1.1 and Tau 1 expression for negative control (a), pLL3.74-dsRed (b), SCN1a WT (c), SCN1a A1685V (d), and SCN1a L986F (e) cells. Blue: nuclei (DAPI), green: Nav_v1.1 (Alexa 488), red: Tau1 (Alexa 647). Glial expression of Nav_v1.1 indicated by * in a. Arrows indicate Nav_v1.1-Tau1 co-localization to the soma only (a, e) or soma and axon initial segment (b, c, d). Scale for a, b, and e are the same. Scale for c and d are the same.

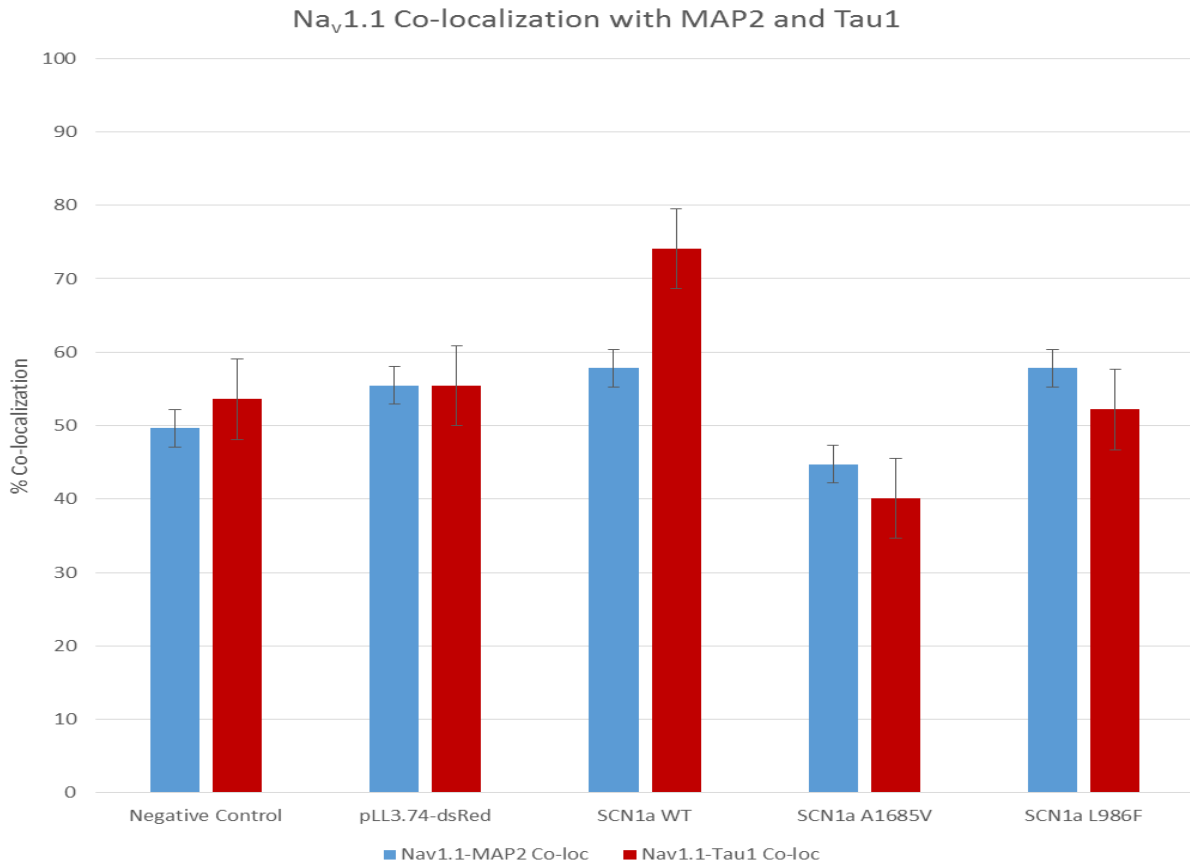


Figure 24: Nav1.1 Co-localization with MAP2 and Tau1

Above: Average Nav_v1.1 co-localization with MAP2 (blue) and Tau1 (red) for various genotypes on DIV7 ± standard error. *: p<0.05 as determined by 1-way ANOVA and post-hoc Scheffe test. Negative control (n=6), pLL3.74-dsRed cells (n=6), SCN1a WT (n=6 for MAP2, 5 for Tau1), SCN1a A1685V (n=6), SCN1a L986F (n=5 for MAP2, 7 for Tau1).

In the case of $\text{Na}_v1.1$ and PV, co-localization was fairly constant across days and genotypes (Figure 26 & Figure 27). $\text{Na}_v1.1$ was expressed in the soma of both neurons and glia, but was also present in the axon initial segment of PV^+ cells, while PV was mainly expressed in neuronal somas (Figure 25). Looking at individual genotypes over time, *SCN1a* WT cells displayed a small decrease between DIV 4 and 8 but, in general, expression remained consistent (Figure 26c). Negative control cells displayed a gradual increase in co-localization from DIV 4 to DIV 12 ($32\% \pm 3$ to $58\% \pm 6$, p value: 0.016; Figure 26a). The remaining pLL3.74-dsRed, A1685V, and L986F cells all showed trends where $\text{Na}_v1.1$ -PV co-localization increased from DIV 4 to 8 then decreased from DIV 8 to 12 (Figure 26 b, d, e). However, this trend was only significant between DIV 4 and 8 for A1685V cells (p value: 0.027).

Examination across genotypes on individual days also showed some variability in trends (Figure 27). On DIV 4, negative control, pLL3.74-dsRed, and L986F cells had $\text{Na}_v1.1$ -PV co-localization values of around 36% (Figure 27a). However, *SCN1a* WT cells had noticeably higher co-localization while A1685V cells had noticeably lower co-localization, leading to a significant difference between the two (p value: 0.008). This disparity in co-localization between $\text{Na}_v1.1$ and PV could indicate an overexpression of $\text{Na}_v1.1$ in PV^+ neurons for WT cells and a reduced expression of $\text{Na}_v1.1$ in PV^+ neurons in A1685V cells early on, possibly due to their respective genotypes. By DIV 8, both WT and A1685V cells displayed $\text{Na}_v1.1$ -PV co-localization near that of the other genotypes (Figure 27 b). Neither DIV 8 nor 12 show any significant differences between genotypes (Figure 27 b and c). The fact that WT and A1685V cell's $\text{Na}_v1.1$ -PV co-localization caught up to that of the remaining genotypes may indicate a subtle compensatory down-regulation of $\text{Na}_v1.1$ expression on PV^+ cells in WT networks and a subtle up-regulation in A1685V cells.

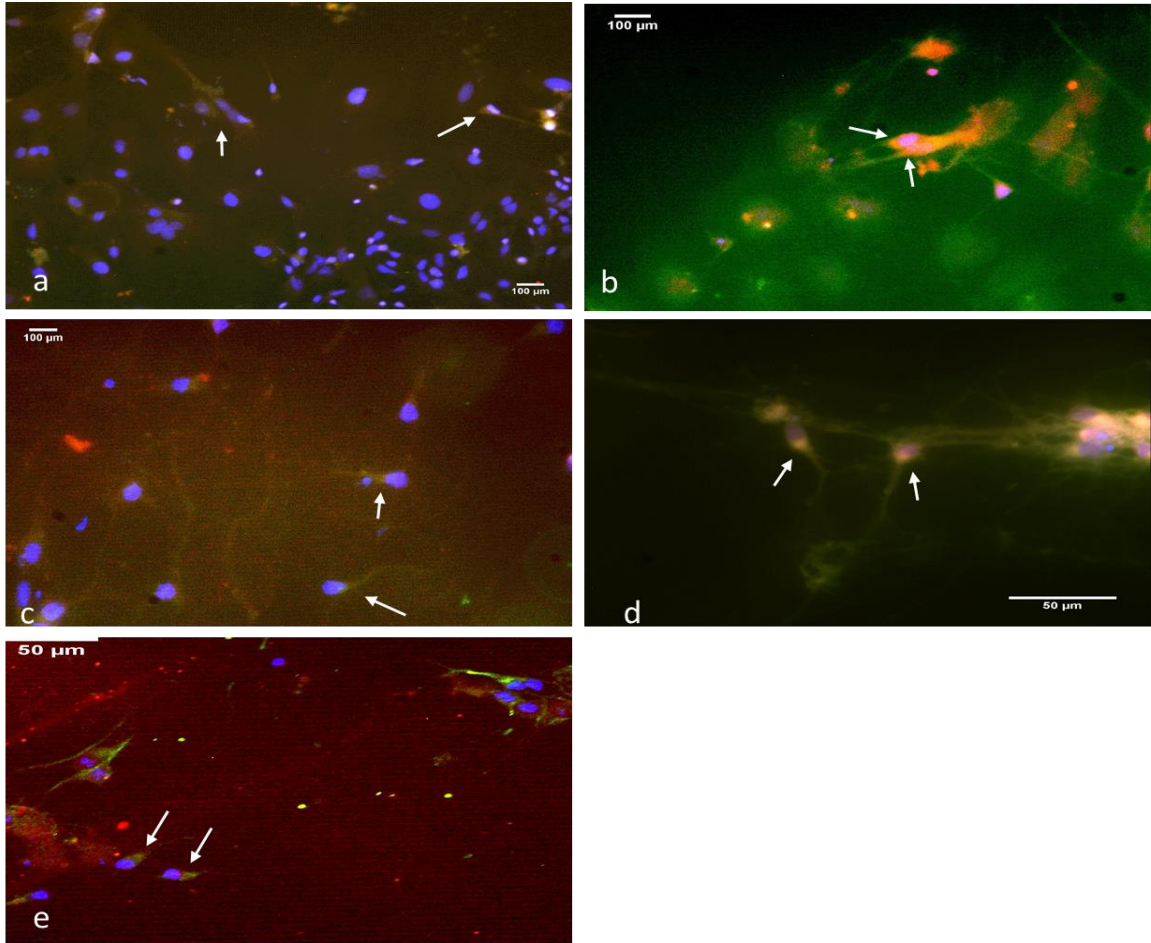


Figure 25: Representative Images of Nav1.1-Parvalbumin Co-expression

Above: Representative images of Nav1.1-PV co-expression for a) negative control cells (DIV 8), b) pLL3.74-dsRed cells (DIV 8), c) SCN1a WT cells (DIV 8), d) SCN1a A1685V cells (DIV8), e) SCN1a L986F cells (DIV 4). DAPI: nuclei (blue), Alexa 488: Nav_v1.1 (green), Alexa 647: PV (red). Arrows indicate PV⁺ cells with Nav1.1 localized to the soma and axon initial segment.

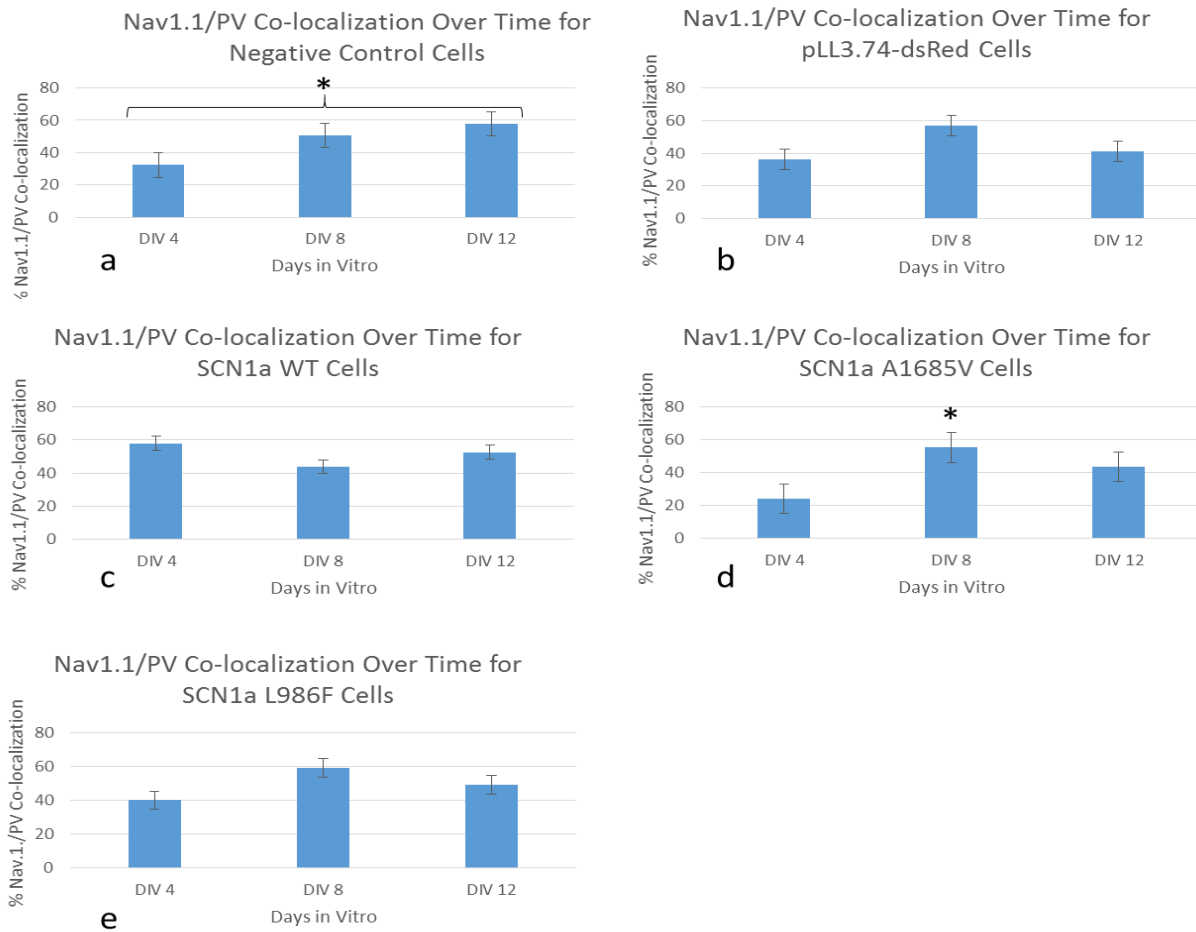


Figure 26: Nav1.1-Parvalbumin Co-localization Over Time for Individual Genotypes

Above: Average Nav1.1-PV co-localization for individual genotypes on DIV 4, 8, and 12 \pm standard error. *: $0.01 < p < 0.05$ as determined by 1-way ANOVA and post-hoc Scheffe test. a) Negative control cells (n=6, 6, 8), b) pLL3.74-dsRed cells (n=5, 6, 6), c) SCN1a WT (n=5, 5, 5), d) SCN1a A1685V (n=5, 6, 6), e) SCN1a L986F (n=5, 5, 5).

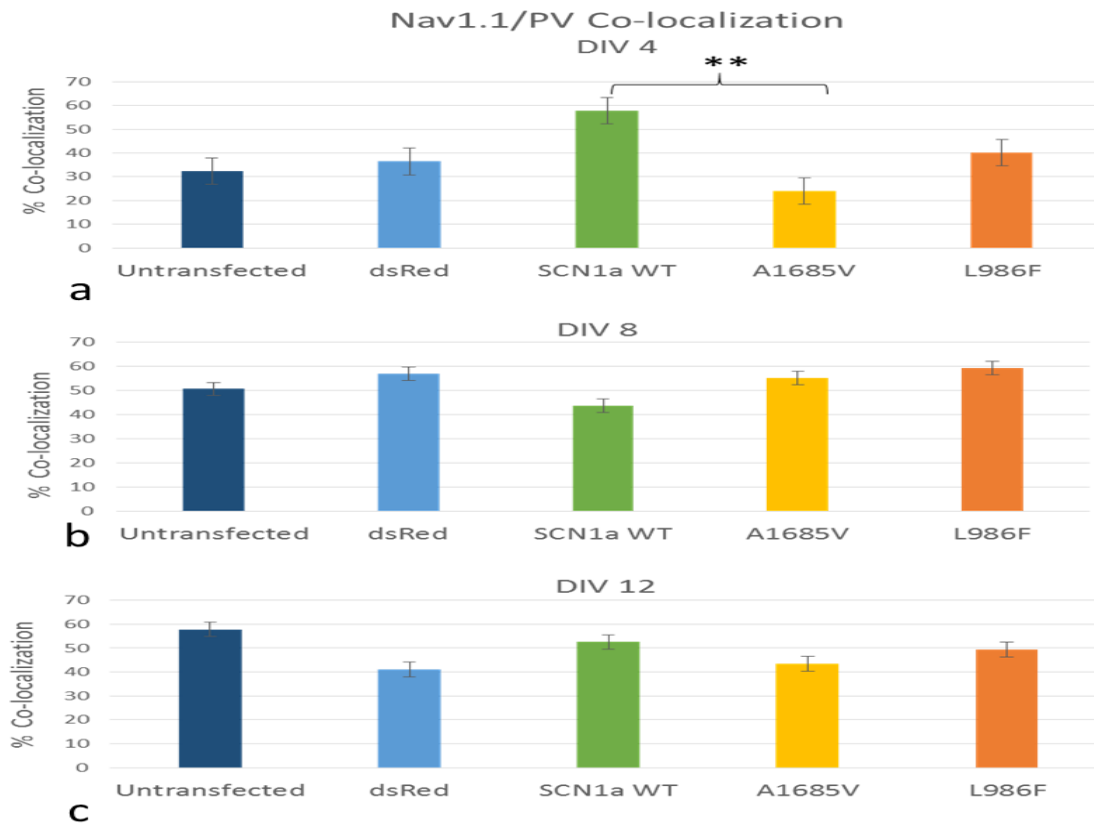


Figure 27: $Na_v1.1$ -Parvalbumin Co-localization Across Genotypes at a Given Age

Above: Average $Na_v1.1$ -PV co-localization for across genotypes on DIV 4, 8, and 12 \pm standard error. **: p value < 0.01 as determined by 1-way ANOVA and post-hoc Scheffe test. DIV 4, 8, and 12 n: Negative control cells (n=6, 6, 8), pLL3.74-dsRed cells (n=5, 6, 6), SCN1a WT (n=5, 5, 5), SCN1a A1685V (n=5, 6, 6), SCN1a L986F (n=5, 5, 5)

Similar co-localization uniformity was observed for Nav1.1 and Vglut1 across genotypes and age (Figure 29 & Figure 30). Nav1.1 was mainly expressed in the soma of both glia and neurons, but was present in the beginnings of dendritic processes in Vglut1⁺ cells (Figure 28). Negative control cells displayed a significant increase in Nav1.1-Vglut1 co-localization from DIV 4 to 8 and 8 to 12 (38% ± 4 vs. 43% ± 4 and 38% ± 4 vs. 75% ± 8; p values: 0, and 0 respectively; Figure 29a). pLL3.74-dsRed (Figure 29b), A1685V (Figure 29d, and L986F; Figure 29e) cells all showed trends with slight increases in co-localization between DIV 4 and 8 but similar or slightly reduced expression on DIV 12. WT cells had fairly similar Nav1.1-Vglut1 co-localization on all days (Figure 29c).

No significant difference in Nav1.1-Vglut1 co-localization was observed across genotypes at a given age (Figure 30). DIV 4 Nav1.1-Vglut1 co-localization was fairly consistent between 38 and 51% (Figure 30a). On Nav1.1-Vglut1 co-localization generally increased from DIV 4 to DIV 8 (Figure 30b), possibly due to changes in Vglut1⁺ cells during synapse development. By DIV 12, Nav1.1-Vglut1 co-localization was again uniform across genotypes (Figure 30c).

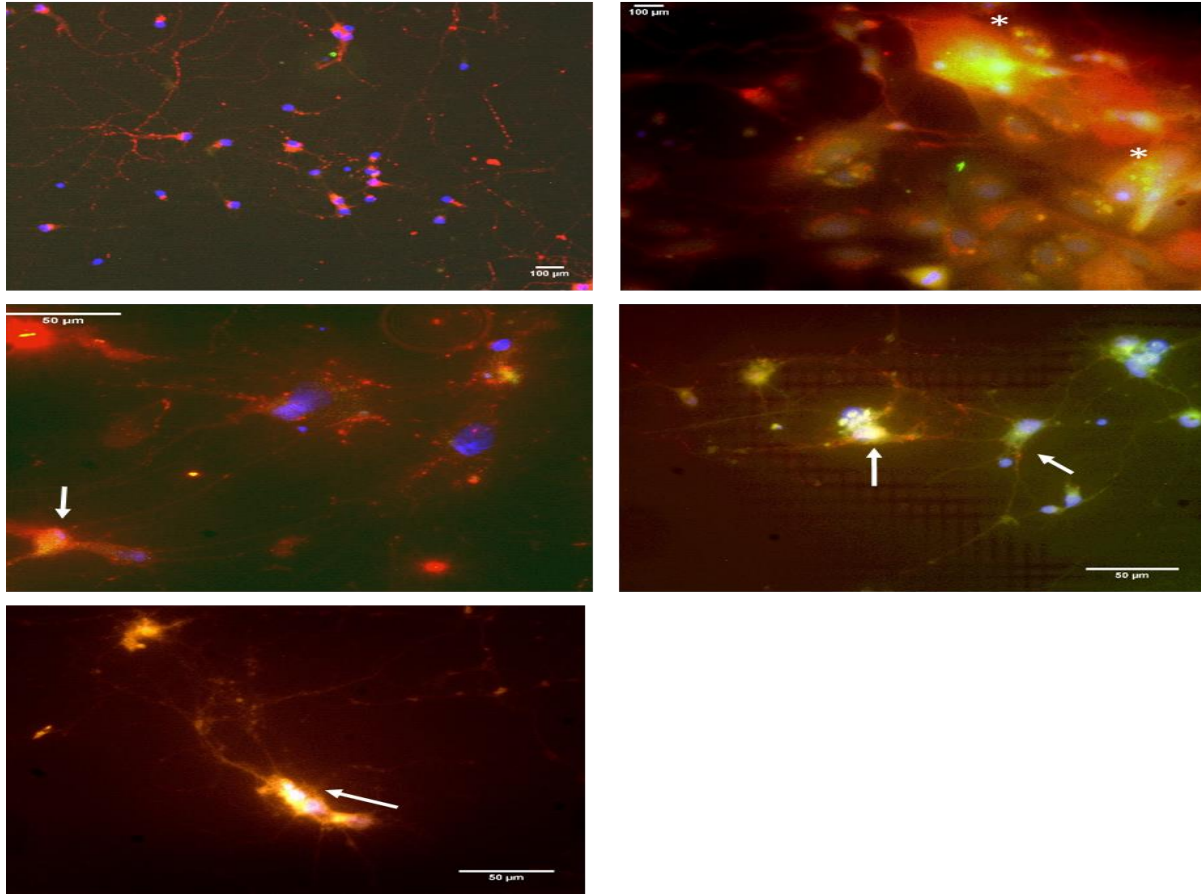


Figure 28: Representative Images of Nav1.1-VGlut1 Co-expression

Above: Representative Images of Nav_v1.1-Vglut1 co-expression. A) Negative control cells (DIV 8); b) pLL3.74-dsRed cells (DIV 8), c) SCN1a WT cells (DIV 8), d) SCN1a A1685V cells (DIV 8), e) SCN1a L986F cells (DIV 12). Arrows indicate Nav1.1 expression in the soma and early dendritic processes. * denotes glial co-localization. DAPI: nuclei (blue), Alexa 488: Nav_v1.1 (green), Alexa 647: Vglut1 (red).

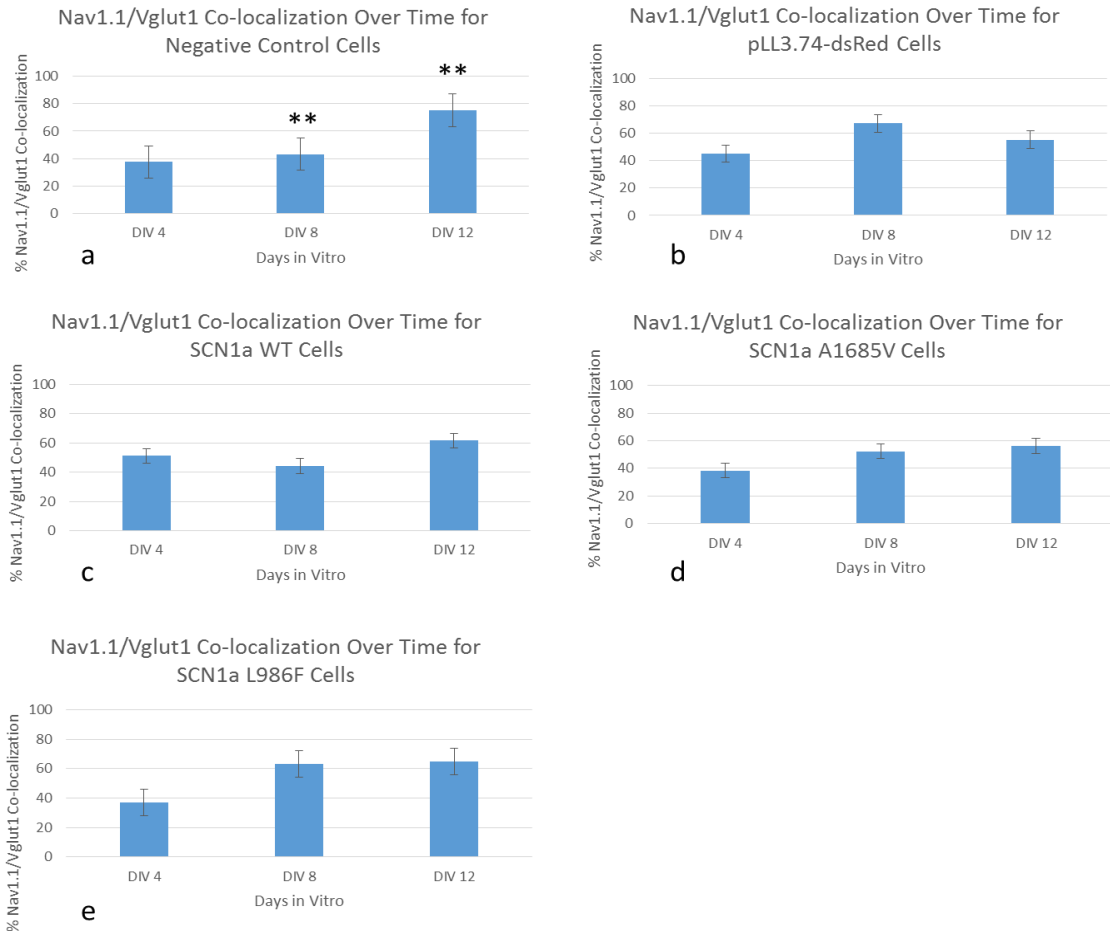


Figure 29: Nav1.1-Vglut1 Co-localization in Individual Genotypes Across Time

Above: Average Nav_v1.1-Vglut1 co-localization for individual genotypes on DIV 4, 8, and 12 ± standard error. **: p value < 0.01 as determined by 1-way ANOVA and post-hoc Scheffe test. a) Negative control cells (n=5, 6, 6), b) pLL3.74-dsRed cells (n=6, 6, 6), c) SCN1a WT (n=5, 5, 6), d) SCN1a A1685V (n=5, 5, 5), e) SCN1a L986F (n=6, 6, 5)

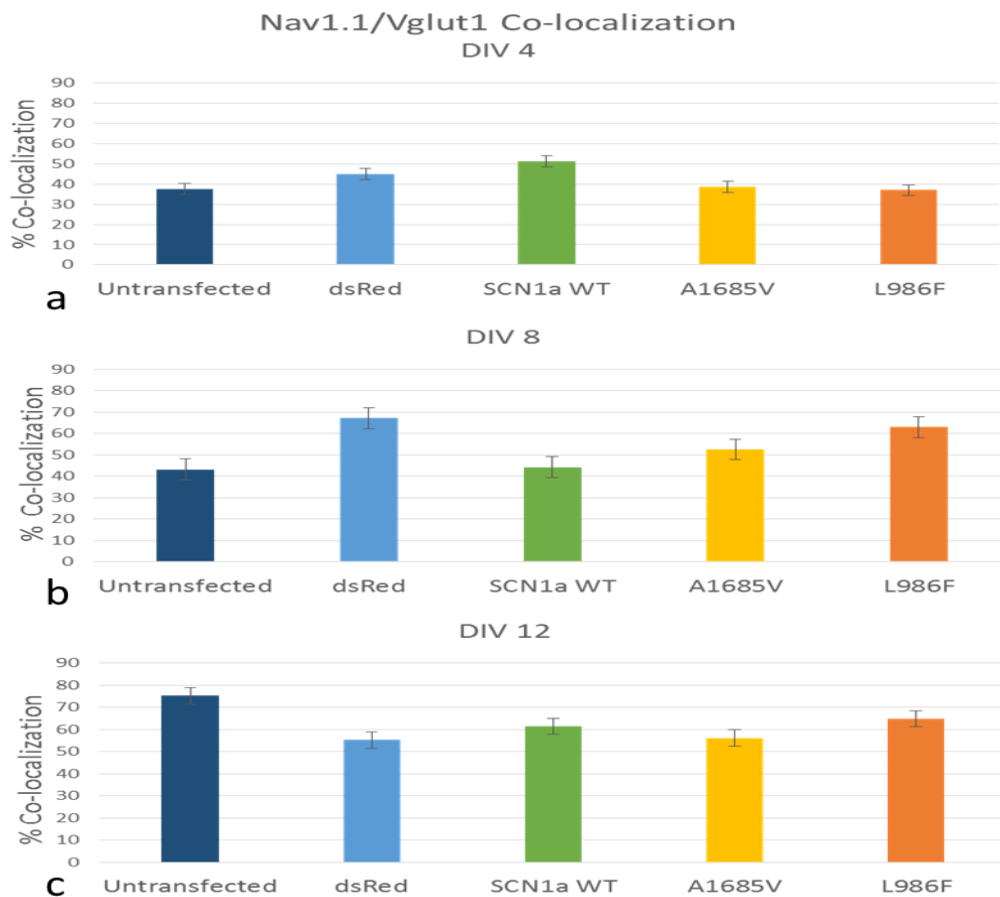


Figure 30: Nav1.1-Vglut1 Co-localization Across Genotypes at a Given Age

Above: Average Nav1.1-Vglut1 co-localization for across genotypes on DIV 4, 8, and 12 \pm standard error. **: p value < 0.01 as determined by 1-way ANOVA and post-hoc Scheffe test. DIV 4, 8, and 12 n: Negative control cells (n=5, 6, 6), b) pLL3.74-dsRed cells (n=6, 6, 6), c) SCN1a WT (n=5, 5, 6), d) SCN1a A1685V (n=5, 5, 5), e) SCN1a L986F (n=6, 6, 5)

3.4 DISCUSSION

The purpose of this chapter was to determine whether transfection with SCN1a plasmids impacts culture composition and Na_v1.1 protein expression and localization. Studies indicate that transfection did not appear to alter the phenotype of transfected vs. un-transfected controls indicating that any changes between controls and experimental genotypes were likely due to the exogenous DNA introduced. Furthermore, the overall ratio of excitatory to inhibitory neurons was consistent with previous studies in *in vitro* neurons. Typically, the majority of dissociated rodent hippocampal cultures are excitatory cells with at least 20% being inhibitory [134, 135]. The fact that the average excitatory to inhibitory ratio remained stable across genotypes indicates that a stable compensatory up-regulation of inhibitory cells or down-regulation of excitatory cells did not take place for the cell markers we studied. However, other compensatory mechanisms may be at play [100]. For instance, other subsets of inhibitory cells may be over-expressed in order to provide additional network inhibition. In this case, we used the inhibitory marker parvalbumin because of its presumed role in epilepsy and previous association with Na_v1.1. However, a more general anti-GABA marker might reveal more subtle changes in Na_v1.1 expression.

Additionally, parvalbumin expression displayed subtle changes over time and may warrant closer inspection. Compared to other genotypes, negative control cells had higher PV expression early on possibly indicating that the transfection process may impact the early development of PV cells (Figure 18a). More interestingly, L986F cells displayed similar PV expression levels to transfection control cells early on (Figure 18a) but had noticeably higher PV expression at DIV 8 (Figure 18b) followed by a drop down to DIV 4 levels on DIV 12 (Figure 18c). This may indicate a compensatory increase in PV expression followed by a return to

baseline expression levels following loss of transfection, but as these trends were subtle, they require more investigation.

Furthermore, $Na_v1.1$ expression appeared consistent across genotypes. It was somewhat surprising that *SCN1a* mutations did not affect overall $Na_v1.1$ expression. However, examination of $Na_v1.1$ expression in axons and dendrites did indicate a possible phenotypic effect of *SCN1a* transfection. Although dendritic expression of $Na_v1.1$ was similar in controls, WT, and L986F cells, it was comparably lower in A1685V cells (Figure 24). Similarly, axonal expression of $Na_v1.1$ was comparable in controls and L986F cells but a decrease in axonal expression was noted for the mild mutant A1685V cells (Figure 24). The combined decrease in $Na_v1.1$ axonal and dendritic expression in A1685V cells compared to other genotypes is likely a result of the introduced $Na_v1.1$ mutation. However, the overall $Na_v1.1$ expression for A1685V cells measured on DIV 8 was not noticeably lower than other genotypes (Figure 15c). This may indicate that although the same number of cells are expressing $Na_v1.1$ in A1685V cells around DIV 7-8, the amount of $Na_v1.1$ being expressed in processes is lower.

Additionally, *SCN1a* WT cells demonstrated increased axonal $Na_v1.1$ expression compared to other genotypes (Figure 24). This may indicate that transfection is leading to $Na_v1.1$ over-expression in WT cultures and is mostly impacting inhibitory cells, possibly because they are believed to express $Na_v1.1$ more readily than excitatory cells [107]. Furthermore, both negative control and *SCN1a* WT cells show a higher ratio of axonal vs. dendritic $Na_v1.1$ expression while pLL3.74-dsRed cells are split evenly. This is not surprising because inhibitory cells are thought to express $Na_v1.1$ more readily than excitatory cells (explaining the slight increase in axonal expression) but the greater ratio of excitatory to inhibitory cells may keep axonal and dendritic expression fairly even, especially when glia are factored in. Glia are known

to express Nav1.1 and reactive glia have been shown to express MAP2, which may skew dendritic expression upward. However, both A1685V and L986F cells show slightly higher levels of dendritic expression instead, possibly indicating that the introduced SCN1a mutation is affecting Nav1.1 expression in inhibitory cells in our SCN1a mutants.

Finally, protein expression decreased in a number of instances between DIV 8 and 12. This may be due to cell death, a loss of transfection stability or a combination of the two. Similar preparations of *in vitro* hippocampal neurons can generally be maintained for 2 to 3 weeks, but cell death often begins around DIV 12. Additionally, nucleofection is only stable for 12-14 days. Therefore, changes in Nav1.1 expression on DIV 12 in WT, A1685V, or L986F cells could be due to a loss of genotype. Additionally, these two constraints may limit future studies involving long-term synapse development as synapses begin maturing around DIV 7 and continue to mature through DIV 21. Therefore, this model is currently limited to examining protein expression and early synapse development, but could provide information regarding early disease development.

3.5 CONCLUSIONS

In summary, this chapter illustrates our ability to examine changes in culture composition following transfection of SCN1a plasmids. While no significant compensatory mechanism was observed, several subtle trends do warrant closer inspection. These include density of Nav1.1 expression in processes of mild mutants, early PV expression in negative control cells, and Nav1.1 co-localization with other inhibitory cell markers.

4.0 FUNCTIONAL ANALYSIS OF DEFINED NETWORKS

4.1 INTRODUCTION

Phenotypic analysis of protein localization is not sufficient to assess the effect of SCN1a mutations on neural networks. Because epilepsy is a disease based in aberrant electrical activity, examining the functional consequences of SCN1a mutations on network activity is critical. This chapter is focused on using calcium imaging to examine if and how SCN1a mutations impact activity in constrained neural networks in the presence of seizure agonists and antagonists.

4.1.1 Calcium Imaging, Epilepsy, and Constrained Neuronal Networks

Calcium is one of many intracellular messengers in the brain. At rest, calcium levels inside the cell are low, but this can rapidly increase during neuronal activity as voltage-gated calcium channels and N-methyl-D-aspartate (NMDA) receptors open to allow calcium to enter the cell. Intracellular calcium signals vary by time course and amplitude, so studying calcium transients can provide insight into cellular activity in both healthy and diseased networks [136]. To that end, calcium imaging has been applied to a number of research areas including the development of epilepsy, or epileptogenesis, in the cortex and hippocampus [137, 138].

In 2001, Yuste *et al.* used the calcium-sensitive dye Fura-2 to examine individual neurons' activity in bicuculline-induced epilepsy-like, or epileptiform events, in mouse

somatosensory cortex slices [138]. Yuste's group applied bicuculline methiodide (BMI) to tissue and observed epileptiform activity after 30 minutes. Bicuculline is a competitive GABA_A receptor antagonist that effectively blocks inhibition in a network, creating the hyperexcitability characteristic of epilepsy. Yuste's work resulted in both fast and slow calcium transients. The majority of calcium transients were classified as fast, correlated with epileptiform events, and were not present when TTX was used to block sodium channel activity. Slow calcium transients, on the other hand, appeared spontaneously and persisted in spite of TTX application.

In 2010, Zeringue *et al.* performed a parallel study using the calcium-sensitive dye Fluo4-AM with *in vitro* cultures of E18-E19 rat hippocampal neurons [92]. In this case, microcontact printing was used to constrain network geometry, creating small networks of 40-60 neurons adhered to poly-L-lysine "rings" on glass coverslips. Following electrical stimulation, the networks displayed a brief increase in electrical activity as expected, typically lasting 60 ms with a 2-4 s decay. However, a subset of control cultures displayed "reverberation," defined as network activity persisting >2 s after the cessation of the input stimulus. This persistent activity involved a 6 fold increase in fluorescence over the first 2 seconds followed by a gradual signal decay. The Zeringue group found that after 10 μ M bicuculline treatment, reverberation was observed in 100% of cultures. However, reverberation was both brighter and longer lasting when BMI was present compared to the control HBS bath. When the calcium chelator EGTA-AM was added, persistent activity was effectively blocked. Zeringue *et al.*'s work raised the question, "if prolonged 'seizure-like' activity can be triggered chemically in constrained networks, can it also be triggered genetically?" Therefore, the working hypothesis for this chapter was that mutations in the voltage-gated sodium channel Na_v1.1 likely impact network

functionality. If this hypothesis were correct, then expression of mutant SCN1a subunits should modify the functional activity of constrained networks.

4.1.2 GEFS⁺ and AEDs

Generalized Epilepsy with Febrile Seizures Plus, Type II (GEFS⁺) is a spectrum epilepsy disorder that ranges from mild, generally controllable seizures with normal development to the more extreme Severe Myoclonic Epilepsy of Infancy (SMEI) which typically presents with intractable seizures and severe developmental delays. Although the majority of GEFS⁺ epilepsies are originally associated with fever-related seizures, over time, patients can exhibit non-febrile, generalized, or partial seizures which are often drug resistant and can sometimes even be exacerbated by anti-epileptic drugs (AEDs) [139]. Liao *et al.* studied the effect of AEDs on GEFS⁺ and SMEI using TSa201 cells [104]. Both GEFS⁺ and SMEI involve a loss of sodium channel function due to SCN1a missense mutations. However, GEFS⁺ is less severe, possibly because its missense mutations, including A1685V, do not involve a change in residue hydrophobicity. While some AEDs had no effect, sodium channel blocking AEDs like lamotrigine (LTG), phenytoin (PHT), and carbamazepine (CBZ) did trigger seizure activity. If SCN1a related seizures are caused by a lack of inhibition, using sodium channel blocking AEDs could intensify the problem by further decreasing the inhibitory activity of available interneuron sodium channels without adequately lowering activity in excitatory cells. Although AED aggravated seizure activity may be linked to dosage, several groups have suggested new AEDs that do not target sodium channels should be explored in an effort to help epilepsy patients with diseases like GEFS⁺ and SMEI [140] [104].

Although some AEDs like CBZ and LTG exacerbate seizures in some GEFS⁺ patients, others, like valproic acid (VPA), have shown some success in controlling GEFS⁺. For instance, in 2010, Escayg *et al* demonstrated that 100-300 mg/kg of VPA administered to SCN1a knock-out mice increased the time between seizure episodes and that the effect was magnified increased with increasing dose. Additionally, VPA helped return heterogeneous knock-out mice's elevated febrile seizure threshold to normal [141].

We focused our study on one AED known to aggravate seizure activity in GEFS⁺ patients (referred to as AED⁻) and one that is known to alleviate them (referred to as AED⁺). In this case, our AED⁻ is carbamazepine (CBZ) and our AED⁺ is valproic acid (VPA). CBZ preferentially binds to voltage-gated sodium channels in the inactive state, causing the channel to become inactive at less negative membrane potentials (essentially making it inactive sooner). CBZ also prolongs the refractory period by delaying the channel's return from inactive to closed, resting state following hyperpolarization [57]. Although CBZ is commonly used for treating some types of epilepsy, it is not generally prescribed for GEFS⁺ as it tends to trigger, rather than prevent, seizures. This is likely because CBZ impacts both excitatory and inhibitory cells, so even though excitatory cell activity is reduced, it is not enough to overcome the further reduction of inhibitory cell activity in a network already displaying decreased inhibition, leading to intensified seizure activity. On the other hand, valproic acid (VPA) is an anti-epileptic drug commonly prescribed to GEFS⁺ patients. VPA serves as an AED in two ways. First, it blocks voltage-gated sodium channels to reduce network excitability [142]. Secondly, it is believed to inhibit release of gamma hydroxybutyrate, a chemical that binds to excitatory receptors, leading to an overall decrease in excitation [143]. Both mechanisms increase the activity of functional inhibitory cells

in a network and help compensate for inhibitory neurons which have been compromised by GEFS⁺ mutations.

In short, GEFS⁺ is a neurological disease characterized by abnormal network functionality, but it is rarely studied *in vitro* in neurons. Calcium imaging is often used to study network functionality in *in vitro* neurons and previous studies indicate that it can be used to study seizure-like behavior in constrained networks. Therefore, we propose to pair calcium imaging with constrained neural networks expressing GEFS⁺-related genetic mutations to assess network functionality.

4.2 MATERIALS & METHODS

4.2.1 Master Fabrication

In this project a polydimethylsiloxane (PDMS) stamp was used to pattern surfaces and constrain network geometry. A silicon master, from which the stamp was cast, was first created. To do so, a 3" silicon wafer (University Wafer) was cleaned with acetone, IPA, and DDW to remove organic residue then dried with a nitrogen gun. After baking for 5 minutes at 200°C to remove solvent residue, ~50 μm of SU-8 3035 (Microchem, Westborough, MA) was applied using a two-step spin process (10 seconds at 500 rpm with a 100 rpm/s ramp up, 30 seconds at 2000 rpm with a 300 rpm/s ramp up). The wafer was then soft baked for 8 minutes, 32 seconds at 95°C and briefly cooled until a thin film formed to prevent the photomask from sticking to the wafer surface. Next, a photomask was placed on the wafer, covered with a thin piece of Pyrex glass to ensure good contact between the wafer and mask, and exposed to UV for 12 seconds. The

master was post-exposure baked for 1 minute at 65°C then 4 minutes at 95°C before being developed by immersing the wafer in SU-8 developer (Microchem, Westborough, MA) for 8 minutes. Following development, the wafer was rinsed with IPA & DDW and gently dried with a nitrogen gun. To improve adhesion and anneal any surface cracks, the master was hard baked for 2 minutes at 150°C. After cooling to room temperature, the master was visually inspected for defects using a stereoscope. The final stamp pattern consisted of a 6x10 grid of annuli, each with an outer diameter of 300 µm and an inner diameter of 100 µm.

4.2.2 Stamp Fabrication

Once a silicon master was fabricated, a PDMS stamp could be created from it. In this case, PDMS (Dow Corning, Midland, MI) was combined in a 10:1 pre-polymer:curing agent ratio. Briefly, the pre-polymer was weighed out in a plastic cup and an appropriate amount of curing agent was added. The solution was then thoroughly mixed and placed in a desiccator to remove any air bubbles that formed during the mixing process. A master containing the desired pattern was rinsed with methanol and DDW and dried with a nitrogen gun before PDMS was slowly poured over it. The PDMS coated master was then baked for two hours at 80°C. Once the wafer cooled to room temperature, the stamping section was removed with a scalpel and spatula before being visually inspected with a stereoscope. Stamps were stored in DDW until needed.

4.2.3 Coverslip Preparation

Prior to experimental use, all glass coverslips were cleaned in an effort to promote neuronal adhesion and growth. Briefly, coverslips were submerged in sterile distilled, deionized water

(DDW) for 15 minutes on a shaker before being transferred to 70% nitric acid and left on a shaker for 24-48 hours. Coverslips were then rinsed in sterile DDW (3 times at 5 minutes each followed by 3 times at 20 minutes each) and stored in 70% ethanol until needed. Immediately before harvesting tissue, cleaned coverslips were briefly flamed, stamped with PLL as outlined in 4.2.2, and placed in plating medium before being stored in a 5% CO₂, 37°C incubator to equilibrate.

4.2.4 Stamping Protocol

A level stamp face is necessary for proper stamping. Therefore, once a stamp was complete, its evenness was evaluated using FITC-tagged PLL. Stamps were cleaned with IPA and DDW then dried with a nitrogen gun to remove any surface debris. Just prior to stamping, the stamp was exposed to an oxygen plasma for one minute. Plasma exposure made the stamp more hydrophilic and promoted even protein adsorption across the stamping surface. Next, a small amount of FITC-tagged PLL (2 µg/µL in PBS) was added to the stamp's surface. The protein was allowed to dry for several seconds. Once it appeared dry, the stamp was gently placed face down on a substrate using tweezers. Care was taken to keep the stamp from shifting once in contact with the substrate. To ensure even pressure was applied across the entire stamping surface, a series of glass plates were added (two 20 g plates and one 40 g plate). The stamp was allowed to dry for one minute before being removed from the substrate using tweezers. Again, care was taken to keep the stamp from dragging along the surface of the substrate. After at least 5 minutes had passed, the stamped coverslip was briefly rinsed with culture water to remove excess protein build-up. Patterned substrates were then visually inspected using a fluorescent microscope. Once a stamp was deemed adequate, the stamping procedure was repeated on clean

coverslips with 1 mg/mL PLL in borate buffer directly before a harvest began. Stamped coverslips were stored in a 5% CO₂, 37°C incubator between stamping and plating.

4.2.5 Neuronal Harvest, Nucleofection, and Culture

Briefly, E18-E19 rat hippocampal neurons were isolated from freshly harvested tissue in accordance with the University of Pittsburgh's IACUC guidelines. Immediately after isolation, cells were nucleofected with 1-3 µg of either pLL3.74-dsRed alone or co-nucleofected with pLL3.74-dsRed and one of three SCN1a plasmids (wild type, A1685V, or L986F) using a Rat Neuron Nucleofector Kit (Lonza, Walkersville, MD). Cells were cultured in media comprised of 96% Neurobasal, 2% B27 (50x), 1% pen-strep, 0.25% 200 mM glutamate, and 0.125% 10 mM glutamate in 10 mM HCl for up to 14 days.

4.2.6 Time-Lapse Calcium Imaging

DIV 10-13 E18-E19 rat hippocampal neurons were incubated with 2.5 mL of Fura2-AM and 2.5 mL of Pluronic 125 in 2.5 mL warm HBS solution for 20 minutes in the dark. Cells were then placed in a clean dish of warm HBS for 20 minutes in the dark. Once cells were ready, warm HBS was added to the perfusion system and the vacuum was adjusted until flow was steady and uniform. After selecting the desired field of view, a bipolar field electrode was placed near a cell on the ring. Cells were selected using the ROI selection tool in MetaFlour software (Molecular Devices, Sunnyvale, CA) and a baseline bright field image was taken. Fluorescence of selected ROIs were then verified and any pLL3.74-daRed⁺ cells were identified. 60 seconds of baseline 340/380 fluorescence was obtained before any stimulation began. Three minutes of stimulus

response data was then obtained, with a 30 V stimulus being applied for 5 seconds (2 s pulses with 200 ms intervals beginning 4 seconds into a trial). Following three trials for a given bath, the subsequent bath was perfused onto the cells for two minutes before a new stimulus trial began. In between coverslips, 50 mL of DDW was perfused through the system to remove any residual bath solution.

Prior to drug trials, baseline trials were performed to ensure that recovery times between stimulation would be sufficient. In this case, cells were exposed only to a control HBS bath. Stimulation was repeated 5 times using experimental stimulation parameters. Traces were visually assessed for dampening and repeatability.

For drug trials, final bath solutions were: HBS, 10 μ M BMI, 0.6 mM VPA, 10 μ M CBZ, and 30 mM high K^+ HBS. Trials were as follows: VPA with BMI (i.e. HBS, BMI, VPA, high K^+ baths applied in sequential order), VPA without BMI (i.e. HBS, VPA, and high K^+ baths applied in sequential order), CBZ with BMI (i.e. HBS, BMI, CBZ, and high K^+ baths applied in sequential order), CBZ without BMI (i.e. HBS, CBZ, and high K^+ baths applied in sequential order). Each drug trial was repeated in three different cultures. Resulting 340/380 fluorescence vs. time profiles were analyzed in Excel and SPSS v.22 (IBM, Chicago, IL). Data was reported as resulting p-value, effect size, and general trend.

4.2.7 Statistical Analysis

Statistical analysis was performed using SPSS v. 22 (IBM, Chicago, IL). Because data was not normally distributed, a non-parametric Kruskal-Wallis test was used to assess significance while η^2 was used to determine effect size [112]. Effect size of 0.2-0.12 was considered small, 0.13-0.25 was considered medium, and 0.26 or higher was considered large. Before beginning

statistical analysis, unresponsive cells were discarded. We defined unresponsive cells as those whose starting Fmax (the maximum 340/380 value recorded during the one minute of baseline activity preceding each stimulation) was less than 0.05 units from its Fmax following stimulation. Once the final data set was ready, we accounted for variable baselines by normalizing data to a trial's average baseline value then logarithmically transforming the data set.

4.2.8 *In Vitro* Toxicology Testing

Because AED studies are not often done in neurons *in vitro*, we elected to determine drug dosing prior to calcium imaging using a Trypan blue exclusion assay [144]. To assess cytotoxicity of given bath solutions, a Trypan blue exclusion assay was used on DIV 10 E18-E19 rat hippocampal neurons. To begin, cells were perfused with warm HBS for 3-5 minutes at room temperature before being exposed to a drug bath for 15 minutes. Immediately following drug exposure, cells were rinsed with warm HBS for 1 hour with solution changes every 10 minutes to remove any drug traces. After 1 hour, cells were briefly placed in a 0.4% Trypan blue solution (<1 min.) and rinsed in room temperature HBS to remove excess dye. Cells were then placed in cold 4% PFA for 30 minutes at 4°C. Afterward, cells were rinsed with PBS and dehydrated in an ethanol series (twice for 30 minutes each in DDW, 3 minutes in 50% ethanol, 3 minutes in 80% ethanol, twice for 3 minutes each in 95% ethanol, and 3 minutes in 100% ethanol). Cells were then mounted with Fluoromount G before being imaged at 20x. The number of Trypan blue positive cells vs. the total number cells in three random ROIs was used to calculate cytotoxicity (cell toxicity was defined as the percent of Trypan blue positive cells in a given ROI). Data is presented as the mean \pm standard error of the mean. A one-way ANOVA was performed to

determine statistically significant differences between groups. Post-hoc analysis was performed using a Scheffe test (SPSS v22, Chicago, IL).

In these studies, we selected three doses to test per drug. These were presumed to be sub-therapeutic, therapeutic, and toxic based on literature review. For CBZ, those doses were 1 μ M (sub therapeutic), 10 μ M (therapeutic), and 100 μ M (toxic). For VPA doses were 0.6 μ M (sub therapeutic), 0.6 mM (therapeutic), and 5 mM (toxic). These ranges were selected for evaluation based on available literature as well as calculations involving common doses and estimated blood brain barrier permeability for each drug. BMI was not subject to toxicity testing as it is commonly used in *in vitro* culture work. These studies used 10 μ M BMI because previous studies showed little results with BMI below 10 μ M [92].

4.3 RESULTS

In this chapter, ring shaped networks of transfected and un-transfected neurons were successfully generated (Figure 31b). Even distribution of the cell adhesion protein poly-L-lysine encouraged cell adhesion across the ring and prevented neurospheres from forming (Figure 31a). The average number of cells per ring network was found to be slightly lower at ~30 cells/ring than the previously reported 40-60 cells/ring in un-transfected ring networks [92]. Overall, our ring networks averaged 31 cells/ring (33 ± 1.66 for negative control networks, 33 ± 2 for pLL3.74-dsRed networks, 30 ± 2 for SCN1aWT networks, 33 ± 2 for SCN1a A1685V networks, and 27 ± 2 for SCN1a L986F networks; Figure 32). The number of cells per ring was uniform across most genotypes with the only exception being a significantly higher number of A1685V cells compared to L986F cells.

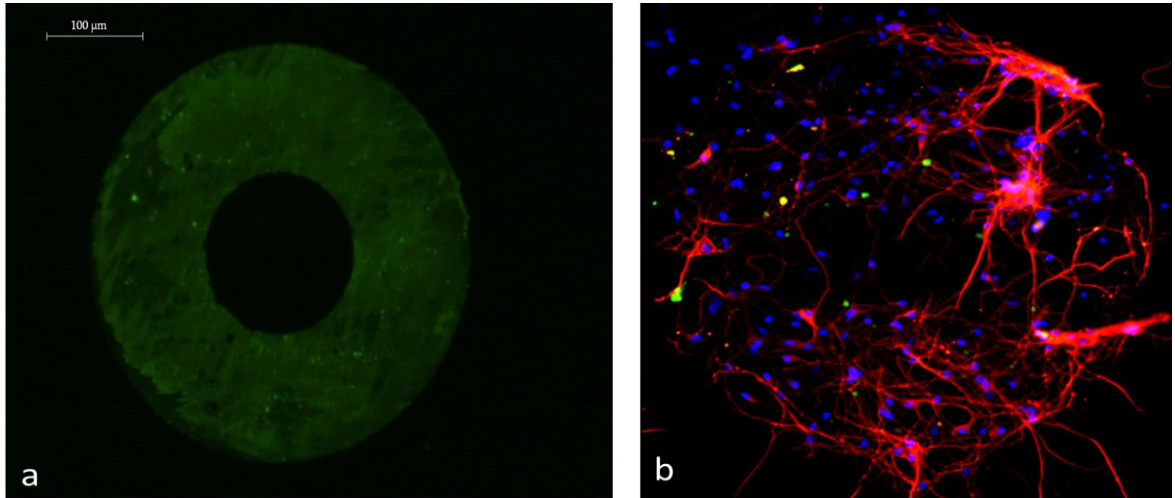


Figure 31: Microcontact Printing Ring Patterns

Above: a) Glass coverslip stamped with FITC-tagged PLL (2 mg/mL in PBS). b) Neurons growing on stamped substrate. Blue: nuclei (DAPI); red: MAP2 (Alexa 647).

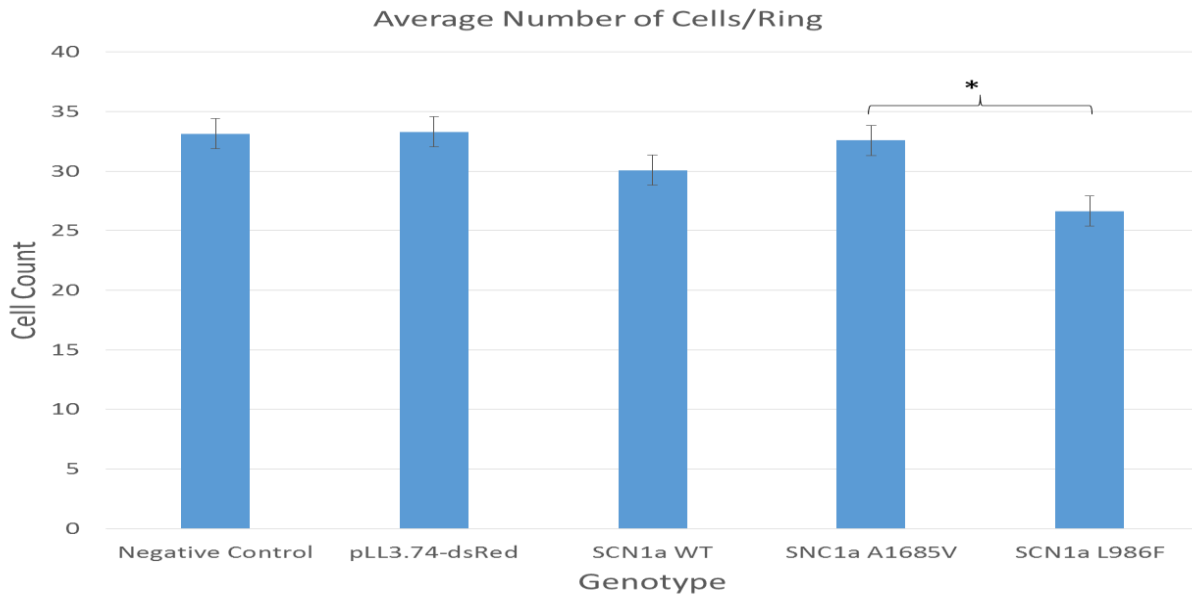


Figure 32: Average Number of Cells per Ring Network

Above: Average number of cells per ring for various genotypes \pm standard error. *: $p < 0.05$ as determined by 1-way ANOVA and post-hoc Scheffe test

Prior to calcium imaging experiments, we assessed drug toxicity using a Trypan blue exclusion assay. VPA and CBZ appeared to have a dose-dependent effect on cell death across all genotypes (Figure 33). Similar levels of cell death occurred in control baths for both drug trials, which is to be expected as the same control bath composition was used in both tests. Valproic acid induced cell death was determined to be $11\% \pm 1$ for HBS control bath, $14\% \pm 1$ for 0.06 mM (sub therapeutic dose), $19\% \pm 1$ for 0.6 mM (therapeutic dose), and $24\% \pm 1$ for 0.6 mM (toxic dose) (Figure 33a). Carbamazepine induced cell death was determined to be $10\% \pm 1$ for HBS control bath, $13\% \pm 1$ for 1 μM (sub therapeutic dose), $17\% \pm 1$ for 10 μM (therapeutic dose), and $22\% \pm 1$ for 100 μM (toxic dose) (Figure 33b). In general, cell death increased with increasing drug dose in both cases, with all genotypes displaying a significantly higher cell death in the toxic dose compared to the control HBS bath. Cell death was approximately the same for the control HBS bath and the low doses of each drug, although the low dose of VPA resulted in a significantly higher cell death in L986F cells while the low dose of CBZ resulted in a significantly higher cell death in SCN1aWT cells.

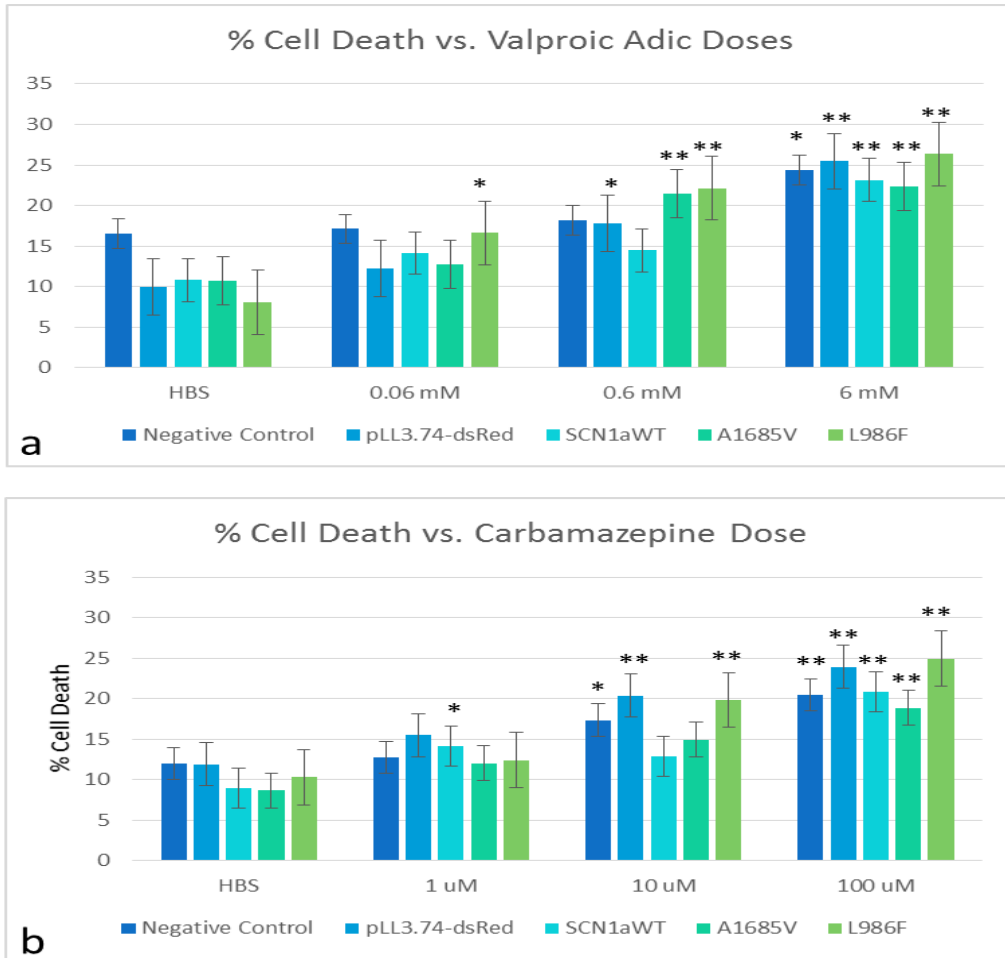


Figure 33: Valproic Acid & Carbamazepine Induced Cell Death

Above: Anti-epileptic drug induced cell death from valproic acid (a) and carbamazepine (b). Data are presented as the mean \pm standard error of the mean. *: $p < 0.05$; **: $p < 0.01$ between a given drug dose and the control HBS bath, as determined by 1-way ANOVA and post-hoc Scheffe test.

Before beginning calcium imaging drug trials, baseline images were collected to evaluate rest times between stimulation. Repeatable traces were obtained for all five stimulations in negative control and pLL3.74-dsRed trials (Figure 34a and b). Wild type networks experienced some dampening, typically beginning at the fourth stimulus (Figure 34c). Both A1685V and L986F cultures displayed more prolonged responses (responses to stimuli that do not recover to pre-stimulus levels) as stimulation progressed (Figure 34d and e). Additionally, they were prone to some signal dampening beginning around the fourth consecutive stimulation (data not shown).

Figure 34 also provides examples of the variety of responses commonly seen during our calcium imaging experiments including: spontaneous activity (panels a, d, and e); prolonged response to stimuli (panels a, b, c, d, and e); and oscillatory behavior (panels c and d). While most genotypes displayed spontaneous and prolonged activity at some point during a trial, transfected cells appeared to be more likely to display prolonged responses and oscillatory behavior.

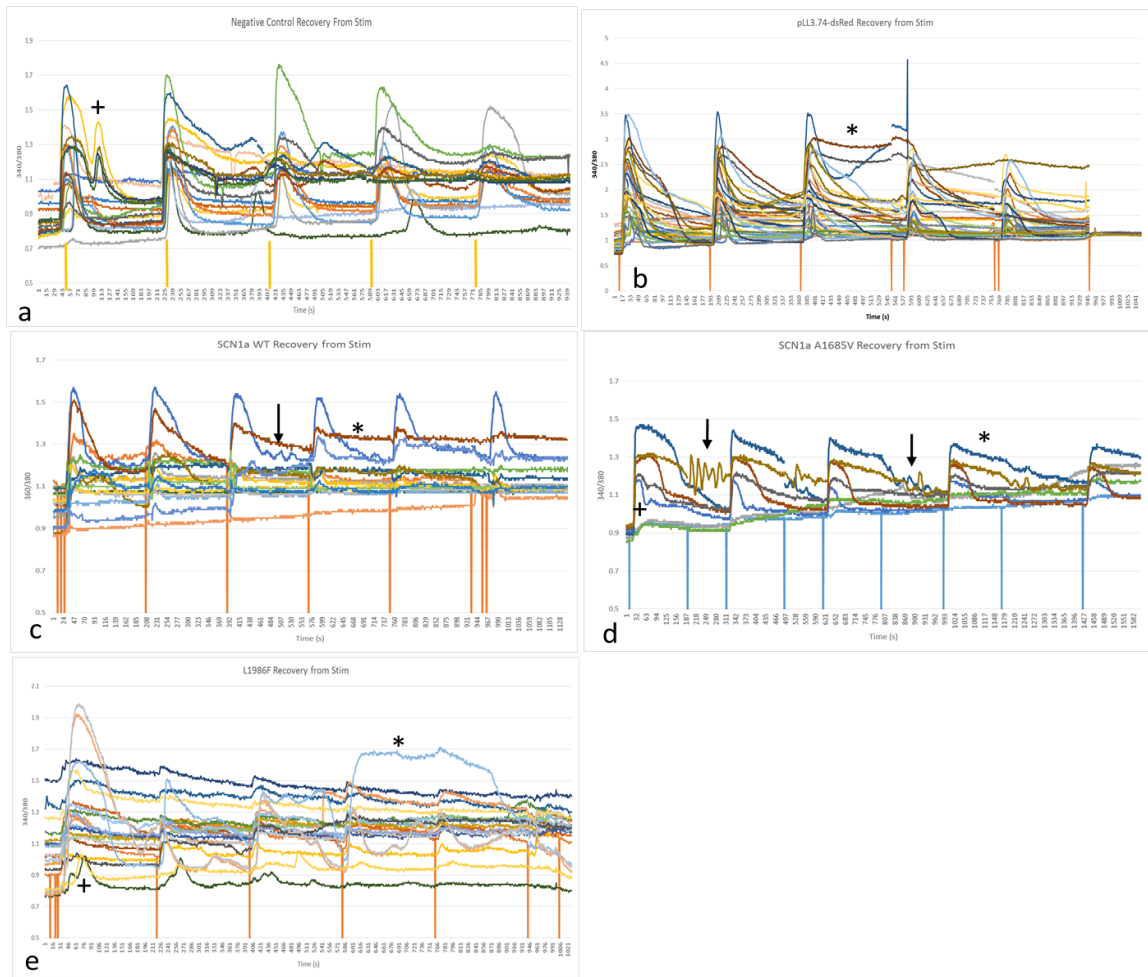


Figure 34: Representative Traces of Baseline Calcium Activity

Above: representative calcium imaging traces of 340/380 vs. time recorded during baseline trials for a) negative control cells, b) pLL3.74-dsRed cells, c) SCN1a WT cells, d) SCN1a A1685V cells, e) SCN1a L986F cells. Arrows: oscillatory behavior; *: prolonged activity; +: spontaneous activity. Stimulations are indicated by vertical lines.

Following preliminary calcium imaging studies, we began initial drug trials. In induced trials, bicuculline methiodide (BMI) was used to induce seizure activity prior to AED application. High K^+ was added at the end of each experiment to ensure that networks were still active. Additionally, drug trials were performed without BMI application to investigate intrinsic changes in network activity. In all cases, calcium responses were fairly variable between trials for the same genotype and same drug, making data analysis challenging. In the end, we decided to focus on three of our five original genotypes (negative control cells, pLL3.74-dsRed, and A1685V cells).

For all experiments, cell activity was assessed by calculating the time needed to reach maximum fluorescence, or Time-to- F_{\max} , following electrical stimulation. We assumed an increase in Time-to- F_{\max} (TTF) to indicate an increase in activity because a higher F_{\max} should take longer to reach or because cells that have prolonged responses to stimuli may have a delayed F_{\max} (Figure 35).

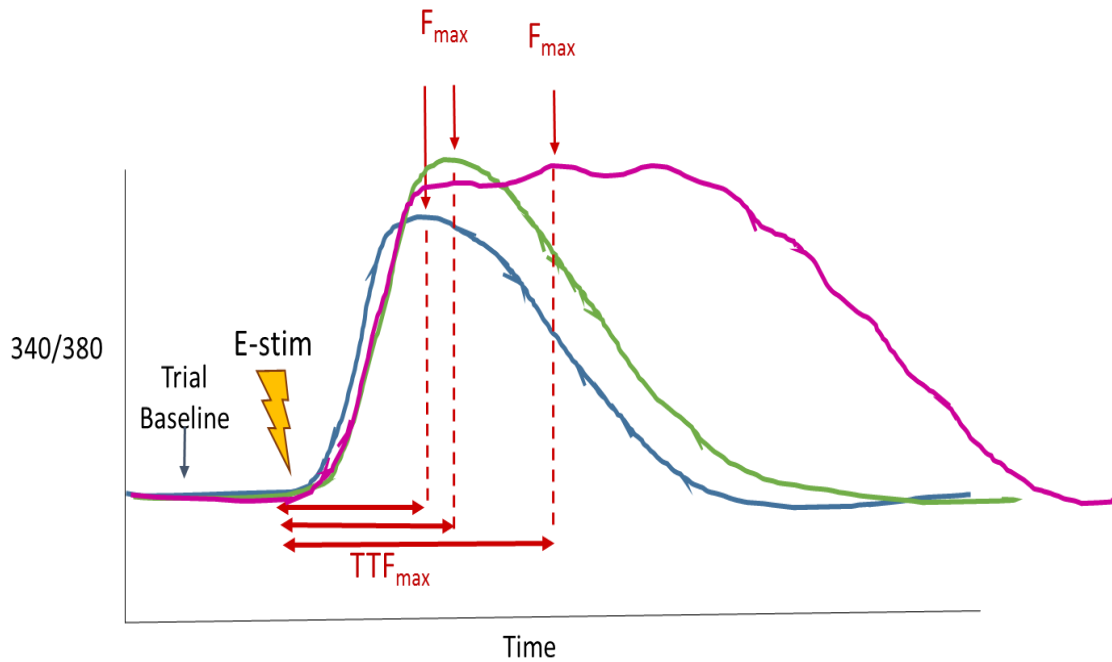


Figure 35: Connection Between Time-to-F_{max} and Cell Activity

Above: Schematic of Time-to-F_{max} (TTF) for a cell with a moderate response (blue), an elevated response (green), and a prolonged response (pink) demonstrating how elevated or prolonged responses are likely to result in a longer TTF.

In BMI + VPA trials, an increase in TTF from HBS to BMI baths was observed in both pLL3.74-dsRed and A1685V, as expected (Table 6). Although this trend was not significant, it did have a small effect size. Negative control cells, on the other hand demonstrated a decrease in TTF. This unexpected result paired with the lack of significance and low effect size may indicate that BMI dose was too low. However, a significant decrease in activity was noted for all genotypes when comparing HBS to VPA and BMI to VPA, also as expected. When looking at HBS to high K^+ results, a medium increase was seen for all genotypes, but this was only significant in transfected and un-transfected controls, possibly indicating that A1685V cells are not recovering as quickly from VPA-reduced activity as the controls. Finally, increases in TTF were observed when comparing BMI to high K^+ and VPA to high K^+ for all genotypes, as expected. However, this trend is only significant for pLL3.74-dsRed cells. The lack of significance when comparing BMI to high K^+ may be because cells reach a maximum increase in activity when exposed to BMI and are therefore not able to exceed that during high K^+ exposure. The lack of significance when comparing VPA to high K^+ may indicate that, although cells respond to high K^+ , their activity is too depressed from VPA exposure to significantly recover in the time allotted. Representative traces illustrate the subtle trends observed as well as the variability within single trials (Figure 37).

In intrinsic VPA trials, a decrease in activity from HBS to VPA was noted for all genotypes, as expected (Table 5). However, this was not statistically significant for any group and the effect size was low. This may indicate that higher than expected doses of VPA are required to significantly impact the network. Additionally, increases in activity were noted for both HBS vs. high K^+ and VPA vs. high K^+ , as expected. However, this trend was not significant for transfected or un-transfected cells which may indicate that although these cells

respond to high K^+ , they were not given sufficient time to recover from VPA depression before high K^+ application. A1685V cells, however, did show a significant increase in activity from HBS to high K^+ and VPA to high K^+ , potentially demonstrating that these mild mutants were either more reactive to high K^+ following VPA exposure or that they were less reactive to VPA than the controls were. Representative traces illustrate the subtle trends observed as well as the variability within single trials (Figure 36).

Table 5: Time-to-Fmax P-values, Effect Size, & Trends for Valproic Acid Trials

P-values, Effect Size, & Trends for Time-to-Fmax Data for Valproic Acid Trials without Bicuculline Methiodide (Normalized & Log Transformed)						
Genotype		HBS-VPA		HBS-High K		VPA-High K
Negative Control						
pLL3.74-dsRed	0.074		0.107		0.107	
SCN1a A1685V	1.000		<i>0.000</i>		<i>0.000</i>	

Above: Arrow direction indicates general trend in Time-to-F_{max}. Arrow color indicates the η^2 effect size (grey: no effect, red: small, yellow: medium, green: large). P-values between 0.01 and 0.05 shown in bold red. P-values less than 0.01 shown in bold, italic red. Significance determined by Kruskal-Wallis test.

Table 6: Time-to-Fmax P-values, Effect Size, & Trends for Induced VPA Trials

P-values & Trends for Time-to-Fmax Data for Valproic Acid Trials with Bicuculline Methiodide (Normalized & Log Transformed)									
Genotype	HBS-BMI	HBS-VPA	HBS-High K	BMI-VPA	BMI-High K	VPA-High K			
Negative Control	0.682		<i>0.000</i> 	0.040 	<i>0.001</i> 	0.776 	1.000		
pLL3.74-dsRed	1.000		<i>0.000</i> 	0.033 	<i>0.000</i> 	<i>0.016</i> 	<i>0.003</i>		
SCN1a A1685V	1.000		<i>0.014</i> 	1.000 	<i>0.000</i> 	1.000 	0.124		

Above: Arrow direction indicates general trend in Time-to-F_{max}. Arrow color indicates η^2 effect size (grey: no effect, red: small, yellow: medium, green: large). P-values between 0.01 and 0.05 shown in bold red. P-values less than 0.01 shown in bold, italic red. Significance determined by Kruskal-Wallis test.

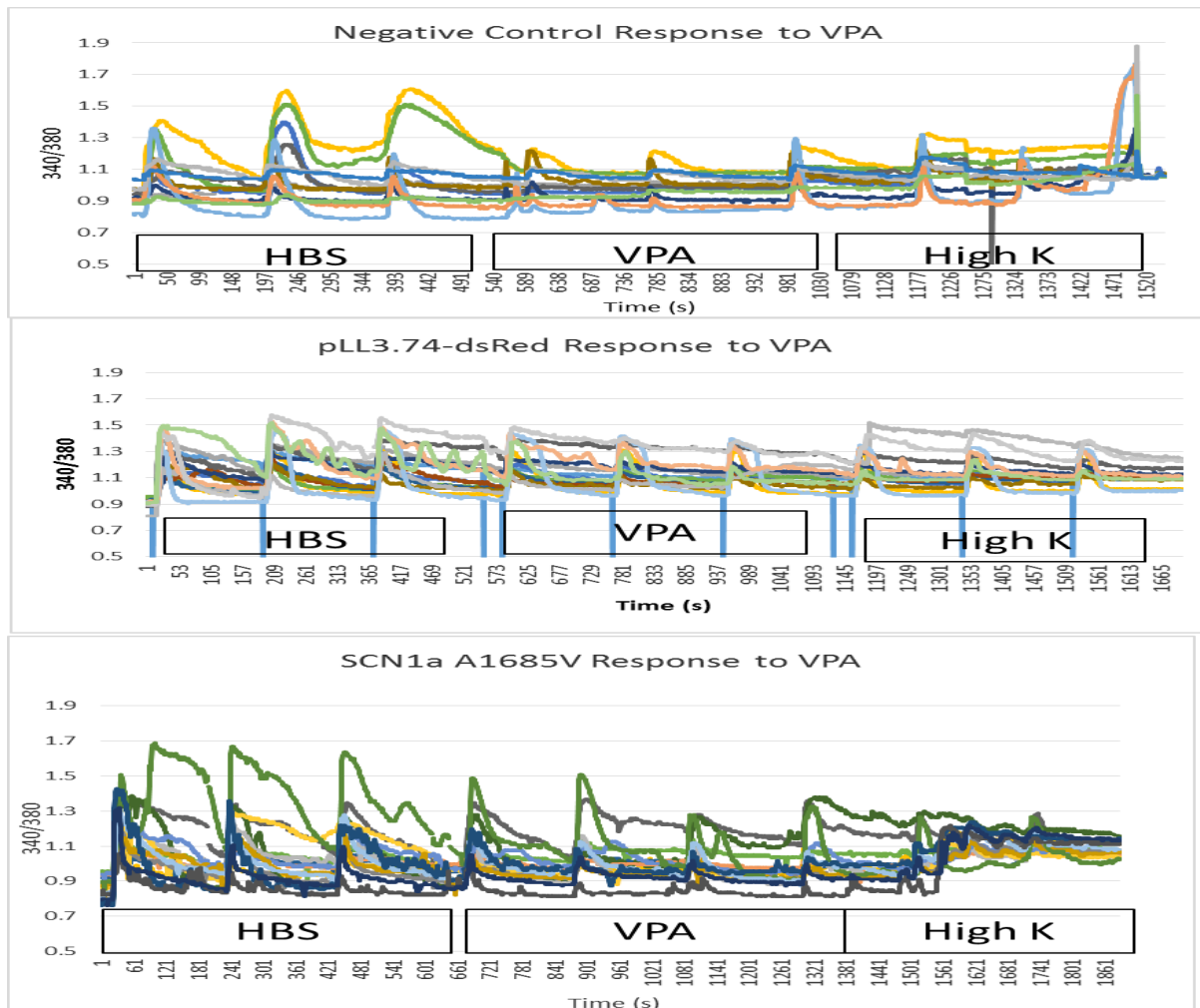


Figure 36: Representative Calcium Traces Following VPA

Above: Representative calcium imaging traces of 340/380 vs. time following VPA trials. Top: Negative control cells, middle: pLL3.74-dsRed cells, bottom: SCN1a A1685V cells. Stimulations are indicated by vertical lines.

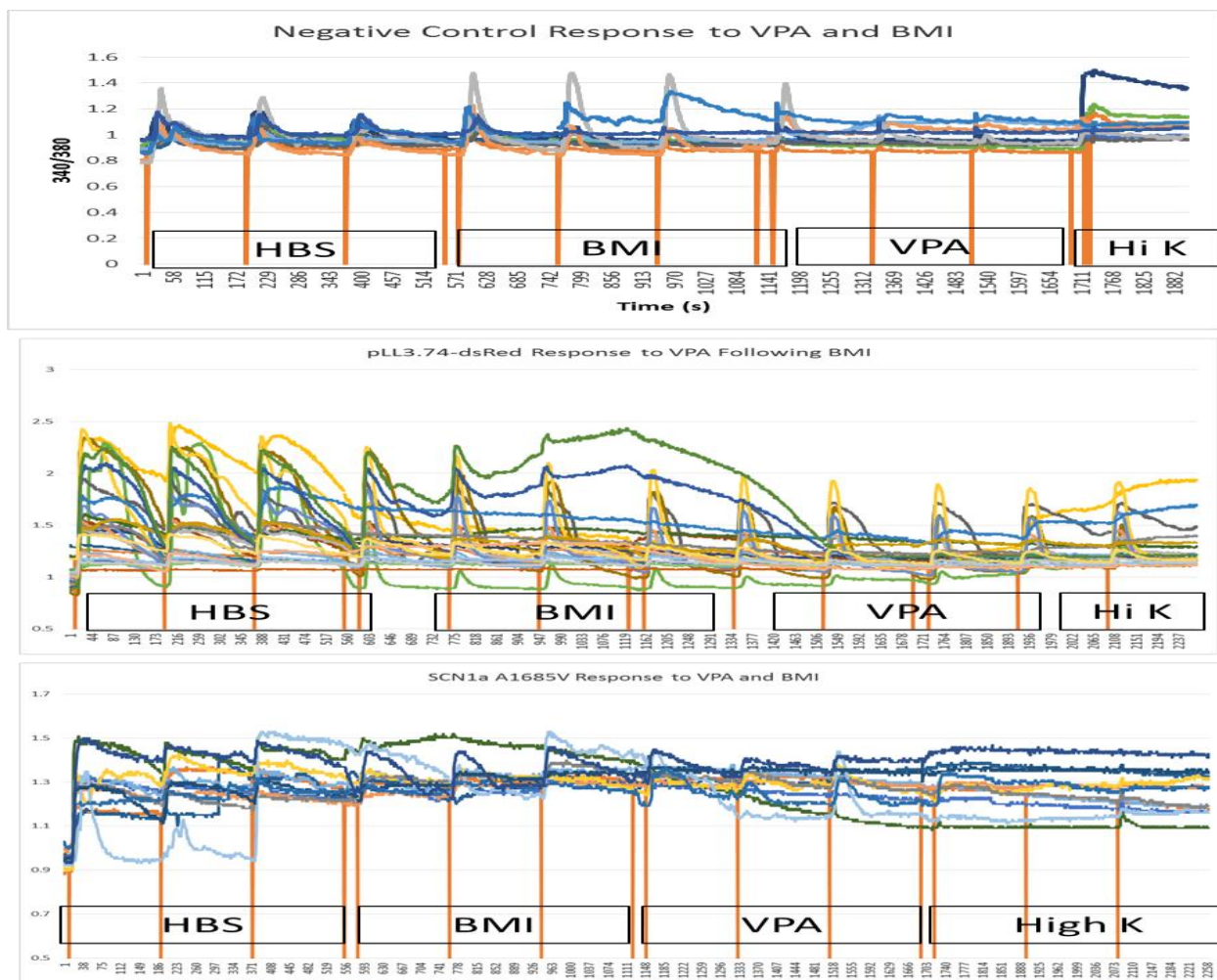


Figure 37: Representative Calcium Traces Following BMI & VPA

Above: Representative calcium imaging traces of 340/380 vs. time following BMI VPA trials.
 Top: Negative control cells, middle: pLL3.74-dsRed cells, bottom: SCN1a A1685V cells.
 Stimulations are indicated by vertical lines.

For CBZ exposure following BMI, all genotypes demonstrated an upward trend in TTF for HBS vs. BMI, HBS vs. high K^+ , BMI vs. high K^+ , and CBZ vs. high K^+ as expected (Table 8). Additionally, negative control cells displayed a decrease in TTF when comparing both HBS to CBZ and BMI to CBZ. This is to be expected because, although CBZ is thought to trigger seizure activity in GEFS⁺ patients, it should cause a decrease in network activity in healthy patients. Surprisingly, pLL3.74-dsRed cells exhibit an increased TTF trend for both HBS vs. CBZ and BMI vs. CBZ. The longer TTF when comparing HBS to CBZ could be attributed to the significant increase between control and BMI baths leading to higher baseline values going into CBZ trials. If cells become too active during BMI exposure, they may not be able to sufficiently recover to below baseline during CBZ exposure. However, this does not explain the increase in TTF from BMI to CBZ. Finally, A1685V cells demonstrate the expected increase in TTF for HBS vs. CBZ but a surprising decrease in TTF from BMI to CBZ. However, these trends are not significant, possibly indicating that our CBZ dose could be increased. One last observation from these trials pertains to A1685V cells. As all of the drugs in this trial would be expected to increase TTF for SCN1a mutants, it is surprising that A1685V does not show any significant gains. This could be caused by a number of things including elevated baseline due to a decrease in network inhibition, insufficient drug doses, or cells that are responding maximally for electrical stimulation regardless of bath. Representative traces illustrate the subtle trends observed as well as the variability within single trials (Figure 39).

As for intrinsic CBZ trials, both transfected and un-transfected cells exhibited a decrease in activity from HBS to CBZ, as expected (Table 7). Interestingly, A1685V cells did show an increase in TTF when exposed to CBZ following HBS, as expected. However, this trend was not significant, possibly indicating that CBZ doses were too low to impact mutant networks. As for

the comparisons between HBS and High K⁺, and CBZ and High K⁺, all genotypes displayed an increase in TTF, as expected. These trends are only significant for negative control cells, which makes sense because they did not demonstrate a significant decrease in TTF following CBZ exposure, so they would presumably have a higher baseline going into high K⁺ exposure compared to pLL3.74-dsRed cells. Neither trend was significant for A1685V cells. A1685V's combination of minimal response to both CBZ and high K⁺, both of which should increase activity, may point to an elevated baseline for this genotype. Representative traces illustrate the subtle trends observed as well as the variability within single trials (Figure 38).

Table 7: Time-to-Fmax P-values, Effect Size, & Trends for Carbamazepine Trials

P-values, Effect Size, & Trends for Time-to-Fmax Data for Carbamazepine Trials without Bicuculline Methiodide (Normalized & Log Transformed)						
Genotype	HBS-CBZ		HBS-High K		CBZ-High K	
Negative Control	0.529		0.039		<i>0.002</i>	
pLL3.74-dsRed	<i>0.000</i>		0.586		0.091	
SCN1a A1685V						

Above: Arrow direction indicates general trend in Time-to-F_{max}. Arrow color indicates η^2 effect size (grey: no effect, red: small, yellow: medium, green: large). P-values between 0.01 and 0.05 shown in bold red. P-values less than 0.01 shown in bold, italic red. Significance determined by Kruskal-Wallis test.

Table 8: Time-to-Fmax P-values, Effect Size, & Trends for Induced CBZ Trials

P-values & Trends for Time-to-Fmax Data for Carbamazepine Trials with Bicuculline Methiodide (Normalized & Log Transformed)									
Genotype	HBS-BMI	HBS-CBZ	HBS-High K	BMI-CBZ	BMI-High K	CBZ-High K			
Negative Control	0.168 	0.620 	<i>0.001</i> 	<i>0.001</i> 	<i>0.000</i> 	<i>0.000</i> 			
pLL3.74-dsRed	<i>0.012</i> 	<i>0.008</i> 	<i>0.000</i> 	1.000 	0.372 	0.958 			
SCN1a A1685V									

Above: Arrow direction indicates general trend in Time-to-F_{max}. Arrow color indicates η^2 effect size (grey: no effect, red: small, yellow: medium, green: large). P-values between 0.01 and 0.05 shown in bold red. P-values less than 0.01 shown in bold, italic red. Significance determined by Kruskal-Wallis test.

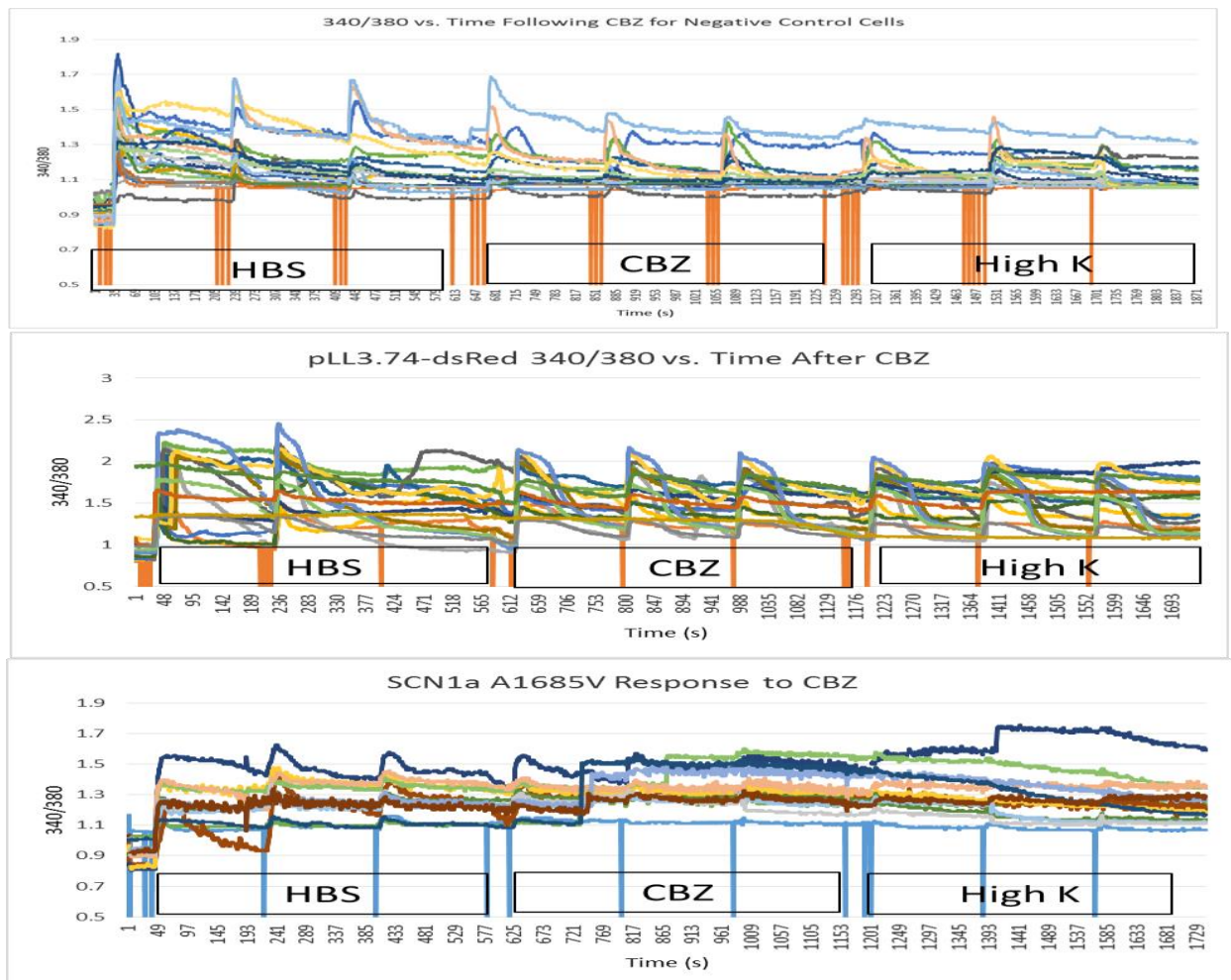


Figure 38: Representative Calcium Traces Following CBZ

Above: Representative calcium imaging traces of 340/380 vs. time following CBZ trials. Top: Negative control cells, middle: pLL3.74-dsRed cells, bottom: SCN1a A1685V cells. Stimulations are indicated by vertical lines.

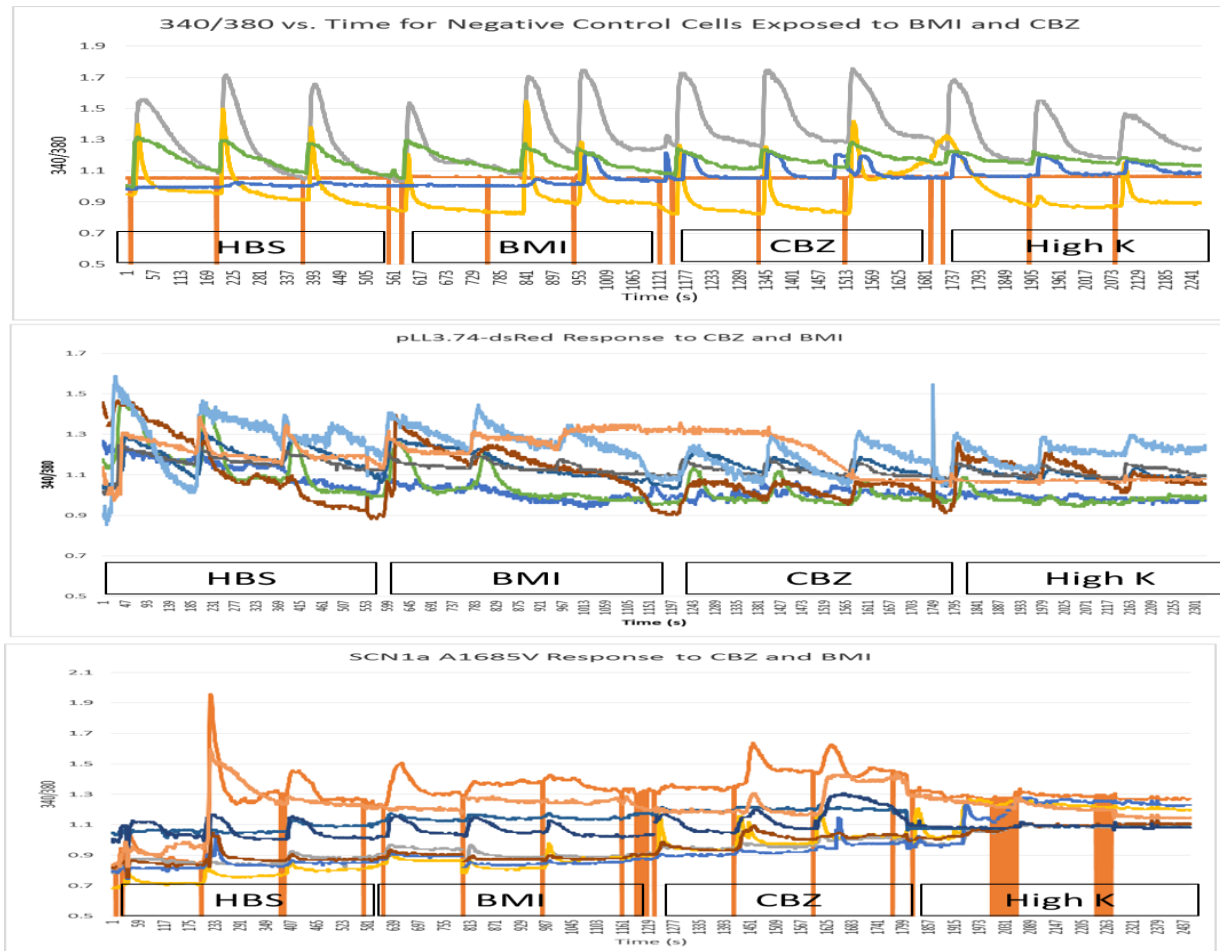


Figure 39: Representative Calcium Traces Following BMI & CBZ

Above: Representative calcium traces of 340/380 vs. time following BMI CBZ trials. Top: Negative control cells, middle: pLL3.74-dsRed cells, bottom: SCN1a A1685V cells. Stimulations are indicated by vertical lines.

4.4 DISCUSSION

This chapter examined the functional activity of small, genetically modified neuronal networks with confined geometry. To our knowledge, this is the first time that transfected neurons have been evaluated as a possible *in vitro* epilepsy model and also the first time an *in vitro* epilepsy model with confined geometry has been proposed.

Networks were composed of similar numbers of cells regardless of cell type, indicating that transfection and SCN1a mutations had little effect on cell viability (Figure 32). However, our severe mutant (L986F) presented with the fewest number of cells per ring which may be a residual effect of this genotype expressing the most extreme mutation possibly causing higher rates of cell death and more delicate cells in general. Additionally, the number of cells per ring was slightly lower than the 40-60 cells/ring reported in previous work [92]. The reduction is likely due to the modified culture method required to sustain transfected cells.

Baseline studies demonstrated a variety of calcium transients including spontaneous activity, oscillatory behavior, and prolonged responses. Prolonged responses may be due to slower recovery times in transfected cells or may originate from glia which tend have slower response times. It is possible that the SCN1a mutations encourage glia to take a more prominent role in network activity.

In all drug trials, calcium responses were fairly variable between trials for the same genotype and same drug making data analysis challenging. Several factors may be responsible for the variation. One possibility is that some of the large, prolonged responses are coming from glia while the briefer responses are neuronal, as our phenotypic analysis showed that cultures were composed of a mix of neurons and glia. Additionally, culture composition between DIV 10 and 13 may be variable, as was noted in our previous phenotypic analysis. Most cultures were

viable for two to three weeks, with some having noticeable cell death around DIV 14 and other lasting until DIV 21. Additionally, nucleofection is only stable for 12-14 days [70]. The majority of calcium imaging experiments were performed between DIV 10 and 13 to allow synapses to mature (begins at DIV 7) and before nucleofection stability declined [93, 145, 146]. However, it is possible that some of the cultures studied began to lose their assigned genotype prior to imaging, which could confound results.

Additionally, much of our interest in confining network geometry lies in the assumption that unpatterned substrates allow *in vitro* cultures to make random intracellular connections that vary from coverslip to coverslip but that constrained networks would exhibit consistent behavior. However, the majority of microcontact printing work up to this point focused on constraining network geometry for logistical purposes such as focusing cells to an electrode, as opposed to minimizing variability in network behavior [93, 147, 148]. The wide range of calcium imaging responses observed in this chapter suggests that controlling network geometry may not be sufficient to reduce *in vitro* variability on a functional level. Instead, an additional step of segregating cell type may be necessary to better mimic the topological organization of various brain regions. To address this possibility, closer examination of functional activity in patterned vs. unpatterned networks is warranted. Additionally, it may be prudent to examine network connectivity prior to and immediately following drug trials using a live cell dye like Lucifer Yellow. This would allow networks to be segregated based on connectivity as opposed to even cell body distribution. It may be that some rings have even cell body distribution but poor connectivity resulting in a varied response from a more well-connected network.

Finally, the drug bath compositions as well as subsequent drug application protocol may need to be examined closer- specifically, drug doses and possible drug interactions. Our drug

doses were based on a combination of available literature pertaining to other *in vitro* work (not necessarily neuronal), *in vivo* data adjusted for blood-brain barrier permeability, and our Trypan blue toxicity testing. However, because few AED trials are done in neurons *in vitro*, it is possible that our “therapeutic” doses were actually sub-therapeutic. Trypan blue exclusion assays illustrated a dose-dependent toxicity to both VPA and CBZ. However, even our “toxic” doses were well below LD₅₀ - the dose at which 50% of cells are killed [149]. Therefore, we should be able to increase to our “toxic” dose without serious detrimental effects to our cells. Furthermore, BMI-AED interaction could have a potentially confounding effect if BMI is failing to thoroughly dissociate uniformly across cultures prior to AED application so rinse times between drug applications may need to be reassessed.

4.5 CONCLUSIONS

This chapter examined the functional activity of small networks of patterned neurons that have been transfected to express epilepsy-related SCN1a mutations. Ring-shaped networks of transfected and un-transfected neurons were successfully created and network activity could be assessed using time-lapse calcium imaging. Additionally, the effect of multiple drugs, including AEDs, were quickly and consistently evaluated. While our goal was to study seizure activity in genetically-based seizures, our methods could easily be modified to study chemically or electrically induced seizures. Although this work acts as a proof-of-concept and lays a foundation for future studies, there are many improvements yet to be made. Several of these are discussed in the following chapter.

5.0 PROJECT SUMMARY

As a whole, this project demonstrated that a genetically based *in vitro* epilepsy model could be created from wild type and genetically modified hippocampal neurons and that these genetically modified cultures could also be geometrically constrained. To our knowledge, this is the first time that a potential *in vitro* epilepsy model has been created using genetic modifications in primary neurons. Additionally, we believe this is the first time that genetically modified neurons have been constrained using microcontact printing. We have successfully demonstrated SCN1a plasmid generation as well as successful transfection and culture of neurons expressing those plasmids (Chapter 2, page 25). Furthermore, we have evaluated the composition of these networks and determined subtle compensatory trends that bear further review (Chapter 3, page 47). Finally, we have evaluated network functionality and observed subtle but promising trends, including responses to AEDs which mimic those seen *in vivo* (Chapter 4, page 83). A neuronal *in vitro* epilepsy model of intrinsic, rather than induced, seizure activity would fill a significant gap in current epilepsy research. Additionally, it would meet the NINDS's suggested guidelines for new epilepsy models including cost-effectiveness, propensity for examining disease mechanisms, ability to be used in high-throughput testing, and potential for use in personalized medicine.

Moving forward, we would suggest the incorporation of two additional technologies and one new direction of investigation that could help build a stronger foundation for our proposed *in*

vitro epilepsy model. The first would be to add a fluorescent reporter gene to the SCN1a plasmids used. This would quickly allow for definite confirmation of experimental cells expressing the SCN1a mutant to rule out the possibility that transfection of the fluorescent marker is occurring without the SCN1a plasmid in some cells. However, the increased plasmid size would warrant a re-evaluation of transfection efficiency.

Secondly, we recommend incorporation of additional methods to confirm other ways to constrain network geometry, whether by other microtechniques or by using other patterns. Microcontact printing has waned in popularity in the past few years because, although easy, inexpensive, and quick, it can be more art than science. Even a small movement of the hand, stamp, or coverslip during stamping can result in poor pattern adherence. Therefore, more substrates than necessary are generally prepped in case a planned coverslip does not display the desired network geometry. While this is a relatively easy fix, if the goal is to create an inexpensive *in vitro* model, an effort should be made to increase pattern repeatability and further reduce costs. One option for doing so would be to explore the use of photosensitive silicone where cells can be directly plated onto a biocompatible master. Additionally, slightly more complex patterns may provide additional control over network geometry which may help reduce culture-to-culture variability.

Lastly, we recommend a closer examination of the role glia play in these networks. Glia are known to be essential to proper neuronal development and synapse maturation *in vitro* [63, 150]. More recently, glia has been implicated in seizure propagation [151, 152]. Therefore, performing a few experiments where cells are cultured using the Banker sandwich method may determine whether the large, prolonged calcium responses can be attributed to glia. Briefly, the Banker method involves plating purely neuronal cultures on one coverslip and sandwiching it

together with a second coverslip containing mature glia [153]. The proximity of the coverslips allows neurons and glia to exchange chemokines, thus ensuring proper synapse development. However, the separate coverslips would also allow both purely neuronal and purely glial cultures to be examined independently once the coverslips were detached. Additionally, the reverse situation can be employed, where glia are transfected to express SCN1a mutations while neurons are not transfected, to examine how $\text{Na}_v1.1$ mutations in glia may drive seizure propagation. Glia's role in epilepsy is not widely understood and has only become a topic of interest in recent years.

Overall, we hope that this project can serve as a building block for future research into the creation of an *in vitro* epilepsy model and that it will open up the discussion of *in vitro* “chips” for high throughput testing of AEDs. One long-term possibility would be to attempt to use a chip for personalized medicine. This appears particularly promising given the recent, disease specific induced neuron work by Goldstein and Liu [154, 155]. Goldstein's group demonstrated an ability to create induced pluripotent stem cells (iPSCs) from primary skin fibroblasts of Alzheimer's patients. The primary fibroblasts could be reprogrammed into iPSCs then differentiated into neuronal cultures that displayed normal electro-physical activity. Even more recently, Liu *et al* used similar techniques to create iPSCs from SMEI patients presenting with SCN1a mutations [155]. These iPSCs were differentiated into neurons which displayed altered sodium channel current consistent with SMEI.

5.1 EPILEPSY ON A CHIP

The idea of using a fairly non-invasive skin biopsy to generate a personalized cell line that could be plated on an inexpensive, high-throughput chip to screen individual or combinations of AEDs for a specific patient could truly be a field-changing product. Specifically, a commercially available epilepsy “chip” could be useful in quickly finding the best AED candidates for treatment in an individual patient, which would greatly cut down on the time between initial diagnosis and controlled seizure status. Additionally, chips could be used to identify patients who are likely to have intractable epilepsies, as their cells would not respond to available AEDs. Lastly, inexpensive, disposable chips could be a useful tool for developing new AEDs because the mechanisms behind different epilepsies, especially intractable epilepsies, could be examined. Once more about the underlying disease mechanism is understood and specific protein targets are identified, more effective AEDs could be developed.

APPENDIX

LIST OF ACRONYMS

AED(s): anti-epileptic drug(s)

AIS: axon initial segment

AraC: cytosine arabinoside

BMI: bicuculline methiodide

CBZ: carbamazepine

DAPI: 4',6-diamidino-2-phenylindole (nuclei stain)

DIV: days *in vitro*

DDW: double distilled water

E18-E19: embryonic day 18-19

Fmax: maximum fluorescence

GEFS⁺: generalized epilepsy with febrile seizures plus, type II

HBS: HEPES-buffered saline

High K⁺: high potassium HBS solution

iPSC: induced pluripotent stem cells

LOF: loss-of-function

MAP2: microtubule-associated protein 1

Nav1.1: voltage-gated sodium channel type 1, α subunit (protein)

PDMS: polydimethylsiloxane

PLL: poly-L-lysine

PV: parvalbumin

ROI: region of interest

SCN1a: voltage-gated sodium channel type 1, α subunit (gene)

SMEI: severe myoclonic epilepsy of infancy

Tau1: microtubule-associated protein Tau1

TTF: time-to-Fmax

Vglut1: vesicular glutamate transporter 1

VPA: valproic acid

WT: wild type

BIBLIOGRAPHY

- [1] J. J. Palop, Chin, J., and Mucke, L., "A network dysfunction perspective on neurodegenerative diseases," *Nature*, vol. 443, 2006.
- [2] National Institute of Neuological Disorders & Stroke. (2009, 8/17/09). http://www.ninds.nih.gov/about_ninds/ninds_overview.htm.
- [3] T. M. Pearce, & Williams, J.C., "Microtechnology: Meet Neurobiology," *Lab on a Chip*, vol. 7, pp. 30-40, 2007.
- [4] E. R. Kandel, Schwartz, J.H., and Jessell, T.M., Ed., *Principles of Neural Science, 4th Ed.* New York: McGraw-Hill, 2000, p.^pp. Pages.
- [5] J. C. Chang, Brewer, G.J. Wheeler, B.C., "Neuronal networks structuring induces greater neuronal activity through enhanced astroglial develoment," *Journal of Neural Engineering*, vol. 3, pp. 217-226, 2006.
- [6] Y. Takii, Kaji, H., Matsue, T., Nishizawa, M., "Microstamp-based micromachining for modulation of growth of cultured cells," *JSME International Journal Series C*, vol. 47, pp. 956-961, 2004.
- [7] C. Wyart, Ybert, C., Bourdieu, L, Herr, C., Prinza, C., Chatenay, D., "Constrained synaptic connectivity in functional mammalian neuronal networks grown on patterned surfaces," *Journal of Neuroscience Methods*, vol. 117, pp. 123-131, 2002.
- [8] C. M. Liu Q.Y., Dumm J., Shaffer K.M., Schaffner A.E., Barker J.L., Pancrazio J.J., Stenger D.A., and Ma W., "Synaptic connectivity in hippocampal neuronal networks cultured on micropatterned surfaces," *Developmental Brain Research*, vol. 120, pp. 223-231, 2000.
- [9] B. S. Chang, Lowenstein, D.H., "Mechanisms of disease: epilepsy," *The New England Journal of Medicine*, vol. 349, pp. 1257-1265, 2003.

- [10] World Health Organization. (2012, July 2, 2014). *Epilepsy Fact Sheet*. Available: <http://www.who.int/mediacentre/factsheets/fs999/en/>
- [11] R. S. Fisher, van Emde Boas, W., Blume, W., Elger, C., Genton, P., Lee, P., Engel, Jr., J., "Epileptic Seizures and Epilepsy: Definitions Proposed by the International League Against Epilepsy (ILAE) and the International Bureau for Epilepsy (IBE)," *Epilepsia*, vol. 46, pp. 470-472, 2005.
- [12] C. P. Panayiotopoulos, *Atlas of Epilepsies* vol. 3. London: Springer.
- [13] D. C. Hesdorffer, Logroscino, G., Benn, E.K.T., Katri, N., Cascino, G., Hauser, W.A., "Estimating risk for developing epilepsy," *Neurology*, vol. 76, pp. 23-27, 2011.
- [14] Center for Disease Control and Prevention. (2011, July 3, 2014). *Epilepsy at a glance*. Available: <http://www.cdc.gov/chronicdisease/resources/publications/aag/epilepsy.htm>
- [15] J. Meacham, "Epilepsy: Overlooked and Underfunded," in *Newsweek*, ed. New York, NY: PR Newswire, 2009.
- [16] M. R. Sperling, "Sudden Unexplained Death in Epilepsy," *Epilepsy Currents*, vol. 1, pp. 21-23, 2001.
- [17] J. G. Boggs, "Mortality associated with Status Epilepticus," *Epilepsy Currents*, vol. 4, pp. 25-27, 2004.
- [18] K. J. Meador, "Epilepsy and risk of suicide: a population-based case-control study," *Lancet Neurology*, vol. 68, pp. 693-698, 2007.
- [19] A. M. Kanner, "Depression in epilepsy: prevalence, clinical semiology, pathogenic mechanisms, and treatment," *Biological Psychiatry*, vol. 54, pp. 388-398, 2003.
- [20] Institute of Medicine Committee on the Public Health Dimensions of the Epilepsies, *Epilepsy across the spectrum: promoting health and understanding*. Washington, DC: National Academies Press, 2012.
- [21] C. D. Lamar, Hurley, R.A., Rowland, J.A., Taber, K.H., "Post-traumatic epilepsy: review of risks, pathophysiology, and potential biomarkers," *The Journal of Neuropsychiatry & Clinical Neurosciences*, vol. 26, pp. iv-113, 2014.
- [22] S. Li, Want, X., Wang, J., Wu, J., "Cerebrovascular and posttraumatic epilepsy," *Neurology Asia*, vol. 9, pp. 12-13, 2004.

- [23] L. Claes, Del-Favero, J., Ceulemans, B., Lagae, L., Van Broeckhoved, C., De Jongh, P., "De novo mutations in the sodium-channel gene SCN1a cause severe myoclonic epilepsy of infancy," *American Journal of Human Genetics*, vol. 68, pp. 1327-1332, 2001.
- [24] A. G. Bassuk, Wallace, R.H., Buhr, A., Buller, A.R., Afawi, Z., Shimojo, M., Miyata, S., Chen, S., Gonzalez-Alegre, P., Griesbach, H.L., Wu, S., Nashelsky, M., Vladar, E.K., Antic, D., Ferguson, P.J., Cirak, S., Voit, T., Scott, M.P., Axelrod, J.D., Gurnett, C., Daoud, A.S, Kivity, S., Neufeld, M.Y., Mazarib, A., Straussberg, R., Walid, S., Dorczyn, A.D., Slusarski, D.C., "A homozygous mutation in human PRICKLE1 causes an autosomal-recessive progressive myoclonus epilepsy-ataxia syndrom," *American Journal of Human Genetics*, vol. 83, pp. 572-581, 2008.
- [25] J. O'Muircheartaigh, Vollmar, C., Barker, G.J., Kumari, V., Symms, M.R., Thompson, P., Duncan, J.S., Koepp, M.J., Richardson, M.P., "Abnormal thalamocortical structural and functional connectivity in juvenile myoclonic epilepsy," *Brain*, vol. 135, pp. 3635-3644, 2012.
- [26] Z. Haneef, Lenartowicz, A., Yeh, H.J., Engel, Jr., J., Stern, J.M., "Network analysis of the default mode network using functional connectivity MRI in Temporal Lobe Epilepsy," *Journal of Visualized Experiments*, vol. 90, p. e51442, 2014.
- [27] Z. Haughn, "Epilepsy: Now and in the future," *Practical Neurology*, vol. 13, pp. 1-16, 2013.
- [28] E. B. Bromfield, Cavazos, J.E., Sirven, J.I., *An Introduction to Epilepsy*. West Harford, CT: American Epilepsy Societ, 2006.
- [29] B. Adamolekun. (2013, July 7, 2014). *Seizure Disorders*. Available: http://www.merckmanuals.com/professional/neurologic_disorders/seizure_disorders/seizure_disorders.html
- [30] M. J. Brodie, Barry, S.J., Bamagous, G.A., Norrie, J.D., Kwan, P., "Patterns of treatment responses in newly diagnosed epilepsy," *Neurology*, vol. 78, pp. 1548-1554, 2012.
- [31] R. Diaz-Arrastia, Agostini, M.A., Van Ness, P.C., "Evolving treatment strategies for epilepsy," *The Journal of the American Medical Association*, vol. 287, pp. 2917-2920, 2002.
- [32] P. Kwan, "Drug treatment of epilepsy: when does it fail and how to optimize its use?," *CNS Spectrums*, vol. 9, pp. 110-119, 2004.

- [33] E. K. St. Louis, Rosenfeld, W.E., Bramley, T., "Antiepileptic drug monotherapy: the initial approach in epilepsy management," *Current Neuropharmacology*, vol. 7, pp. 77-82, 2009.
- [34] S. U. Schuele, Luders, H.O., "Intractable epilepsy: management and therapeutic alternatives," *The Lancet Neurology*, vol. 7, pp. 514-524, 2008.
- [35] B. M. Uthman, Reichel, A.M., Dean, J.C., Eisenschenk, S., Gilmore, R., Reid, S., Roper, S.N., Wilder, B.J., "Effectiveness of VNS in epilepsy patients: a 12 year observation," *Neurology*, vol. 63, pp. 1124-1126, 2004.
- [36] J. Engle, J., "Surgery for Seizures," *The New England Journal of Medicine*, vol. 334, pp. 647-653, 1996.
- [37] J. Regis, Barolomei, F., Hayashi, M., Chauvel, P., *Advances in epilepsy surgery and radiosurgery* vol. 84. Vienna, Austria: Springer Vienna, 2002.
- [38] C. H. Halpern, Samadani, U., Litt, B., Jaggi, J.L., Baltuch, G.H., "Deep brain stimulation for epilepsy," *Neurotherapeutics*, vol. 5, pp. 59-67, 2010.
- [39] R. A. Lehne, Rosenthal, L., *Pharmacology for nursing care*. St. Louise, Missouri: Elsevier, 2013.
- [40] G. H. Baltuch, Villemure, J-G., *Operative techniques in epilepsy surgery*. New York, NY: Thieme Medical Publishers, 2008.
- [41] P. Garcia, "Brain stimulation for epilepsy: stimulating results?," *Epilepsy Currents*, vol. 6, pp. 192-194, 2006.
- [42] A. Carius, Wintermantel, A., "Vagus nerve stimulation therapy in epilepsy patients: long-term outcome and adverse effects: a retrospective analysis," *Nervenarzt*, vol. 84, pp. 1473-1485, 2013.
- [43] University of Pittsburgh Department of Neurological Surgery. (2014, 11/10/14). *Adult Epilepsy Surgical Options*.
- [44] J. de Tisi, Bell, G.S., Peacock, J.L., McEvoy, A.W., Harkness, W.F., Sander, J.W., Duncnan, J.S., "The long-term outcome of adult epilepsy surgery, patterns of seizure remission, and relapse: a cohort study," *Lancet*, vol. 378, pp. 1388-1395, 2011.
- [45] J. S. Hauptman, Pedram, K., Sison, C.A., Sankar, R., Salamon, N., Vinters, H.V., Mathern, G.W., "Pediatric epilepsy surgery: long-term 5-year seizure remission and medication use," *Neurosurgery*, vol. 71, pp. 985-993, 2012.

- [46] World Health Organization. World Federation of Neurology, "Atlas: country resources for neurological disorders," World Health Organization & World Federation of Neurology, Geneva, Switzerland 2004.
- [47] E. Vegni, Leone, D., Canevini, M.P., Tinuper, P., Moja, E.A., "Sudden unexplained death in epilepsy (SUDEP): a pilot study on truth telling among Italian epileptologists," *Neurological Sciences*, vol. 32, pp. 332-335, 2011.
- [48] B. Morton, Richardson, A., Duncan, S., "Sudden unexplained death in epilepsy (SUDEP): don't ask, don't tell?," *Journal of Neurology, Neurosurgery, Psychiatry, with Practical Neurology*, vol. 77, pp. 199-202, 2006.
- [49] National Institute of Neurological Disorders & Stroke. (2000, July 10, 2014). *2000 Epilepsy research benchmarks: a guide for the general public*. Available: <http://www.ninds.nih.gov/research/epilepsyweb/benchmarks.htm>
- [50] National Institute of Neurological Disorders & Stroke. (2005, July 10, 2014). *2005 Epilepsy Research Benchmarks: Stewards Report*. Available: <http://www.ninds.nih.gov/research/epilepsyweb/epilepsybenchmarks.htm>
- [51] National Institute of Neurological Disorders & Stroke. (2007, July 10, 2014). *2007 Epilepsy Research Benchmarks*. Available: http://www.ninds.nih.gov/research/epilepsyweb/2007_benchmarks.htm
- [52] A. Pitkanen, Schwartzkroin, P.A., Moshe, S.L., *Models of Seizures and Epilepsy*. San Diego, CA: Elsevier Academic Press, 2005.
- [53] G. A. Hortopan, Dinday, M.T., Baraban, S.C, "Zebrafish as a model for studying genetic aspects of epilepsy," *Disease Models & Mechanisms*, vol. 3, pp. 144-148, 2010.
- [54] L. Parker, Howlett, I.C., Rusan, Z.M., Tanouye, M.A., "Seizure and epilepsy: studies of seizure disorders in *Drosophila*," *International Review of Neurobiology*, vol. 99, pp. 1-21, 2011.
- [55] Y. Yang, Frankel, W.N., "Molecular Mechanisms of Epileptogenesis," in *Molecular Mechanisms of Epileptogenesis*, H. E. S. D. K. Binder, Ed., ed Georgetown, TX: Landes Bioscience/Kluwer, 2004.
- [56] H. Kupferber, "Animal models used in the screening of antiepileptic drugs," *Epilepsia*, vol. 42, pp. 7-12, 2001.
- [57] S. D. Shorvon, Perucca, E., Fish, D., Dodson, E., Ed., *The Treatment of Epilepsy*. Oxford: Blackwell Publishing, 2004, p.^pp. Pages.

- [58] A. C. Michael, Borland, L., *Electrical/chemical Methods for Neuroscience*. Boca Raton, FL: CRC Press, 2007.
- [59] R. Burgess, *Understanding Nanomedicine: An Introductory Textbook*. Singapore: Pan Stanford Publishing, 2012.
- [60] A. Cestelli, Savettieri, G., Salemi, G., Di Liegro, I. . , "Neuronal cell cultures: a tool for investigations in developmental neurobiology," *Neurochemical Research*, vol. 17, pp. 1163-1180, 1992.
- [61] R. G. Harrison, "The outgrowth of the nerve fiber as a mode of protoplasmic movement," *Journal of Experimental Zoology*, vol. 9, pp. 787-846, 1910.
- [62] R. Dulbecco, Freeman, G., "Plaque production by the polyoma virus," *Virology*, vol. 8, pp. 396-397, 1959.
- [63] F. W. Pfrieger, "Roles of glial cells in synapse development," *Cellular and Molecular Life Sciences*, vol. 66, pp. 2037-2047, 2009.
- [64] G. M. Beaudoin III, Lee, S.H., Yuan, Y., Ng, Y.G., Reichardt, L.F., Arikath, J., "Culturing pyramidal neurons from the early postnatal mouse hippocampus and cortex," *Nature Protocols*, vol. 7, pp. 1741-1754, 2012.
- [65] M. Akay, *Handbook of Neural Engineering*. Hoboken, NJ: Wiley-IEEE Press, 2007.
- [66] D. P. Martin, Wallace, T.L., Johnson, Jr., E.M., "Cytosine arabinoside kills postmitotic neurons in a a fashion resembling trophic factor deprivation: evidence that a deoxycytidine-dependent process may be required for nerve growth factor signal transduction," *Journal of Neuroscience*, vol. 10, pp. 184-193, 1990.
- [67] P. J. Hollenbeck, Bamberg, J.R., *Neurons: methods and applications for the cell biologist*. San Diego, CA: Academic Press, 2003.
- [68] G. Banker, Goslin, K., *Culturing Nerve Cells*. Cambridge: MIT Press, 1998.
- [69] G. J. Brewer, Torricelli, J.R., Evence, E.K., Price, P.J., "Optimized survival of hippocampal neurons in B27-supplemented neurobasal, a new serum-free medium combination," *Journal of Neuroscience Research*, vol. 35, pp. 567-576, 2004.
- [70] Lonza, "Amata rat neuron nucleofector kit for primary rat hippocampal or cortical neurons," Lonza, Ed., ed. Cologne, Germany: Lonza, 2009, pp. 1-5.

- [71] F. Griffith, "The Significance of pneumococcal types," *Journal of Hygiene*, vol. 27, pp. 113-159, 1928.
- [72] M. Mandel, Higa, A., "Calcium dependent bacteriophage DNA infection," *Journal of Molecular Biology*, vol. 53, 1970.
- [73] S. C. Baraban, "Emerging epilepsy models: insights from mice, flies, worms, and fish," *Current Opinion in Neurology*, vol. 20, pp. 164-168, 2007.
- [74] G. Avanzini, Noebels, J., *Genetics of epilepsies and genetic epilepsies*. Paris, France: John Libbey Eurotext, 2009.
- [75] T. Sugawara, Tsurubuchi, Y., Fujiwara, T., Mazaki-Miyazaki, E., Nagata, K., Montal, M., Inoue, Y., Yamakawa, K., "Nav1.1 channels with mutations of severe myoclonic epilepsy of infancy display attenuated currents," *Epilepsy Research*, vol. 54, pp. 201-2017, 2003.
- [76] M. Mantegazza, Gambardella, A., Rusconi, R., Schiavon, E., Annesi, F., Cassulini, R.R., Labate, A., Carrideo, S., Chifari, R., Canevini, M.P., Canger, R., Franceschetti, S., Annesi, G., Wanke, E., Quattrone, A., "Identification of an Nav1.1 sodium channel (SCN1a) loss-of-function mutation associated with familial simple febrile seizures," *Proceedures of the National Academy of Sciences*, vol. 102, pp. 18177-18182, 2005.
- [77] Y. Sugiura, Ogiwara, I., Hoshi, A., Ugawa, Y., "Different degrees of loss of function between GEFS+ and SMEI Nav1.1 missense mutants at the same residue induced by rescuable folding defects," *Epilepsia*, vol. 53, pp. e111-e114, 2012.
- [78] A. Vogt, Lauer, L., Knoll, W., and Offenhausser A., "Micropatterned substrates for the growth of functional neuronal networks of defined geometry," *Biotechnology Progress*, vol. 19, pp. 1562-1568, 2003.
- [79] A. Folch, Toner, M., "Microengineering of cellular interactions," *Annual Review of Biomedical Engineering*, vol. 2, pp. 227-256, 2000.
- [80] R. Singhvi, Stephanopoulos, G., Wang, D.I.C., "Review: Effects of substratum morphology on cell physiology," *Biotechnology and Bioengineering*, vol. 43, 1994.
- [81] P. Clark, "Cell behavior on micropatterned surfaces," *Biosensors and Bioelectronics*, vol. 9, pp. 657-661, 1994.
- [82] J. C. Chang, Brewer, G.J., Wheeler, B.C., "A modified microstamping technique enhances polylysine transfer and neuronal cell patterning," *Biomaterials*, vol. 24, pp. 2863-2870, 2003.

- [83] N. R. Wilson, Ty, M.T., Ingber, D.E., Sur, M., Liu, G., "Synaptic reorganization in scaled networks of controlled size," *Journal of Neuroscience*, vol. 27, pp. 13581-13589, 2007.
- [84] S. W. Kam L., Turner J. N., and Bizios R., "Axonal outgrowth of hippocampal neurons on micro-scale networks of polylysine-conjugated laminin," *Biomaterials*, vol. 22, pp. 1049-1054, 2001.
- [85] W. G. Vogt A.K., Meyer W., Knoll W., and Offenhausser A., "Synaptic plasticity in micropatterned neuronal networks," *Biomaterials*, vol. 26, pp. 2549-2557, 2005.
- [86] E. Ostuni, Whitesides, G.M., "Patterning mammalian cells using elastomeric membranes," *Langmuir*, vol. 16, pp. 7811-7819, 2000.
- [87] M. Scholl, Sprossler, C., Denyer, M., Krause, M., Nakajima, K., Maelicke, A., and W. Knoll, and Offenhausser, A., "Ordered networks of rat hippocampal neurons attached to silicon oxide surfaces," *Journal of Neuroscience Methods*, vol. 104, 2000.
- [88] A. Tourovskaia, Barber, T., "Micropatterns of chemisorbed cell adhesion repellent films using oxygen plasma etching elastomeric masks," *Langmuir*, vol. 19, pp. 4754-4764, 2003.
- [89] O. Shefi, Golding, I., Segev, R., Ben-Jacob, E., Ayali, A., "Morphological characterization of in vitro neuronal networks," *Physical Review E*, vol. 66, 2002.
- [90] R. Sorkin, Gabay, T., Blinder, P., Baranes, D., Ben-Jacob, E., Hanein, Y., "Compact self-wiring in cultured neural networks," *Journal of Neural Engineering*, vol. 3, pp. 95-101, 2006.
- [91] D. A. Stenger, Hickman, J.J., Bateman, K.E., Ravenscroft, M.S., Ma, W., Pancrazio, J.J., Shaffer, K., Schaffner, A.E., Cribbs, D.H., Cotman, C.W., "Microlithographic determination of axonal/dendritic polarity in cultured hippocampal neurons," *Journal of Neuroscience Methods*, vol. 82, pp. 167-173, 1998.
- [92] A. Vishwanathan, Bi, G-Q., Zeringue, H.C., "Ring-shaped networks: a platform to study persistent activity," *Lab on a Chip*, 2010.
- [93] M. Jungblut, Knoll, W., Thielemann, C., Pottek, M., "Triangular neuronal networks on microelectrode arrays: an approach to improve the properties of low-density networks for extracellular recording," *Biomedical Microdevices*, vol. 11, pp. 1269-1278, 2009.
- [94] G. Grynkiewicz, Poenie, M., Tsien, R.Y., "A New Generation of Ca²⁺ Indicators with Greatly Improved Fluorescence Properties," *The Journal of Biological Chemistry*, vol. 260, pp. 3440-3450, 1985.

- [95] Life Technologies, *The Molecular Probes Handbook*, 11 ed.: Life Technologies, 2010.
- [96] R. Singh, Andermann, E., Whitehouse, W.P.A., Harvey, A.S., Keene, D.L., Seni, M-H., Crossland, K.M., Andermann, F., Berkovic, S.F., Scheffer, I.E., "Severe myoclonic epilepsy of infancy: extended spectrum of GEFS+?," *Epilepsia*, vol. 42, pp. 837-844, 2001.
- [97] T. Takahashi, Fukuyama, Y. , *Biology of Seizure Susceptibility in Developing Brain*. Surrey: John Libbey Eurotext, 2008.
- [98] A. Hahn, Neubauer, B.A., "Sodium and potassium channel dysfunctions in rare and common idiopathic epilepsy syndromes," *Brain Development*, vol. 31, pp. 515-520, 2009.
- [99] National Institutes of Health. (2014, July 12, 2014). *SCN1a*.
- [100] A. Escayg, Goldin, A.L., "Sodium channel SCN1a and epilepsy: mutations and mechanisms," *Epilepsia*, vol. 51, pp. 1650-1658, 2010.
- [101] M. H. Meisler, Kearney, J.A. , "Sodium Channel Mutations in Epilepsy and Other Neurological Disorders," *Journal of Clinical Investigation*, vol. 115, pp. 2010-2017, 2005.
- [102] I. Soltesz, Staley, K., *Computational neuroscience in epilepsy*. San Diego, CA: Elsevier Academic Press, 2008.
- [103] C. Lossin, Rhodes, T.H., Desai, R.R., Vanoye, C.G., Wang, D., Carniciu, S., Devinsky, O., George, Jr. A.L., "Epilepsy-associated dysfunction in the voltage-gated neuronal sodium channel SCN1a," *Journal of Neuroscience Methods*, vol. 23, pp. 11289-11295, 2003.
- [104] W.-P. Liao, Shi, Y-W., Long, Y-S., Zeng, Y., Li, T., Yu, M-J., Su, T., Deng, P., Lei, Z-G., Xu, S-J., Deng, W-Y., Liu, X-R., Sun, W-W., Yi, Y-H., Xu, Z.C., Duan, S., "Partial epilepsy with antecedent febrile seizures and seizure aggravation by antiepileptic drugs: associated with loss of function Nav1.1," *Epilepsia*, vol. 51, pp. 1669-1678, 2010.
- [105] F. Kalume, Yu, F.H., Westenbroek, R.E., Scheuer, T., Catterall, W.A., "Reduced sodium current in purkinje neurons from Nav1.1 mutant mice: implications for ataxia in severe myoclonic epilepsy in infancy," *The Journal of Neuroscience*, vol. 27, pp. 11065-11074, 2007.
- [106] F. H. Yu, Mantegazza, M., Westenbroek, R.E., Robbins, C.A., Kalume, F., Burton, K.A., Spain, W.J., McKnight, G.S., Scheuer, T., Catterall, W.A., "Reduced sodium current in

- GABAergic interneurons in a mouse model of severe myoclonic epilepsy of infancy," *Nature Neuroscience*, vol. 9, pp. 1142-1149, 2006.
- [107] I. Ogiwara, Miyamoto, H., Morita, N., Atapour, N., Mazaki, E., Inoue, I., Takeuchi, T., Itohara, S., Yanagawa, Y., Obata, K., Furuichi, T., Hensch, T.K., Yamakawa, K., "Nav1.1 localizes to axons of parvalbumin-positive inhibitory interneurons: a circuit basis for epileptic seizures in mice carrying an SCN1a gene mutation," *Neurobiology of Disease*, vol. 27, pp. 5903-5914, 2007.
- [108] I. Ohmori, Kahlig, K.M., Rhodes, T.H., Wang, D.W., George Jr., A.L., "Nonfunctional SCN1a is common in severe myoclonic epilepsy of infancy," *Epilepsia*, vol. 47, pp. 1636-1642, 2006.
- [109] C. H. Thompson, Porter, J.C., Kahlig, K.M., Daniels, M.A., George Jr., A.L., "Nontruncating SCN1a mutations associated with severe myoclonic epilepsy of infancy impair cell surface expression," *Journal of Biological Chemistry*, vol. 287, pp. 42001-42008, 2012.
- [110] B. Alberts, Johnson, A., Lewis, J., Raff, M., Roberts, K., Walter, P., *Molecular Biology of the Cell*, 5th ed. New York, NY: Garland Sciences, 2008.
- [111] N. Eijkelkamp, Linley, J.E., Baker, M.D., Minett, M.S., Cregg, R., Werdehausen, R., Rugiero, F., Wood, J.N., "Neurological perspectives on voltage-gated sodium channels," *Brain*, vol. 135, pp. 2585-2612, 2012.
- [112] B. H. Munro, *Statistical methods for health care research*, 5th ed. Philadelphia, PA: Lippincott, Williams, & Wilkens, 2005.
- [113] G. Dityateva, Hammond, M., Thiel, C., Ruonala, M.O., Delling, M., Siebenkotten, G., Nix, M., Dityatev, A., "Rapid and efficient electroporation-based gene transfer into primary dissociated neurons," *Journal of Neuroscience Methods*, vol. 130, pp. 65-73, 2003.
- [114] A. Gartner, Collin, L., Lalli, G., "Nucleofection of primary neurons," *Methods in Enzymology*, vol. 406, pp. 374-388, 2006.
- [115] O. Gresch, Engel, F.B., Nesic, D., Tran, T.T., England, H.M., Hickman, E.S., Korner, I., Gan, L., Chen, S., Castro-Obregon, S., Hammermann, R., Wolf, J., Muller-Hartmann, H., Nix, M., Siebenkotten, G., Kraus, G., Lun, K., "New non-viral method for gene transfer into primary cells," *Methods*, vol. 32, pp. 151-163, 2004.

- [116] M. Zeitelhofer, Vessey, J.P., Thomas, S., Kiebler, M., Dahm, R., "Transfection of cultured primary neurons via nucleofecion," *Current Protocols in Neuroscience*, vol. 47, pp. 1-21, 2009.
- [117] J. K. Rathenberg, J.T., Moss, S.J., "Palmitoylation regulates the clustering and cell surface stability of GABA_A receptors," *Molecular and Cellular Neuroscience*, vol. 26, pp. 251-257, 2004.
- [118] D. Karra, Dahm, R., "Transfection techniques for neuronal cells," *The Journal of Neuroscience*, vol. 30, pp. 6171-6177, 2010.
- [119] W. R. J. Whitaker, Faull, R.L.M., Waldvogel, H.J., Plumpton, C.J., Emson, P.C., Clare, J.J., "Comparative distribution of voltage-gated sodium channel proteins in human brain," *Molecular Brain Research*, vol. 88, pp. 37-53, 2001.
- [120] R. E. Westenbroek, Merrick, D.K., Catterall, W.A., "Differential subcellular localization of the RI and RII Na⁺ channel subtypes in central neurons," *Neuron*, vol. 3, pp. 695-704, 1989.
- [121] K. Krishnamurthy, Smith-Parker, A., Burton, S.D., Zeringue, H.C., "SCN1a point mutations on neuron connectivity," in *35th Annual Northeast IEEE Bioengineering Conference*, Boston, MA, 2009.
- [122] B. Gong, Rhodes, K.J., Bekele-Arcuri, Z., Trimmer, J.S., "Type I and Type II Na⁺ channel alpha-subunit polypeptides exhibit distinct spatial and temporal patterning, and association with auxiliary subunits in rat brain," *The Journal of Comparative Neurology*, vol. 412, pp. 342-352, 1999.
- [123] A. Duflocq, Le Bras, B., Bullier, E., Couraud, F., Davene, M., "Nav1.1 is predominantly expressed in nodes of Ranvier and axon initial segments," *Molecular and Cellular Neuroscience*, vol. 39, pp. 180-192, 2008.
- [124] M. Kempf, Clement, A., Faissner, A., Lee, G., Brandt, R., "Tau binds to the distal axon early in development of polarity in a microtubule- and microfilament-dependent manner," *The Journal of Neuroscience*, vol. 16, pp. 5583-5592, 1996.
- [125] A. Van Wart, Trimmer, J.S., Matthews, G., "Polarized distribution of ion channels within microdomains of the axon initial segment," *Journal of Comparative Neurology*, vol. 500, pp. 339-352, 2006.
- [126] J. A. Black, Liu, S., Waxman, S.G., "Sodium channel activity modulates multiple functions in microglia," *Glia*, vol. 57, pp. 1072-1081, 2008.

- [127] E. R. O'Connor, Sontheimer, H., Spencer, D.D., de Lanerolle, N.C., "Astrocytes from human hippocampal epileptogenic foci exhibit action potential-like responses," *Epilepsia*, vol. 39, pp. 347-354, 1998.
- [128] T. Klausberger, Marton, L.F., O'Neill, J., Huck, J.H., Dalezios, Y., Fuentealba, P., Suen, W.Y., Papp, E., Kaneko, T., Watanabe, M., Csicsvari, J., Somogyi, P., "Complementary roles of cholecystokinin- and parvalbumin-expressing GABAergic neurons in hippocampal network oscillations," *Journal of Neuroscience*, vol. 25, pp. 9782-9793, 2005.
- [129] J. Engel, J., Pedley, T.A., Aicardi, J., *Epilepsy: A Comprehensive Textbook*, 2nd ed. Philadelphia, PA: Lippincott, Williams, & Wilkins, 2008.
- [130] W. S. van der Hel, Verlinde, S.A.M.W., Meijer, D.H.M., de Wit, M., Rensen, M.G., van Gassen, K.L.I., van Rijen, P.C., van Veelen, C.W.M., de Graan, P.N.E., "Hippocampal distribution of vesicular glutamate transporter I in patients with temporal lobe epilepsy," *Epilepsia*, vol. 50, pp. 1717-1728, 2009.
- [131] J. Freneau, R.T., Troyer, M.D., Pahner, I., Nygaard, G.O., Tran, C.H., Reimer, R.J., Bellocchio, E.E., Fortin, D., Storm-Mathisen, J., Edwards, R.H., "The expression of vesicular glutamate transporters defines two classes of excitatory synapse," *Neuron*, vol. 31, pp. 247-260, 2001.
- [132] P. Bezzi, Gundersen, V., Galbete, J.L., Seifert, G., Steinhauser, C., Pilate, E., Volterra, A., "Astrocytes contain a vesicular compartment that is competent for regulated exocytosis of glutamate," *Nature Neuroscience*, vol. 7, pp. 613-620, 2004.
- [133] E. Herzog, Gilchrist, J., Gras, C., Muzerell, A., Ravassard, P., Giros, B., Gaspar, P., El Mestikaway, S., "Localization of Vglut3, the vesicular glutamate transporter type 3, in the rat brain," *Neuroscience*, vol. 123, pp. 983-1002, 2004.
- [134] G. A. Banker, Cowan, W.M., "Further observations on hippocampal neurons in dispersed cell culture," *Journal of Comparative Neurology*, vol. 187, pp. 469-493, 1979.
- [135] G. M. J. Beaudoin III, Lee, S-H., Singh, D, Yuan, Y., Ng, Y-G., Reichardt, L.F., Arikath, J., "Culturing pyramidal neurons from the early postnatal mouse hippocampus and cortex," *Nature Protocols*, vol. 7, pp. 1741-1754, 2012.
- [136] C. Grienberger, Konnerth, A., "Imaging calcium in neurons," *Neuron*, vol. 73, pp. 862-885, 2012.

- [137] D. A. Sun, Sombati, S., Blair, R.E., DeLorenzo, R.J., "Calcium-dependent epileptogenesis in an in vitro model of stroke induced "epilepsy"," *Epilepsia*, vol. 43, pp. 1296-1305, 2002.
- [138] T. Badea, Goldber, J, Mao, B., Yuste, R., "Calcium imaging of epileptiform events with single-cell resolution," *Journal of Neurobiology*, vol. 48, pp. 215-227, 2001.
- [139] J. W. Wheless, and Sankar, R., "Treatment strategies for myoclonic seizures and epilepsy syndromes with myoclonic seizures," *Epilepsia*, vol. 44, p. 27, 2003.
- [140] C. S. Horn, Ater, S.B., Hurst, D.L., "Caramazepine-exacerbated epilepsy in children and adolescents," *Pediatric Neurology*, vol. 2, pp. 340-345, 1986.
- [141] M. S. Martin, Dutt, K., Papale, L.A., Dube, C.M., Dutton, S.B., de Haan, G., Shankar, A., Tufik, S., Meisler, M.H., Baram, T.Z., Goldin, A.L., Escayg, A., "Altered function of the SCN1a voltage-gated sodium channel leads to g-Aminobutyric acid-ergic (GABAergic) interneuron abnormalities," *Journal of Biological Chemistry*, vol. 285, pp. 9823-9834, 2010.
- [142] W. Loscher, "Basic pharmacology of valproate: a review after 35 years of clinical use for the treatment of epilepsy," *CNS Drugs*, vol. 16, pp. 669-694, 2002.
- [143] C. L. Faingold, Fromm, G.H., *Drugs for the control of epilepsy: action on neuronal networks involved in seizure disorders*. Boca Raton, FL: CRC Press, 1992.
- [144] M. S. Gold, Reichling, D.B., Hampl, K.F., Drasner, K., Levine, J.D., "Lidocaine toxicity in primary afferent neurons from the rat," *The Journal of Pharmacology and Experimental Therapeutics*, vol. 285, pp. 413-421, 1998.
- [145] Y.-C. Lin., Haung, Z-H., Jan, I-Sam, Yeh, C-C., Wu, H-J., Chou, Y-C., Chang, Y-C., "Development of excitatory synapses in cultured neurons dissociated from the cortices of rat embryos and rat pups at birth," *Journal of Neuroscience Research*, vol. 67, pp. 484-493, 2002.
- [146] C. C. Swanwick, Murthy, N.R., Mtchedlishvili, Z., Sieghart, W., Kapur, J., "Development of g-aminobutyric acid-ergic synapses in cultured hippocampal neurons," *The Journal of Comparative Neurology*, vol. 495, pp. 497-510, 2006.
- [147] R. Fricke, Zentis, P.D., Rajappa, L.T., Hofmann, B., Banzet, M., Offenhausser, A., Meffert, S.H., "Axon guidance of rat cortical neurons by microcontact printed gradients," *Biomaterials*, vol. 32, pp. 2070-2076, 2011.

- [148] C. D. James, Davis, R., Meyer, D.M., Turner, A., Turner, S., Withers, G., Kam, L., Banker, G., Craighead, H., Isaacson, M., Turner, J., Shain, W., "Aligned microcontact printing of micrometer-scale poly-L-lysine structures for controlled growth of cultured neurons on planar microelectrode arrays," *IEEE Transactions on Biomedical Engineering*, vol. 47, pp. 17-21, 2000.
- [149] F. C. Lu, Kacew, S., *Lu's Basic Toxicology*, 4th ed. New York, NY: Taylor & Francis, 2002.
- [150] F. W. Pfrieger, Barres, B.A., "Synaptic efficacy enhanced by glial cells in vitro," *Science*, vol. 277, pp. 1684-1687, 1997.
- [151] O. Devinsky, Vezzani, A., Najjar, S., de Lanerolle, N.C., Rogawski, M.A., "Glial cells and epilepsy: excitability and inflammation," *Trends in Neurosciences*, vol. 36, pp. 174-184, 2013.
- [152] F. E. Dudek, "Role of glial cells in seizures and epilepsy: intracellular calcium oscillations in spatial buffering," *Epilepsy Currents*, vol. 2, pp. 137-139, 2002.
- [153] S. Kaech, Banker, G., "Culturing hippocampal neurons," *Nature Protocols*, vol. 1, pp. 2406-2415, 2006.
- [154] M. A. Israel, Yuan, S.H., Bardy, C., Reyna, S.M., Mu, Y., Herrera, C., Hefferan, M.P., Van Gorp, S., Nazor, K.L., Boscolo, F.S., Carson, C.T., Laurent, L.C., Marsala, M., Gage, F.H., Remes, A.M., Koo, E.H., Goldstein, L.S., "Probing sporadic and familial Alzheimer's disease using induced pluripotent stem cells," *Nature* vol. 482, pp. 216-220, 2012.
- [155] Y. Liu, Lopez-Santiago, L.F., Yuan, Y., Jones, J.M., Zhang, H., O'Malley, H.A., Patino, G.A., O'Brien, J.E., Rusconi, R., Gupta, A., Thompson, R.C., Natowicz, M.R., Meisler, M.H., Isom, L.L., Parent, J.M., "Dravet Syndrome patient-derived neurons suggest a novel epilepsy mechanism," *Annals of Neurology*, vol. 74, pp. 128-139, 2013.